United States Nuclear Regulatory Commission

Protecting People and the Environment

NUREG/CR-7015
BNL-NUREG-91346-2010

Analysis of JNES Seismic Tests on Degraded Piping

Office of Nuclear Regulatory Research

NUREG/CR-7015
BNL-NUREG-91346-2010

Analysis of JNES Seismic Tests on Degraded Piping

Manuscript Completed: May 2010
Date Published: July 2010

Prepared by
[1] T. Zhang, [1]F.W. Brust, [1]D.J. Shim, and [1]G. Wilkowski
[2] J. Nie, [2]C. Hofmayer

[1]Engineering Mechanics Corporation of Columbus
3518 Riverside Drive
Suite 202
Columbus, OH 43221

[2]Brookhaven National Laboratory
P.O. Box 5000
Upton, NY 11973-5000

S. Ali, NRC Project Manager

NRC Job Code N6076

Office of Nuclear Regulatory Research

ABSTRACT

This report describes efforts conducted by Engineering Mechanics Corporation of Columbus (Emc^2) under subcontract to Brookhaven National Laboratory (BNL) for the U.S. Nuclear Regulatory Commission to analyze and better understand a series of degraded pipe tests under seismic loading that were conducted in Japan. These efforts were undertaken as part of collaborative efforts between the United States Nuclear Regulatory Commission (NRC) and the Japan Nuclear Energy Safety Organization (JNES), who conducted a multi-year test program for the Ministry of Economy, Trade and Industry (METI) of Japan to investigate the behavior of typical Nuclear Power Plant piping systems under large seismic loads. JNES provided the test results for the evaluations given in this report. Emc^2 worked with BNL on the degraded piping system analyses. This report describes Emc^2's post-test analyses of the large-scale piping system tests and discusses insights gained from this program. The analyses in these efforts are of value to understanding margins that degraded piping has under seismic loading for: (a) Transition Break Size rule for CFR 50.46a applications, (b) Leak-Before-Break analyses in NRC's SRP 3.6.3, and (c) pipe flaw tolerance by ASME code evaluations.

The JNES tests analyzed were of both the simple degraded component tests, e.g., a nozzle with a short section of straight pipe and a circumferential surface crack in the joining girth weld; as well as combined component tests from a 1/3-scale section of the main recirculation system of a BWR. The combined component tests had circumferential cracks at a nozzle girth weld and elbow girth weld of the main pipe run, and at a tee girth weld in the branch pipe. The combined component tests were conducted at room temperature with pressure and simulated seismic loading in one direction.

Emc^2's analyses used a "cracked-pipe element" (CPE) concept, where the element represented the global moment-rotation response due to the crack. This approach was developed to simplify the dynamic finite element analysis. The failure modes automatically captured by this method are ductile tearing during the final failure event, and very low cyclic fatigue damage with large-scale plasticity. Crack growth due to high-cycle fatigue or low-cycle fatigue with small-scale plasticity requires a separate analysis than the current "cracked-pipe element" approach. This "cracked-pipe element" methodology was developed in the International Piping Integrity Research Group (IPIRG) programs that the USNRC and Japan were members of in the early 1990's. In this program, the validation efforts increased in complexity by comparisons with pipe tests with circumferential through-wall and surface cracks under quasi-static bending, fully reverse cyclic loading, and inertial loading to examine dynamic loading aspects with cyclic hysteresis loops of a circumferential through-wall crack. Those pipe tests data were developed in prior USNRC or IPIRG programs. The JNES simple component test was used to fine-tune the "cracked-pipe element" model since the toughness of the weld metal in the JNES tests was not available.

In the JNES combined-component experiment where leakage occurred (Test FTP-4), it was determined that the loading at the crack location was in the small-scale plasticity range of the "cracked-pipe elements." Hence, the leakage was caused by low-cycle fatigue with very small-scale yielding, rather than by ductile tearing or low-cycle fatigue with larger plasticity that would occur if the loading were near the ultimate load capacity of the cracked pipe. The procedure used to make predictions of low-cycle fatigue crack growth were based on the Dowling ΔJ procedure, which is an extension of linear elastic based fatigue crack growth methodology extended into the nonlinear plasticity regime. The predicted moments from the CPE approach were accounted for using a cycle-by-cycle crack growth procedure. Only moments large enough to produce significant crack growth per cycle need be included, and the U.S. Air Force fatigue crack growth code, AFGROW, was used to make these predictions. The predictions using this approach compare quite well with the experimental measurements where leakage occurred during the sixth load block.

As part of the analyses for the FTP-4 experimental case, the amplitude of the seismic loading was increased until failure of the surface crack occurred by cyclic tearing in the ABAQUS model with the "cracked-pipe element" with just one loading block. The margins on the applied accelerations in the FTP-4 test were about a factor of 5.0. The material property parameters were then changed for the cracked-pipe sections as well as the rest of the model to estimate the margins if the JNES test was conducted at the BWR operating temperature at 288°C (550°F). The margin at this temperature was conservatively estimated to be 3 on the applied acceleration in the FTP-4 test. This was a slightly conservative analysis since the viscous damping of the uncracked piping system at this higher level of excitation was kept at 2% (the "cracked-pipe element" and the elbows behave plastically and contributed to the increased overall damping effect). The minor conservatism from the damping at the higher excitation is also true for the room temperature case as well.

To better assess how a full-scale pipe system might behave with similar loading and crack size, an elastic-plastic correction factor for larger-diameter pipe was applied to the load capacity of the FTP-4 pipe analysis at 288°C. An evaluation of one of the component tests showed that the JSME Z-factor for GTAW/SMAW welds was quite close to the experimental results, whereas the ASME code would have over predicted the test failure load by 30-percent. Using the JSME GTAW/SMAW Z-factor equation, the full-scale pipe system margins on failure load and acceleration that were applied in this test for a similar non-dimensional crack size were conservatively estimated to be 1.06 and about 2, respectively. Results here suggest that larger cracks could be tolerated in this system test.

These margins were still above the assumed nonlinear stress correction used in the NRC's work on "Seismic Considerations for the Transition Break Size" in NUREG-1903, although analyses as conducted in this report would have to be performed for the crack sizes and typical pipe system used in the Transition Break Size seismic analysis to better quantify the margins that might exist. Such margins would also affect LBB analyses, ASME code criteria, and on-going probabilistic pipe fracture analyses such as the NRC's xLPR efforts that are just starting up.

FOREWORD

This research work was performed as part of the Implementing Agreement made between the U.S. Nuclear Regulatory Commission (NRC) and the Japan Nuclear Energy Safety Organization (JNES) of Japan in the area of seismic engineering research.

This report is focused on the analysis performed by Engineering Mechanics Corporation of Columbus (Emc2) under subcontract to Brookhaven National Laboratory (BNL) for the NRC to simulate and better understand a series of degraded pipe tests under seismic loading that were conducted in Japan. JNES provided the test results for the evaluations given in this report. Emc2 worked with BNL on the degraded piping system analyses. This report provides a comprehensive coverage of the modeling and analysis effort of the large-scale piping system tests and presents insights gained from this program. The analyses in this effort provide an overall value to understanding margins that degraded piping has under seismic loading for: (a) application to the Transition Break Size rule for CFR 50.46a applications, (b) Leak-Before-Break analyses in NRC's SRP 3.6.3, and (c) pipe flaw tolerance by ASME Section XI code evaluations.

The report is informative and insightful, particularly in the application of the connector element of the ABAQUS computer code in the finite element analyses to simulate the global response of a cracked pipe. The analysis documented in this report also utilized the Dowling ΔJ procedure and the U.S. Air Force fatigue crack growth code, AFGROW, to simulate the cycle-by-cycle crack growth. Very good agreement was established between the behaviors of the analyzed piping system vs. the piping test system subjected to the simulated seismic loading in the JNES test program.

These analyses showed that the JNES pipe test failures are due to low-cycle fatigue with small-scale yielding, and there were large margins on acceleration needed to cause failure in a single large seismic event compared to the input acceleration in the JNES tests. Based on extrapolated results to full-scale behavior, these analyses showed large margins for the acceleration to cause failure relative to the typical design peak ground acceleration (PGA) values for U.S. plants.

The margins seen in the analyses of the JNES tests of the tolerable accelerations relative to the design PGA values for U.S. plants are much larger than the maximum nonlinear stress correction factors used in the Transition Break Size work. However, further analyses similar to those described in this report would have to be conducted for the crack sizes and typical pipe system used in the Transition Break Size seismic analysis to better quantify the margins that might exist. Similar margins would also affect Leak-Before-Break analyses, ASME code criteria, and on-going NRC probabilistic pipe fracture analysis efforts.

TABLE OF CONTENTS

ABSTRACT iii
FOREWORD v
EXECUTIVE SUMMARY xi
ACKNOWLEDGMENTS xv
ACRONYMS xvii
1 INTRODUCTION 1
2 DESCRIPTION OF JNES TEST PROGRAM 5
2.1 Introduction 5
2.2 Simple Component Tests 7
2.3 Combined-Component Tests 8
3 EMC^2 CREATED MODELS 11
3.1 Introduction 11
3.2 Component/Pipe System Models 11
3.3 Cracked-Pipe-Element Modeling 13
3.3.1 Models and Analyses 13
3.3.2 Additional Comments on Modeling Low-Cycle Fatigue Damage 31
3.3.3 Validation of Fracture Analysis in Component Systems 33
3.4 Analysis of JNES Pipe System Test 38
3.4.1 Damping Considerations 42
3.5 Determining Margins on Acceleration Amplitudes for Pipe Break 57
3.6 Low-Cycle Fatigue Crack Growth Assessment 59
3.7 Summary of Results 68
4 CONCLUSIONS AND RECOMMENDATIONS 71
5 REFERENCES 75

List of Figures

Figure 1 Illustration of JNES component tests 3
Figure 2 Typical flaw put in JNES stainless steel weld 6
Figure 3 IGSCC cracks that were found in BWR piping (from JNES paper, Ref. 4) 6
Figure 4 Comparison of ASME and JSME Z-factors for stainless steel welds 7
Figure 5 Different circumferential flaws used in JNES tests (from Reference 4) 8
Figure 6 Illustration of section of actual pipe loop used in 1/3-scale testing 9
Figure 7 Photo showing actual 1/3-scale combined-component system on shaker table (Test FTP-4). 9
Figure 8 Finite element mesh of the FTP-4 piping system 11
Figure 9 Comparison of natural frequency and mode shapes by JNES and Emc^2 12
Figure 10 Moment versus rotation-due-to-the-crack curves from initial loading to full break of a pipe with a circumferential crack 13
Figure 11 Simulation of a crack in IPIRG program during the early 1990's 14
Figure 12 Simulation of a crack in current program using ABAQUS 14
Figure 13 Photographs of pipe specimen for Experiment 1.1.1.28, the crack location in the weld and the circumferential crack growth from one crack tip 16
Figure 14 Moment versus rotation-due-to-the-crack comparisons between ABAQUS and test for Experiment 1.1.1.28 16

Figure 15 Comparison of applied load and far-field displacements between ABAQUS and test data from Experiment 1.1.1.28 17
Figure 16 Post-test photograph of pipe specimen for Experiment 1.2.1.3 18
Figure 17 Illustration of crack growth for circumferential surface cracks 19
Figure 18 Moment-rotation input curve for Experiment 1.2.1.3 19
Figure 19 Moment versus rotation-due-to-the-crack comparison between ABAQUS and test results from Experiment 1.2.1.3 20
Figure 20 Applied load versus load-line displacement curve comparison between ABAQUS and test results from Experiment 1.2.1.3 20
Figure 21 Photograph of pipe specimen for Experiment 1.2-5 21
Figure 22 Schematic of test apparatus for Experiment 1.2-5 22
Figure 23 Upper envelope to cyclic experimental moment versus crack rotation-due-to-the-crack data from Experiment 1.2-5 23
Figure 24 Comparison of moment versus rotation-due-to-the-crack from the FEA and measurements for Experiment 1.2-5 23
Figure 25 Load versus load-line displacement history by FEA and measurement for Experiment 1.2-5 24
Figure 26 Comparison of moment versus rotation-due-to-the-crack curves from the FEA (with 70% reduction factor) and measurement for Experiment 1.2-5 24
Figure 27 Comparison of load versus load-line displacement curves from the FEA (using 70% reduction factor) and measurement for Experiment 1.2-5 25
Figure 28 Post-test photograph of pipe specimen in Experiment 1.1-3 26
Figure 29 Schematic of overall test setup showing dimensions and major transducer locations for Experiment 1.1-3 26
Figure 30 Post-test photograph of specimen 1.1-3 27
Figure 31 Plot of load-line displacement for actuators as a function of time for Experiment 1.1-3 27
Figure 32 Moment versus rotation-due-to-the-crack curve from Experiment 1.1-3 and upper envelope used for the FE input 29
Figure 33 Moment versus rotation-due-to-the-crack comparison between the FEA output (*kinematic-hardening* rule) and measurement for Experiment 1.1-3 29
Figure 34 Displacement at the ends of the pipe masses versus time comparison between the FEA (*kinematic-hardening* rule) output and measurements for Experiment 1.1-3 30
Figure 35 Moment versus rotation-due-to-the-crack curve comparison between FEA (*isotropic-hardening* rule) output and measurements from Experiment 1.1-3 30
Figure 36 Displacement at the ends of the pipe masses versus time comparison between the FEA (*isotropic-hardening* rule) output and measurements for Experiment 1.1-3 31
Figure 37 Schematic of area under load-displacement curve to calculate ΔJ during low-cycle fatigue with compressive loading 33
Figure 38 Dimension of reducer, the schematic view of crack and testing setup 35
Figure 39 Stress-strain curve (from JNES) and J-R curve for TP308 TIG weld at 20°C used for initial estimate of toughness of GTAW 35
Figure 40 Moment versus rotation-due-to-the-crack curves for circumferential surface and through-wall cracks in pipes under bending with internal pressure (Type A surface crack in 203-mm (8-inch) nominal diameter TP316 stainless steel pipe and girth weld) 36
Figure 41 Moment versus rotation-due-to-the-crack curves from circumferential surface to through-wall cracks. Case (b) represents the moment-rotation curve produced using an 85% reduction of the load obtained from past NRC programs. The "cracked-pipe element" for the JNES combined-component test analyses used the Case (b) curve. 36
Figure 42 Load versus load-point displacement history for JNES Test EM-3 and ABAQUS predictions 37

Figure 43 Load versus load-line displacement history from JNES Test ES-1 data and ABAQUS predictions for cyclic loading 37
Figure 44 Mesh and crack locations of the scaled PLR system (Test FTP-4) 39
Figure 45 Location and directions of simulated cracking of Type A for test FTP-4 40
Figure 46 Applied acceleration histories for PLR system in Test FTP-4 (Load blocks CO-30, CO-33, and CO-35) 40
Figure 47 Different intervals of applied acceleration histories for PLR system (Test FTP-4, load steps CO-30, CO-33, and CO-35) 41
Figure 48 Moment versus rotation-due-to-the-crack curves for Type A flaws in the main pipe and branch pipe flaw locations at room temperature 42
Figure 49 Moment versus rotation-due-to-the-crack curves for Type A flaws in the main pipe and branch pipe flaw locations at high temperature (288°C, 550°F) 42
Figure 50 Plasticity contour plot of FTP-4 test system with no damping 44
Figure 51 Displacement measurement locations DO1 and DO4 for FTP-4 test system 45
Figure 52 Comparison of displacement history between the measured and predicted values at Location DO1 46
Figure 53 Comparison of displacement history between the measured and predicted values at Location DO1at different times 47
Figure 54 Comparison of displacement history between the measured and predicted values at Location DO7 48
Figure 55 Calculated applied moment (MN-m) at elbow crack location at room temperature for loading block CO-35 50
Figure 56 Calculated applied moment (MN-m) at reducer crack location at room temperature for loading block CO-35 51
Figure 57 Calculated applied moment (KN-m) at branch connection crack at room temperature for loading block CO-35 52
Figure 58 Calculated moment (MN-m) at elbow crack location at high temperature (288°C) using loading block CO-35 53
Figure 59 Calculated moment (MN-m) at reducer crack location at high temperature (288°C) using loading block CO-35 54
Figure 60 Calculated moment (kN-m) at branch crack location at high temperature using loading block CO-35 55
Figure 61 Calculated moment versus rotation-due-to-the-crack history at reducer crack at high temperature during loading block CO-35 56
Figure 62 Broken FTP-4 combined-component system at room temperature 58
Figure 63 Broken FTP-4 combined-component system at high temperature 58
Figure 64 Predicted moment versus time history for reducer crack for spectrum CO-30 63
Figure 65 Binned Stress cycles calculated from the predicted moments for all spectra (CO-30 to CO-35). σ = 138 MPa corresponds to a moment of 0.1 MN-m, σ = 155 MPa corresponds to a moment of 0.112 MN-m, σ = 173 MPa corresponds to a moment of 0.125 MN-m, and σ = 189 MPa corresponds to a moment of 0.1375 MN-m. Each 'line' represents a cycle applied. 66
Figure 66 Low-cycle fatigue crack growth predictions 67

List of Tables

Table 1 Summary of margins for different cases 70

EXECUTIVE SUMMARY

This report describes modeling efforts conducted by Engineering Mechanics Corporation of Columbus (Emc^2) under subcontract to Brookhaven National Laboratory (BNL) for the U.S. Nuclear Regulatory Commission to analyze and better understand a series of degraded pipe tests under seismic loading that were conducted in Japan. These efforts were a part of collaborative efforts between the United States Nuclear Regulatory Commission (NRC) and the Japan Nuclear Energy Safety Organization (JNES), who conducted a multi-year test program for the Ministry of Economy, Trade and Industry (METI) of Japan to investigate the behavior of typical Nuclear Power Plant (NPP) piping systems under large seismic loads. JNES provided the test results for the evaluations given in this report. Emc^2 worked with BNL on the degraded piping system analyses. This report describes Emc^2's post-test analyses of the large-scale piping system tests and presents insights gained from this program. The analyses in this effort are of value to understanding margins that degraded piping has under seismic loading for: (a) application to the Transition Break Size rule for CFR 50.46a applications, (b) Leak-Before-Break (LBB) analyses in NRC's SRP 3.6.3, and (c) pipe flaw tolerance by ASME Section XI code evaluations. These aspects are briefly discussed below.

The JNES tests[(a)] analyzed were of both the simple degraded component tests, e.g., a nozzle with a short section of straight pipe and a circumferential surface crack in the joining girth weld; as well as combined component tests involving a 1/3-scale section of the main recirculation system of a BWR. The component tests were conducted under monotonic loading as well as cyclic loading. The combined component tests had circumferential cracks at a reducer girth weld and elbow girth weld of the main 8-inch diameter pipe, and at a tee girth weld in the 4-inch diameter branch pipe. (A reducer was used rather than a nozzle for experimental simplicity.) In one test, a leak developed, and the flawed locations were at TP316 stainless steel girth welds with the flaw planned to be 75% of the thickness and 60-degrees of the circumference; the actual dimensions of the flaws varied somewhat in the test. The cracks were simulated using an electric discharge machined flaw [0.7 mm (0.028 inch) width] in the gas tungsten arc girth welds. The tests were conducted at room temperature with BWR pressures. The combined-component tests were conducted with pressure and simulated seismic loading in one direction.

Emc^2's analyses involved using a special "cracked-pipe element" (CPE) concept at all node locations where the cracks were located. The CPE represented the global moment-rotation response due to the respective circumferential cracks at each location. This approach was developed to simplify the dynamic finite element analysis, i.e., the FE models were reduced to 20 to 25 elements with up to 3 cracks where a full 3D analysis might take 15,000 elements per crack location and still not allow for crack growth during the FE analyses. The failure modes automatically captured by this analysis method are ductile tearing during the final failure event, and very low cyclic fatigue damage. High-cycle fatigue and low-cycle fatigue with small-scale plasticity are not automatically captured by this type of analysis, i.e., the cyclic stresses need to be input to another fatigue-crack-growth program. The nonlinear global response behavior for the "cracked-pipe element" was externally calculated by elastic-plastic fracture mechanics (EPFM) analyses that had been validated in numerous large projects for the USNRC[(b)]. This "cracked-pipe element" methodology was developed in the International Piping Integrity Research Group (IPIRG) programs[(c,d)] that the NRC and Japan were members of in the early 1990's. The "cracked-pipe element"

(a) K. Suzuki and H. Kawauchi, "Test Programs for Degraded Core Shroud and PLR System Piping (Seismic Test Results and Discussion on JSME Rules Application," 2008 ASME PVP conferences, July 27-31, Chicago, IL.

(b) Wilkowski, G. M., Olson, R. J., and Scott, P. M., "State-of-the-Art Report on Piping Fracture Mechanics," NUREG/CR-6540, BMI-2196, February 1998.

(c) Wilkowski, G., and others, "International Piping Integrity Research Group (IPIRG) Program, Final Report," NUREG/CR-6233 Vol. 4, June 1997.

originally used a relatively simple combination of springs, gap, and truss elements to construct the "cracked-pipe" global response behavior using the ANSYS computer code. In the current project, a single connector element in the ABAQUS computer code was used to represent the "cracked-pipe element." Prior to analyzing the JNES tests, a series of validation efforts based on other cracked-pipe tests (from various past NRC or IPIRG funded programs) was conducted. The complexity of the validation efforts increased from: (a) a simple circumferential through-wall crack in a pipe under quasi-static monotonic four-point bending to predict far-field displacements during large crack growth past maximum load, (b) a circumferential surface crack in a pipe under quasi-static bending to predict the transition from a surface crack to a through-wall crack during monotonic four-point bending, (c) fully reverse cyclic loading for a circumferential through-wall-cracked pipe in four-point bending to examine the best options for capturing hysteresis energy and low-cycle fatigue damage, and (d) an inertially loaded pipe test with a circumferential through-wall crack to examine dynamic loading aspects with cyclic hysteresis loops. These analyses showed that reasonable predictions could be made using the ABAQUS connector element to model the complete transition of a circumferential surface crack to a through-wall crack under cyclic dynamic loading when the loads were close to the failure loads, i.e., when significant plasticity occurs. Of course, a few secondary aspects need to be fixed in the connector element for it to perform perfectly since that element was not developed to perform analyses such as in this application.

The JNES component test with the reducer and straight-pipe section and a circumferential surface crack at the girth weld was used to fine-tune the calibration of the connector element model. The connector element model requires input of the circumferential surface and through-wall crack moment versus rotation-due-to-the-crack responses from the J-estimation schemes. The J-estimation schemes require input of the pipe size, flaw size and orientation, material strength, and toughness. The toughness of the weld metal in the JNES tests was not available, so that an initial estimate was first used and then it was fine-tuned using the simple component tests.

The FTP combined-component test was analyzed in detail. The combined-component test had three crack locations and multiple applied simulated-seismic block loadings. Each seismic block loading had a total time of 65 seconds that included about 30 seconds of strong motion. As previously noted, the tests included pressure (water added to the mass of the system), dead-weight loads, and inertial loading from the shaker table. The simulated-seismic loading was in only one direction. Since the tests were at room temperature, there were no thermal expansion stresses. Additionally, all fixed points of the pipe loop were on the same shaker table, so there were no seismic anchor motion stresses from relative motions of the anchor points.

There were many loading blocks applied to each of the four different combined-component tests (FTP-1, FTP-2, FTP-3, and FTP-4); however, leakage only occurred in one test (FTP-4), so the analysis was concentrated on that case. For FTP-4, the final six loading blocks were numerically simulated, and each loading block had similar peak amplitudes applied to the test system. Comparisons were also made between the ABAQUS FE analyses results to the measured displacements and strains in the experiment. Reasonably good agreement was obtained when allowing plasticity in the cracked locations and allowing elbow elements to become plastic (actually, all uncracked elements (pipe and elbows) are permitted to become plastic, but only one elbow element became plastic), and then applying 2.0-percent Rayleigh damping to the rest of the system that behaved elastically (with alpha = 1.148 and beta = 1.157E-4). In the experiment where leakage occurred (FTP-4 final load block), it was determined that the loading at the crack location was just above the elastic range of the "cracked-pipe elements." Hence, the leakage was

(d) Hopper, A. T., Wilkowski, G. M., Scott, P. M., Olson, R. O., Rudland, D., Kilinski, T., Mohan, R., Ghadiali, N., and Paul, D., "The Second International Piping Integrity Research Group (IPIRG-2) Program - Final Report," NUREG/CR-6452, February 1997.

caused by low-cycle fatigue with small-scale yielding, rather than by ductile tearing or low-cycle fatigue with large plasticity that would occur if the loading were near the ultimate load capacity of the cracked-pipe component. This is consistent with the fact that it took 6 loading blocks to cause the leakage, whereas in the IPIRG program the pipe-system experiments were conducted to failure in one simulated seismic loading block.

The analysis predictions using the CPE approach did not predict leakage or any crack growth. This indicates that cyclic ductile tearing with large-scale plasticity was not the crack growth mode here since the applied accelerations were not high enough. Hence, the leakage was caused by low-cycle fatigue with very small-scale yielding, rather than by ductile tearing or low-cycle fatigue with larger plasticity that would occur if the loading were near the ultimate load capacity of the cracked pipe. The procedure used to make predictions of low-cycle fatigue crack growth were based on the Dowling ΔJ procedure, which is an extension of linear-elastic fatigue crack growth methodology extended into the nonlinear plasticity regime. The predicted moments from the CPE approach used a cycle-by-cycle crack growth procedure. The U.S. Air Force fatigue crack growth code, AFGROW (Version 4, 10/2008), was used to make these predictions. AFGROW is a completely validated code that is used by many organizations to make fatigue crack growth predictions using complicated loading spectra. The predictions using this approach compare quite well with the experimental measurements where leakage occurred during the sixth load block.

The fatigue crack growth predictions are presented in the form of crack size versus load cycles. For values of closure load expected in the JNES tests, leakage was predicted very near the sixth and final loading block, as seen experimentally. The crack growth for the cycles is examined by comparing growth per cycle throughout the loading spectra.

As part of the analyses for the FTP-4 experimental case, the amplitude of the seismic loading was increased until failure of the surface crack occurred by cyclic tearing in the ABAQUS model. The margins on the applied accelerations in the FTP-4 test were about a factor of 5. The damping ratio was kept the same and the elbow was allowed to become plastic as well as all the crack locations. At this high loading level, the actual viscous damping ratio might be slightly higher so that the estimated margin is a little conservative.

The material property parameters were then changed for the cracked-pipe sections as well as the rest of the model to estimate the margins if the JNES test was conducted at BWR operating temperature of 288°C (550°F). The margin at 288°C (550°F) was estimated to be a factor of 3 on the applied acceleration amplitude in the FTP-4 test. Again, this is a conservative margin since the damping of the entire system was kept at 2% although the crack location and elbows were allowed to plastically deform in the FE analysis. Interestingly, the room temperature FE results showed that after the crack at the nozzle failed, then the crack at the tee girth weld also failed in the same seismic loading block. The crack at the tee was the lowest loaded crack when all cracked sections were originally intact.

Finally, an estimate was made as to what the margins were on the moments and accelerations relative to those needed for failure if elastic-plastic fracture mechanics was considered for the full-scale pipe system. To do this, first the appropriate Z-factor relationship was determined, using the JNES monotonic component test EM-3. Using the failure stress from that pipe test, the calculated Z-factor was 1.38, which is close to the JSME Z-factor value of 1.31 for GTAW/SMAW welds in that pipe size. To predict the margin that might exist for a full-scale pipe system, the JSME Z-factor equation was then used rather than the ASME Z-factors. This resulted in an estimate that the full-scale pipe system at operating temperature might have a margin of 1.06 on the failure load with the same non-dimensional loads and applied acceleration-time history. Although the dynamic “cracked-pipe element” analysis was not run for the full-scale pipe system, the margins on acceleration were scaled to the FTP moment and acceleration margins, and estimated to be between 1.92 and 2.39. Again, these estimated margins were slightly

conservative since the viscous damping was kept at 2% for these analyses (plasticity development in the elbows and the cracks account for the majority of increased damping effect). This suggests that larger cracks can be tolerated in this system. It is difficult to predict how a large-diameter cracked pipe system would respond to this motion without conducting the actual analysis.

In conclusion, these analyses showed that the JNES FTP-4 pipe test should have failure due to low-cycle fatigue with small-scale yielding, and there were large margins on acceleration needed to cause failure in a single loading block (i.e., failure during one seismic event) even for extrapolated results to full-scale behavior and typical U.S. design PGA values. These margins are lower bounding since they did not account for slightly increased viscous damping in the rest of the uncracked pipe system, and are qualitatively instructive in understanding the safety factors that might actually exist under seismic loading. In the Transition Break Size work[(f)], it was known that such margins might exist between elastically calculated seismic stresses for fracture analysis involving beyond-design-basis earthquakes using nonlinear-fracture behavior. A correction factor of 1 to 2.8 was applied to the elastically scaled seismic stresses for events with probabilities of occurrence of 10E-6 from actual plant seismic-hazard curves. (The correction factor of 1 corresponds to the stresses being purely elastic for flawed pipe failure and the factor of 2.8 corresponds to stresses that would cause failure of unflawed pipe.) The correction factor of 1 to 2.8 changes as the flaw size changes. This result is consistent with results from the BINP program[(e)]. It is comforting that the margins seen in the analyses of these JNES tests of the tolerable accelerations relative to the SSE design PGA values for U.S. plants are much larger than the nonlinear-stress correction factors (1 to 2.8) used in the Transition Break Size work. However, analyses as conducted in this report would have to be conducted for the crack sizes and typical pipe system used in the Transition Break Size[(f)] seismic analysis to better quantify the margins that might exist. Similar margins would also affect LBB analyses, ASME code criteria, and on-going probabilistic pipe fracture analyses such as the NRC's xLPR efforts that are just starting up[(g)].

Finally, it should be noted that it is also possible to expand the current "Cracked-Pipe-Element" analysis capability to account for low-cycle fatigue with small-scale-plasticity or high-cycle fatigue crack growth. This can be done by including the design of the CPE with the Dowling low-cycle fatigue analysis into a UMAT in ABAQUS that had to be conducted manually in this project.

(e) Scott, P. M. et al., "The Battelle Integrity of Nuclear Piping (BINP) Program Final Report," NUREG/CR-6837, Vol. 2, June 2005.

(f) Chokshi, N.C., Shaukat, S.K., Hiser, A.L., DeGrassi, G., Wilkowski, G., Olson, R., and Johnson, J.J., "Seismic Considerations for the Transition Break Size," NUREG-1903, February 2008.

(g) The xLPR is an effort being coordinated by the U.S. NRC-RES and EPRI to develop a new probabilistic pipe fracture code. Dr. A. Csontos is the NRC-RES project manager. No reports are available at this time

ACKNOWLEDGMENTS

The research program described in this report was conducted by Engineering Mechanics Corporation of Columbus in support of Brookhaven National Laboratory (BNL) efforts, which have been sponsored by the Office of Nuclear Regulatory Research of the U.S. Nuclear Regulatory Commission. The BNL staff provided valuable review comments and direction during the course of the program. The authors would like to express their gratitude to Dr. Syed Ali, NRC Project Manager, for the technical and administrative support he provided in performing this study.

This research program was performed as part of the Implementing Agreement between the U.S. Nuclear Regulatory Commission and the Japan Nuclear Energy Safety Organization (JNES) in the Area of Seismic Engineering Research. This agreement is an item of the Implementing Arrangement between the United States Nuclear Regulatory Commission and the Nuclear and Industrial Safety Agency (NISA) of Japan for Cooperation in the Field of Nuclear Regulatory Matters and Nuclear Safety Research and Development.

All of the test results and information about the test models for the JNES degraded piping tests included in this report were provided by JNES and are greatly appreciated. The authors especially thank Dr. Katsumi Ebisawa, Dr. Kenichi Suzuki, Mr. Yuichi Uchiyama, and Mr. Hiroshi Abe of JNES and Dr. Akihito Otani of IHI Corporation for their support throughout this collaborative study and the time they took for supplying detailed review comments that were quite valuable in the revisions made for this final report.

During the initiation of the contract between BNL and Emc^2, Mr. Giuliano DeGrassi of BNL passed away. He developed the scope of work for the Emc^2 contract and served as the original technical point of contact. We will miss his cheerful attitude and his technical expertise in the seismic analyses of piping systems.

ACRONYMS

3D – Three dimensional
ASME – American Society of Mechanical Engineers
BNL – Brookhaven National Laboratory
BWR – Boiling water reactor
CD – Compact disc
CPE – Cracked pipe element
CPU – Central processing unit
CT – Compact tension
DM – Design Method
EDM – Electronic discharge machining
Emc^2 – Engineering Mechanics Corporation of Columbus
EPFM – Elastic plastic fracture mechanics
FE – Finite element
FEA – Finite element analysis
GTAW – Gas tungsten arc weld
HAZ – Heat affected zone
IGSCC – Intergranular stress corrosion crack
In – Inconel alloy
IPIRG – International Piping Integrity Research Group
JAERI – Japan Atomic Energy Research Institute
JNES – Japan Nuclear Energy Safety Organization
JSME – Japanese Society of Mechanical Engineers
LBB – Leak-Before-Break
LEFP – Lineal elastic fracture mechanics
LOCA – Loss of Coolant Accident
LVDT – linear variable differential transducer
METI – Ministry of Economy, Trade and Industry
NIED – National Research Institute for Earth Science and Disaster Prevention
NISA – Nuclear and Industrial Safety Agency
NPP – Nuclear Power Plant
NRC – Nuclear Regulatory Commission
NUPEC – Nuclear Power Engineering Corporation
OBE – Operating Basis Earthquake
PLR – Primary Loop Recirculation
PWR – Pressurized Water Reactor
SAW – Submerged arc weld
SMAW – Shielded-metal-arc weld
SRP – Standard review plan
SSE – Safe-Shutdown Earthquake
TBS – Transition Break Size
TWC – Through-wall crack
US – Ultimate strength

1 INTRODUCTION

During 2004 to 2006, the Japan Nuclear Energy Safety Organization (JNES) conducted a Degraded Piping and Components Test Program to investigate the behavior of typical Nuclear Power Plant (NPP) piping systems under large seismic loads. The objectives of this multi-year program were to: (1) obtain a better understanding of the vibration characteristics and seismic strength of degraded structures and components having cracks due to aging, (2) ensure a margin of seismic design safety by considering age-related cracking, and (3) verify the JSME Rules on Fitness-for-Service for NPPs in Japan. This program included shaker-table testing of four 1/3-scale models of a primary loop recirculation piping system typical in BWRs in Japan, in addition to various component tests and 1/2.5 scale core shroud model tests. The shaker table tests of the 1/3-scale piping system models are also referred to as combined-component tests in this report, to be compatible with various JNES documents[1,4]. This report presents an analytical assessment of some selected piping system/component tests.

As part of the joint efforts between the United States and Japan on seismic issues, the U.S. Nuclear Regulatory Commission (NRC) and Brookhaven National Laboratory (BNL) collaborated with JNES by assessing the test data of this program and exchanging research information. In accordance with the collaboration agreement, JNES provided their test results to NRC and BNL in the form of presentations and also provided electronic data for some selected component and combined-component tests to be utilized by BNL. To best assess the dynamic characteristics of the cracked component under simulated seismic excitations, the NRC agreed to have BNL subcontract the analytical part of this program to Engineering Mechanics Corporation of Columbus (Emc^2), for their well-known knowledge and skill in fracture mechanics.

In this report, results of analyses of the JNES component and combined-component tests are presented. Emc^2 conducted these analyses under subcontract to BNL. The staff at Emc^2 have been involved with degraded piping analyses under quasi-static and dynamic loading for decades[2]. The objectives of the efforts in this report are to provide insights to assessment procedures used for degraded piping relative to: (a) application to the Transition Break Size rule for CFR 50.46a applications, (b) leak-before-break analyses in NRC's SRP 3.6.3, and (c) pipe flaw tolerance by ASME Section XI code evaluations. These aspects are briefly discussed below.

In the Seismic LOCA analyses work that was conducted in support of the proposed CFR 50.46a rule change[3], a relatively simple degraded piping analysis was conducted for non-design basis seismic events. The NRC will develop a Regulatory Guide over the next few years for the proposed CFR 50.46a changes. For seismic loading, there needs to be a screening criterion to determine when a plant should conduct additional analyses, as well as how those analyses should be conducted for seismic considerations. The JNES pipe system tests[4] offer a unique opportunity to check the margins in the simplified analyses conducted in Reference (3). This is because of two reasons: (1) The JNES tests involve a more complicated pipe system with degraded pipe under simulated seismic loading than has been evaluated in the past International Piping Integrity Research Group (IPIRG) pipe loop tests,[5,6] and (2) The JNES pipe loop is more prototypical by being a 1/3-scale simulation of an actual BWR primary pipe loop. The results from the JNES work will be helpful in evaluating the margins associated with the simple static analyses used in the "Seismic LOCA" report.

Another application of the lessons learned from this project is for Leak-Before-Break (LBB) applications as per NRC's Standard Review Plan 3.6.3. Seismic loading of piping with hypothetical flaws is typically part of the SRP 3.6.3 fracture evaluations. A technical basis for a new Regulatory Guide for LBB[7] recommended three optional approaches, where the most detailed option allowed for detailed seismic analyses as being done in this project.

Finally, the lessons learned from this project can be useful for an assessment of pipe flaw evaluation criteria such as in the ASME and JSME codes. The ASME Section XI pipe flaw evaluation criteria are flexible enough to handle all levels of seismic loading that could occur, not just restricted to maximum design levels for operating basis earthquake (OBE), safe-shutdown earthquake (SSE), or the S1 and S2 loading in the Japanese seismic design approaches. The results from analyses of the JNES pipe-system experiments would show the magnitude of inherent margins in the ASME (or JSME) code procedures.

Such margin assessments would also be helpful if a non-design basis earthquake occurred, such as happened at the Kashiwazaki nuclear plant site in Japan, and provide a basis for return-to-service capabilities of the piping system with some level of degradation and loads beyond the SSE or S2 design-basis seismic levels.

The JNES pipe system tests[4] offer a unique opportunity to check the margins in the simplified analyses for the various above applications. The JNES tests involve a more complicated pipe system with degraded pipe under simulated seismic loading than has been evaluated in the past International Piping Integrity Research Group (IPIRG) pipe loop tests[5,6]. The IPIRG pipe system tests involved a relatively simple expansion loop of about 100 feet total length, but was complicated in other ways. It was run at 288°C (550°F) with water in 16-inch diameter pipe and cracks in high and low toughness materials, and had seismic anchor motion and thermal expansion stresses as well as pressure, dead-weight, and inertial stresses. The JNES pipe loop is a 1/3-scale simulation of an actual BWR primary pipe loop (largest pipe was 8-inch diameter).

JNES funded work in Japan that involved conducting tests on a 1/3-scale BWR pipe loop at the National Research Institute for Earth Science and Disaster Prevention (NIED) facility, see Figure 1(a). Several circumferential flaws were put in the piping system (called a combined-component test) that was mounted on the 14.5 by 15-meter shaking table. The pipe system was shaken in one horizontal direction, and different geometries of circumferential flaws were put in the pipe system. The simulated seismic loading was generally more than 1.5 times of the Japanese S2 level (the original plan was $1.5 \times S2 \approx 1.5$ g, while the actual measurement at the shaking table top was about 2 g), and leakage occurred in the last of the 6 large seismic loading series for the FTP-4 test. There were also quasi-static component tests loaded to failure by monotonic loading, constant amplitude loading, or simulated seismic loading, see Figure 1(b).

The analyses used in this project were conducted to determine whether the “straight pipe” flaw evaluation procedures for circumferential cracks are applicable to the component tests with cracks in girth welds next to elbows and at nozzles, and then determine the margins for cracks in piping at such locations under simulated seismic loading. The prior NRC-funded work[5,6,8,9] involved development of J-estimation schemes to make these predictions of moment versus rotation due to the crack in a pipe girth weld, so that a “cracked-pipe” element could be created to simulate circumferential crack behavior at any node point in simple pipe beam-element analysis used for plant piping seismic evaluations. Most of the past work was with circumferential cracks in welds joining straight pipes. The JNES work involves a more prototypical pipe system, and the cracks are at more prototypical locations than the IPIRG program tests, i.e., in girth welds by nozzles and at elbow girth welds to straight pipe.

A summary of conclusions including regulatory insights and lessons learned from the program, and recommendations for further research are presented in Section 5.0.

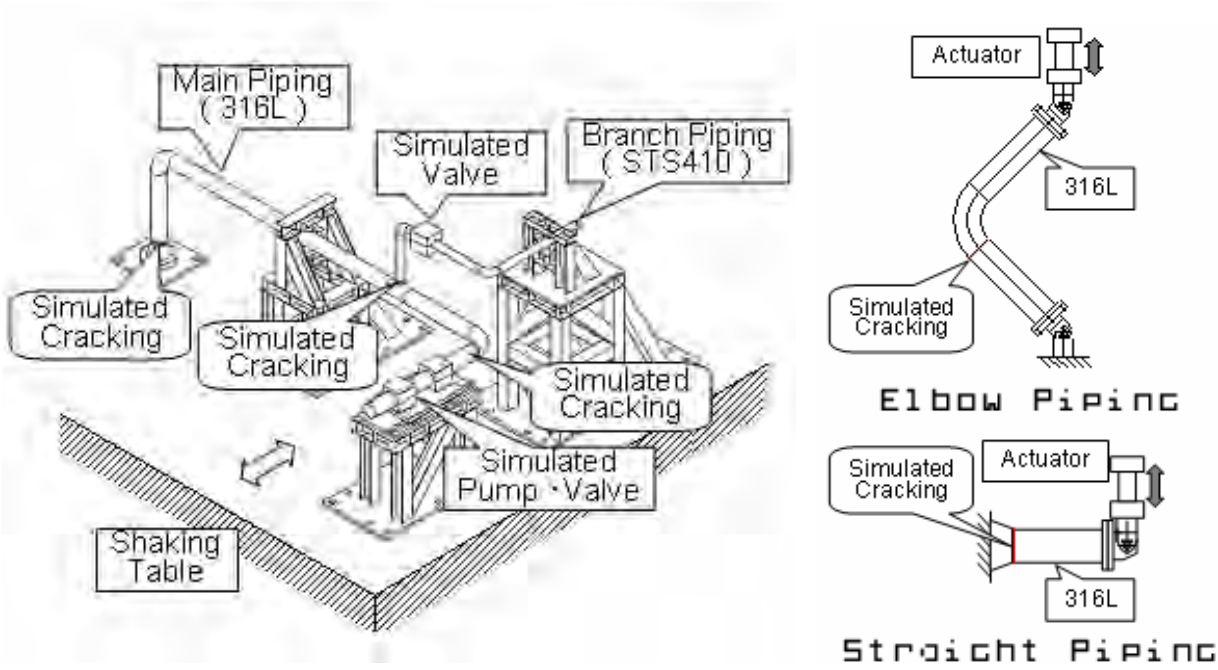

(a) Pipe system (combined component) tests (b) Component tests

Figure 1 Illustration of JNES component tests

2 DESCRIPTION OF JNES TEST PROGRAM

2.1 Introduction

The goals of the JNES test program were to obtain a better understanding of the vibration characteristics and seismic strength of cracked piping components and combined-component piping systems, assess seismic margins of these degraded components and combined-components, and verify the JSME Rules on Fitness-for-Service for NPPs in Japan. In order to gain a better understanding of the piping system behavior subjected to simulated cracks, JNES conducted a series of cracked-piping component static and dynamic tests, as well as combined-component tests with cracks using a shaking table. Selected results of these tests were provided by JNES for use in this study. The combined-component tests used a 1/3-scale model of a section of a BWR recirculation line. Accordingly, the pipe in the scaled tests was 8-inch diameter for the main loop and 4-inch diameter for the branch section. The flaws were circumferential surface flaws made with an electric discharge machined (EDM) notch having a width of about 0.7 mm (0.028 inch), see Figure 2. The flaws started in the HAZ and finished in the weld metal, as was typical of cracks found in service, see Figure 3. The girth welds in the tests were GTAW, whereas in service SAW or SMAW welds would be used in U.S. BWR plants and older Japanese BWR plants. According to JSME rules, GTAW welds have the same toughness as SMAW welds; however, in the ASME rules the SAW/SMAW welds (welds made using a flux shielding) have a lower toughness than TIG or GTAW welds (welds made with inert gas shielding). The toughness correction on the limit-load solution for circumferential cracks in pipes is called a Z-factor, i.e., defined as the ratio of the failure stress at limit load divided by the failure stress under ductile tearing conditions. The limit-load predicted failure stress is divided by Z to predict the failure stress for flawed pipe which does not achieve complete cross section plasticity at failure (for instance, for lower toughness material and large diameter pipe) where limit load plasticity does not occur for fracture. The Z-factors are a function of the pipe diameter and are shown in Figure 4 for stainless steel welds by the ASME and JSME codes. The higher the Z-factor is, the lower the toughness of the material. The differences between the two codes should be examined further. For instance, there are SAW and SMAW pipe test data and statistical J-R curve data from test specimens from NRC-funded work that show essentially no difference between SAW and SMAW fracture behavior[8,10]. However, in the U.S. it has been assumed that TIG/GTAW (any inert gas weld) are high enough in toughness that the Z-factor should be 1.0 (i.e., limit-load controlled). That assumption was backed up by only 4-inch diameter pipe tests[11]. Additionally, over time these welds could lose some toughness from thermal aging, so that older welds should perhaps have an additional aging term on the Z-factor.

One observation regarding the JNES tests is the width of the EDM notch. In the IPIRG program, the simulated seismic tests included a shim in the surface flaw notched region, so that reverse cyclic loads could only close the crack to an amount representative of having a tight crack at the start of the test. Without the shim present, compressive plasticity might be larger than with a tight crack. This reverse compressive plasticity could cause more damage to the crack tip region if it occurs. Of course, as the crack starts to grow from the machined notch, there would be crack closure on those new crack faces.

Another observation regarding the EDM notch is that the bluntness of the notch will raise the apparent toughness at crack initiation. During the NRC pipe fracture programs, fracture toughness tests were conducted with EDM notches that were fatigue pre-cracked leading to a tight crack. The result was that the EDM-notched specimens had initiation toughness values of 1.7 times higher than the fatigue pre-cracked specimen tests. Given that the surface flaws are in smaller-diameter pipe, the notches are in GTAW welds rather than SAW/SMAW in U.S. and older Japanese plants, and the notch acuity aspects, the 1/3-scale tests may fail at limit-load conditions. The actual full-scale BWR pipe loop would be expected to fail at roughly 60-percent of limit-load due to the lower toughness weld, sharp crack, and larger-diameter pipe. The 60-percent value comes from the ASME pipe flaw evaluation procedures where an elastic-plastic toughness correction (Z-factor) is required on the limit-load solutions for

SAW/SMAW welds but not GTAW welds. The differences in the GTAW Z-factors are examined later in this report.

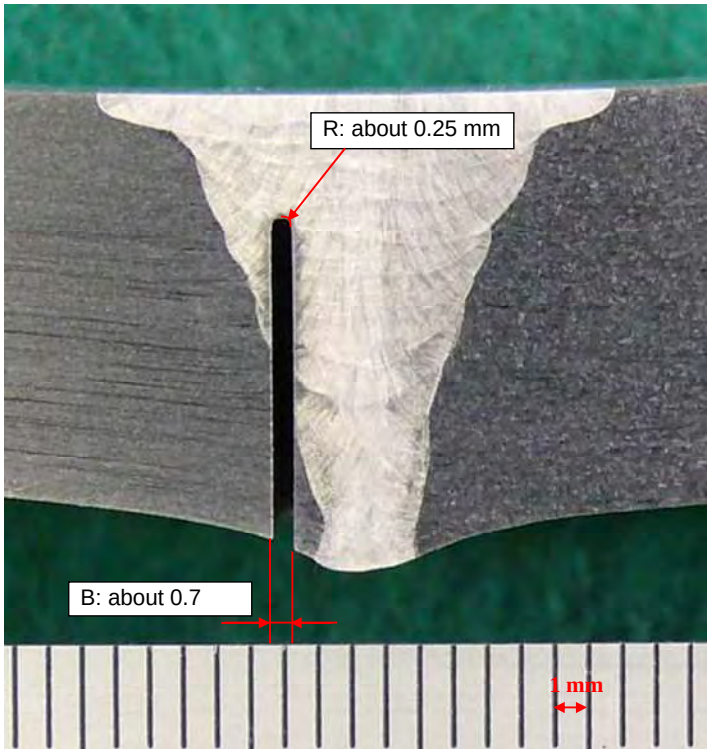

Figure 2 Typical flaw put in JNES stainless steel weld

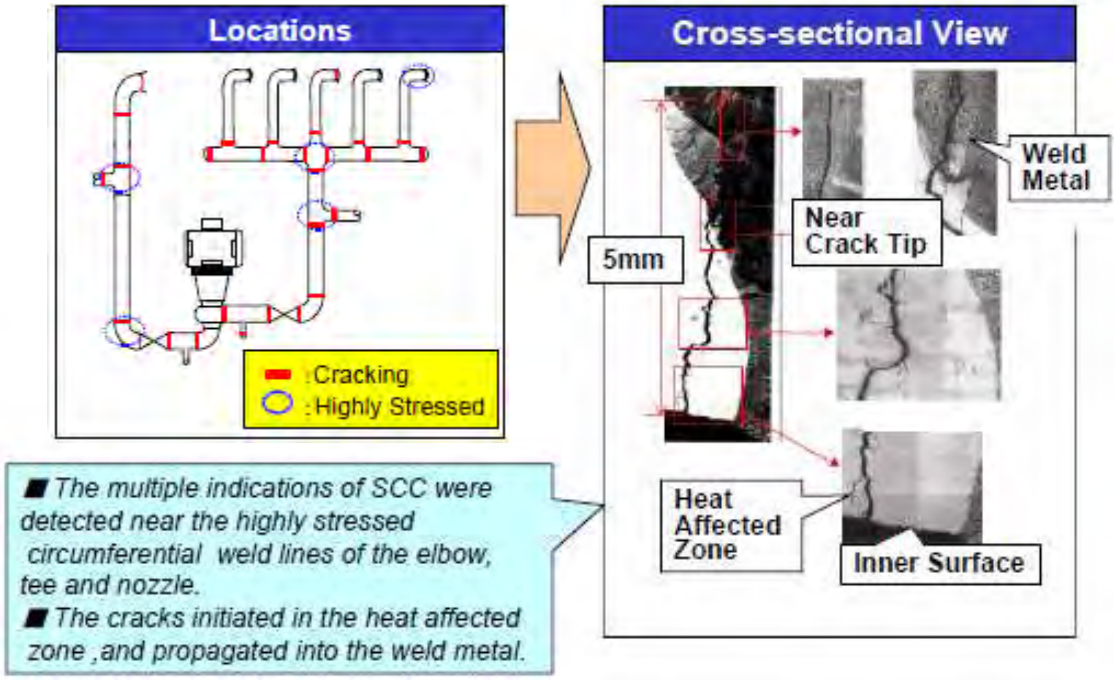

Figure 3 IGSCC cracks that were found in BWR piping (from JNES paper, Ref. 4)

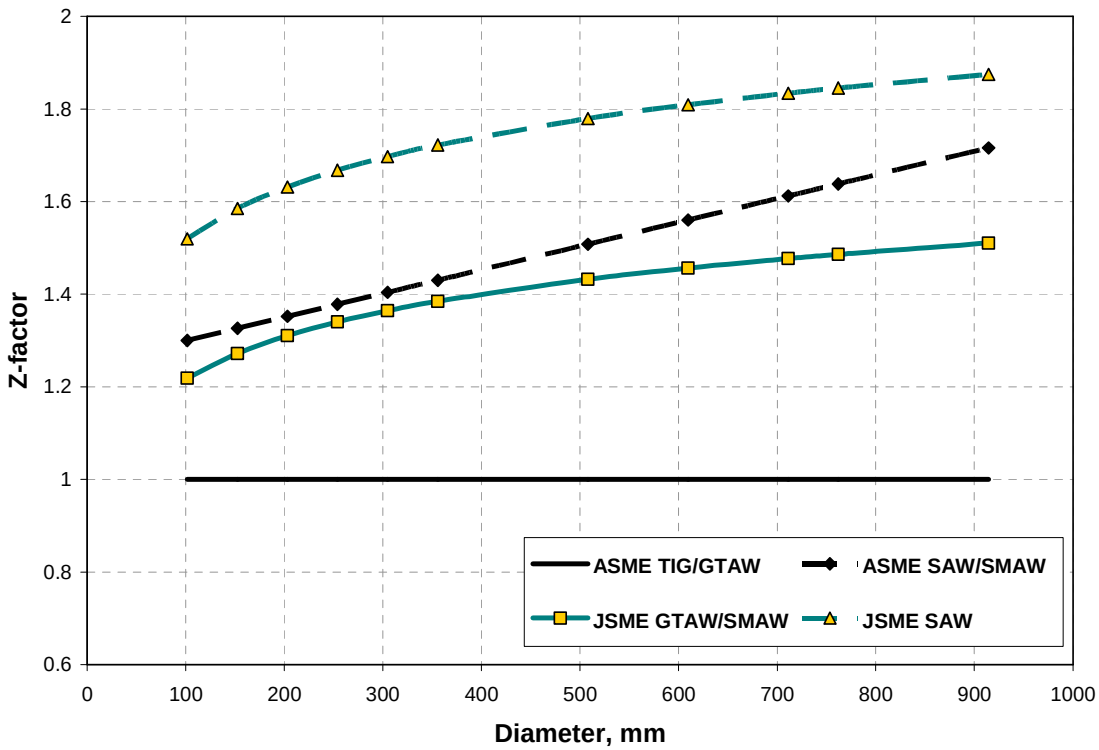

Figure 4 Comparison of ASME and JSME Z-factors for stainless steel welds

2.2 Simple Component Tests

The simple component tests were first conducted by JNES. These tests involved relatively simple sections of pipes with fittings (elbows and reducers to simulate a nozzle) with the similar cracks in the girth welds between the straight pipe and the fitting. More complete descriptions of these tests are provided in References (1) and (4).

The simple component tests were conducted with monotonic increasing displacement, constant frequency sinusoidal cyclic loading, and simulated seismic loading blocks. The loads and far-field displacements were measured. However, no local crack growth monitoring was done other than observing leakage. Examples of local crack growth monitoring would have been measurement of the crack-mouth-opening displacement (by clip gages or LVDTs), and crack growth (by d-c electric potential measurements across the crack)[12].

The shapes of the cracks were called either Type A or Type B. The Type A crack was 60-degrees of the circumference in total length and had a depth of 75-percent of the thickness. The Type B crack was 360-degrees around the circumference and had a depth of 50-percent of the pipe thickness (see Figure 5). The Type A crack was the maximum flaw size allowed in the JSME code at the time their program started, while the Type B crack was a change being evaluated as part of a code case to the JSME code. Both flaw sizes are allowed by the ASME Section XI criteria, as long as the applied loads are low enough with appropriate safety factors.

Of the different simple component tests that were conducted in the JNES program, the monotonic tests with a crack in a girth weld between straight pipe and a reducer were of prime interest for calibration of the nonlinear behavior of the “cracked-pipe” element being used. These tests were done with internal pressure and at room temperature.

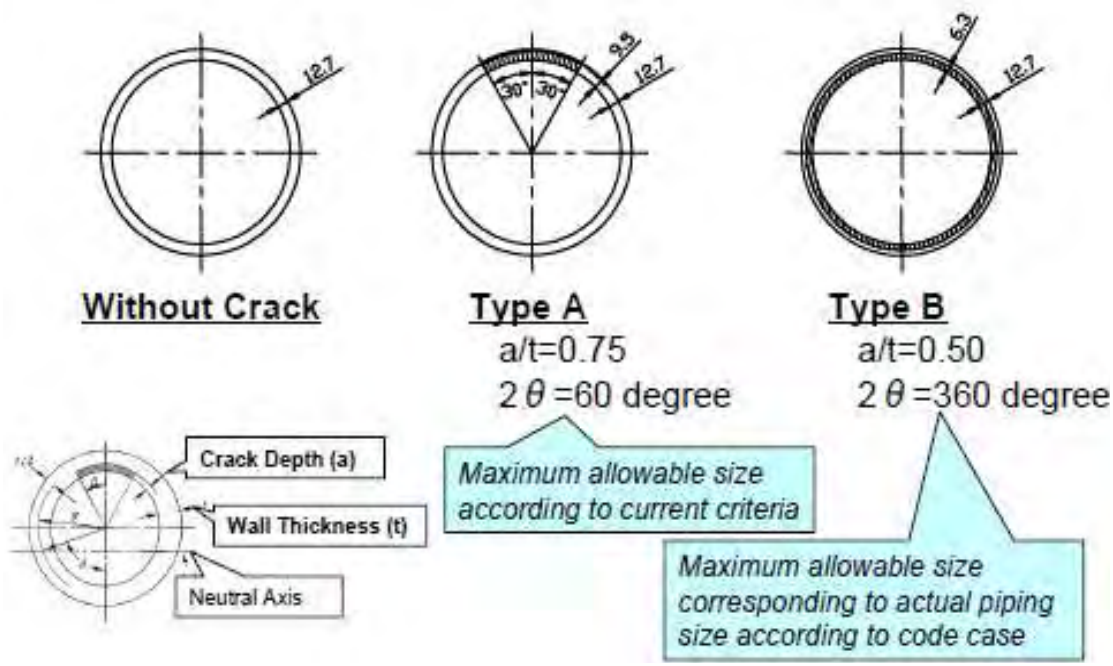

Figure 5 Different circumferential flaws used in JNES tests (from Reference 4)

2.3 Combined-Component Tests

The combined-component tests were a 1/3-scale model of a section of a BWR pipe main recirculation loop that was between the reactor pressure vessel and the recirculation pump, see Figure 6. There is a slight difference in the geometry of the test models between FTP-1 to FTP-3 and Test FTP-4. The main pipe in the 1/3-scale model was 8-inch nominal diameter, and the branch pipe was 4-inch nominal diameter. Figure 7 shows a photograph of the 1/3-scale combined-component test system on the shaker table. Most of the pipe was TP316 stainless steel, but some of the branch pipe was ST410 carbon steel (similar to A333 Grade 6 pipe in the U.S.). The 1/3-scale size was selected to be compatible with the existing shaker table size. The first natural frequency of the 1/3 scale model was about 5 Hz, while the first natural frequency of the actual full-scale pipe was 4.1 to 9.8 Hz. Additional information on these tests is provided in References (1) and (4).

Strain gage measurements were made in several circumferential planes along the pipe length. Displacement measurements were also made at several locations. These data are used later in this report to validate the FE analyses. As in the simple component tests, no local measurements were made of the crack opening displacement for crack growth during the tests. Such measurements are difficult to make with internal surface flaws, but can be done.

The stiffness values of the different frames (green beams in Figure 7) supporting the ends of the combined-component system were provided by JNES along with the dimensions of the pipe segment.

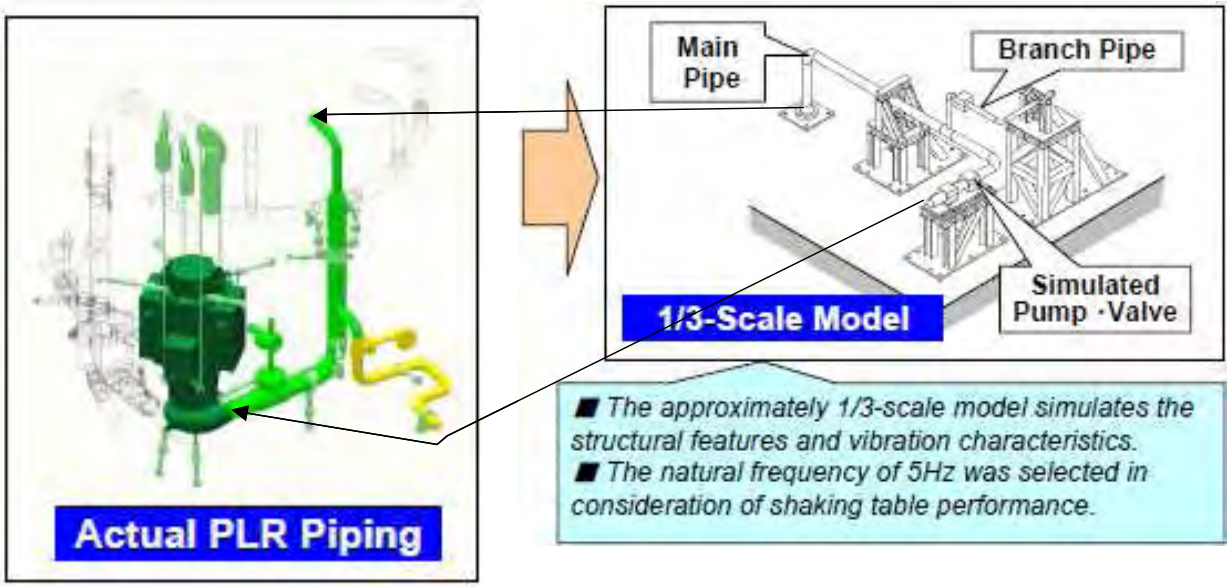

Figure 6 Illustration of section of actual pipe loop used in 1/3-scale testing

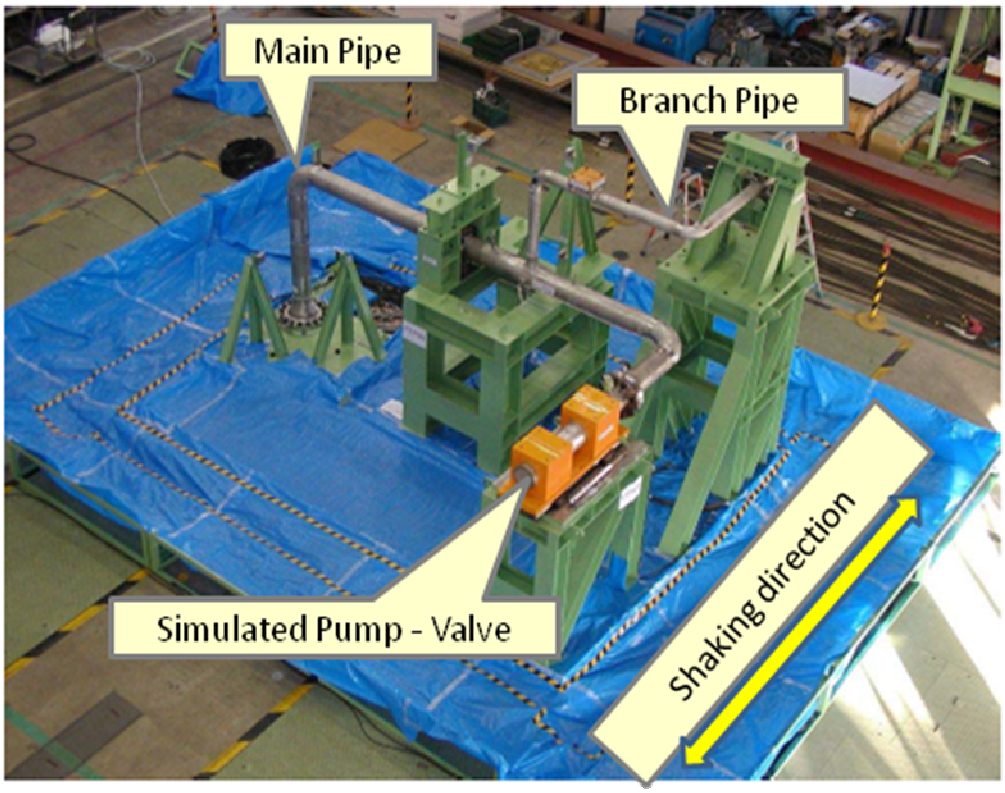

Figure 7 Photo showing actual 1/3-scale combined-component system on shaker table (Test FTP-4)

3 EMC^2 CREATED MODELS

3.1 Introduction

One of the objectives of the Emc^2/BNL collaboration effort was to obtain modeling information from JNES that could not be developed from technical papers and presentations to date. Some of this information was critical to the dynamic analyses of the pipe systems, such as stiffness of beam structures supporting the ends of the piping, dynamic time-history input, material property data, etc.

3.2 Component/Pipe System Models

JNES provided on CD detailed information about the pipe system models, including dimensions and finite element models of the piping system in SAP and NASTRAN formats. From this information, an uncracked-pipe finite element model was developed in the ABAQUS finite element code (Release 6.8) framework since ABAQUS is the finite element code used for most problems at Emc^2. Figure 8 is the mesh of the piping system and the nodes are marked as red circles. This model was debugged and results that compare well with the JNES uncracked-pipe system were obtained. Figure 9 presents the first three natural frequencies and their mode shapes. Figure 9(a) is the comparison of first natural frequency and its distortion mode shape between JNES and Emc^2. The natural frequency from the JNES analysis (SAP) is 5.0 Hz versus 5.028 Hz determined by the Emc^2 analysis (ABAQUS), which compares well. The second and third natural frequencies and corresponding mode shapes are also extremely close and are given in Figure 9(b) and Figure 9(c). This validation shows that the model information from JNES (originally written in SAP and converted to NASTRAN) was correctly input into ABAQUS.

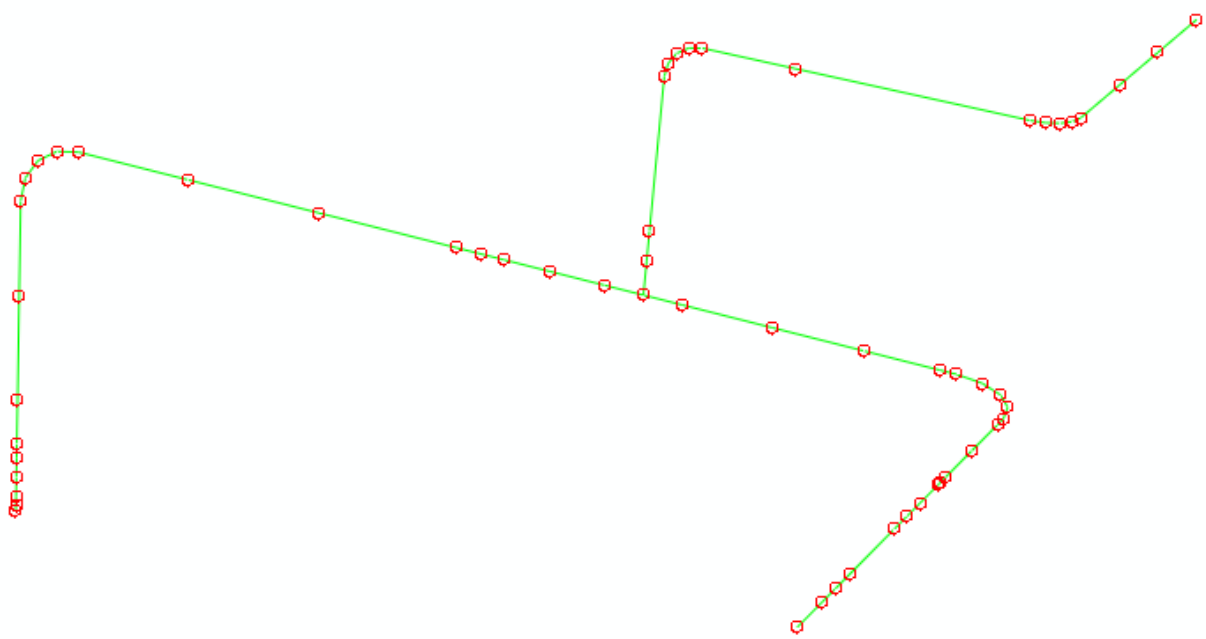

Figure 8 Finite element mesh of the FTP-4 piping system

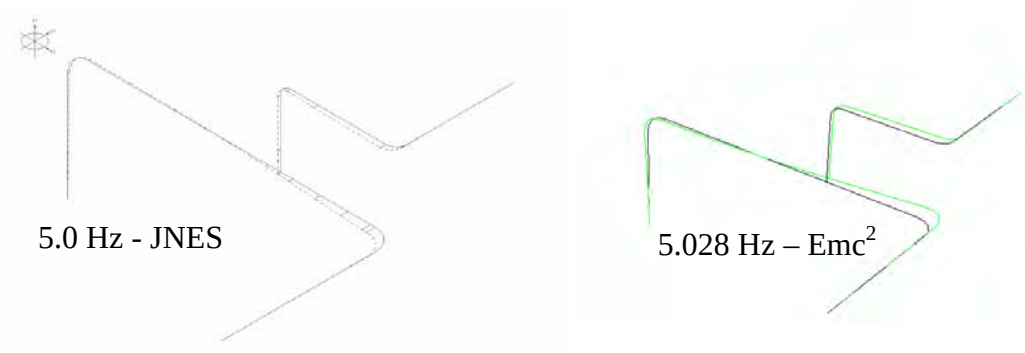

(a) First natural frequency of JNES versus Emc^2 predictions

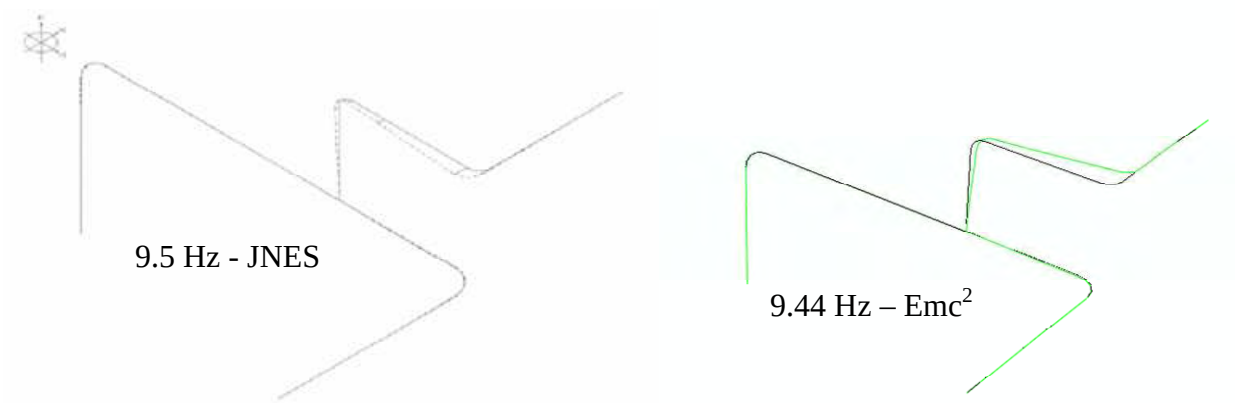

(b) Second natural frequency of JNES versus Emc^2 predictions

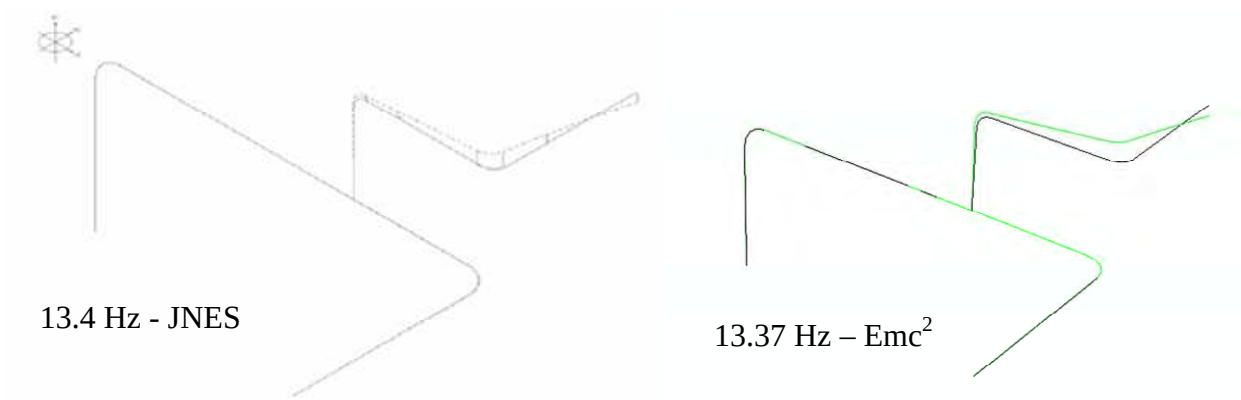

(c) Third natural frequency of JNES versus Emc^2 predictions for FTP-4

Figure 9 Comparison of natural frequency and mode shapes by JNES and Emc^2

Once the above analysis had been accomplished, the focus was on creating the actual finite element (FE) models with the crack present. Generally, these "cracked-pipe elements" are simple beam-element models with nonlinear springs at the node points where the cracks will be located. The nonlinear spring stiffness is essentially the global moment versus rotation due to the crack that comes from much more

sophisticated nonlinear fracture mechanics analyses. By using the "cracked-pipe element" approach, all of the detailed fracture mechanics analyses can be simplified for the dynamic time-history FE analyses. This approach has worked well in past IPIRG seismic pipe-system and other analyses[5,6,13]. By including only the global behavior due to the cracked section, all of the fracture mechanics analyses are essentially made external to the seismic pipe system analysis. As an example of the simplification, many of the FE models used in the following validation efforts used 20 to 25 elements, where a full 3D FE analysis with all the refinement for the fracture analyses included in those models would require 15,000 to 45,000 solid elements per case.

3.3 Cracked-Pipe-Element Modeling

3.3.1 Models and Analyses

The process of a circumferential surface-crack growth in the piping system can go through the experience of starting with surface-crack growth through the thickness and subsequently transitioning to a circumferential through-wall crack, and finally from a through-wall crack to a complete pipe break. Figure 10(a) schematically shows the moment-rotation curve for a pipe with a circumferential surface-crack developing to a circumferential through-wall crack. The crack experiences elastic loading, plastic deformation, reaches the maximum load capacity, and then grows the crack through the thickness. Figure 10(b) is the moment-rotation curve for a pipe with a circumferential through-wall crack from loading until break. It is seen that the load capacity decreases after reaching the maximum point. The whole process from a surface crack to through-wall crack and break is schematically presented in Figure 10(c). From surface crack transition to a through-wall crack, there is often a sudden decrease in load, the extent of which depends on the surface crack length. By subtracting the elastic and plastic rotations of the uncracked pipe from the total rotations including the crack, the rotation due solely to the crack can be determined. It is the moment versus rotation due to the crack that is calculated by various fracture mechanics analyses[2] and then implemented into the "cracked-pipe element."

During the early 1990's, multiple springs, slider and pin elements in ANSYS had to be used to simulate the whole process in the IPIRG program as shown in Figure 11. In this project, a new type element of ABAQUS 6.8, connector element, was to simulate the elastic, plastic, and post maximum load (damage) behavior of a crack as shown in Figure 12.

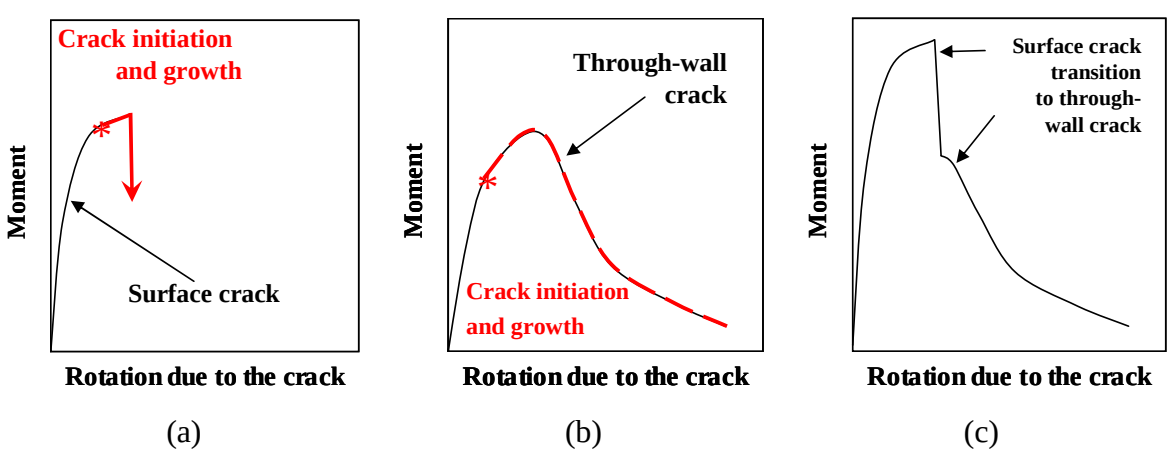

Figure 10 Moment versus rotation-due-to-the-crack curves from initial loading to full break of a pipe with a circumferential crack

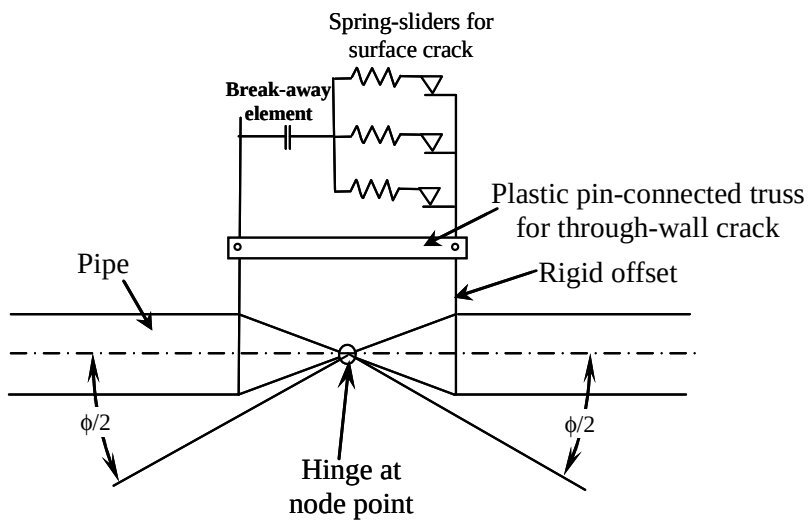

Figure 11 Simulation of a crack in IPIRG program during the early 1990's

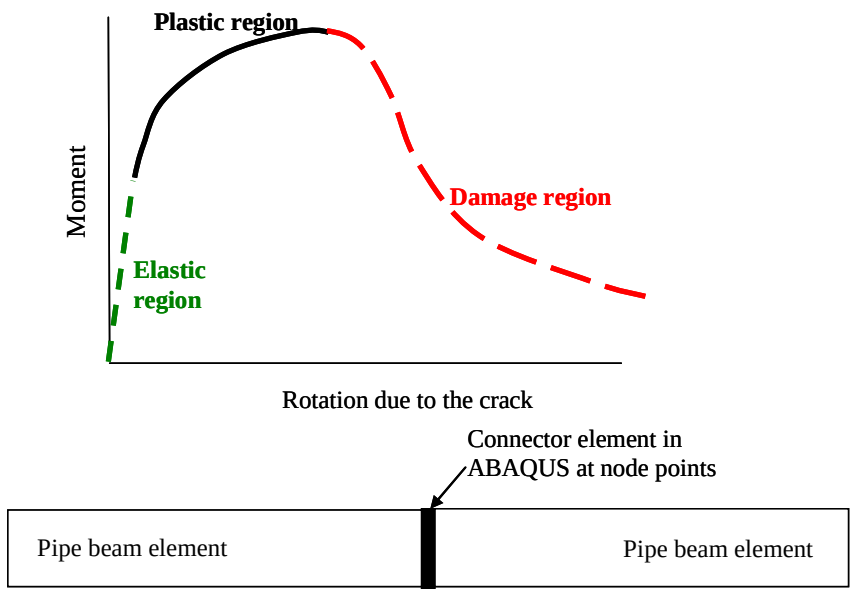

Figure 12 Simulation of a crack in current program using ABAQUS

The "connector element" of ABAQUS 6.8 was used in this project to simulate the crack behavior, i.e., the moment versus rotation-due-to-the-crack response at a node point where the crack is to be located. The "connector element" can be used to model complicated local behavior at a node point such as elastic behavior (linear and non-linear), plasticity (isotropic and kinematic type hardening), and damage (failure behavior until breakage occurs). In addition, this type of element can define admissible relative motion under crack closure conditions, in which the pipe takes the compressive loads as if it was un-cracked when the crack faces come in contact under compressive loading. Note that the JNES pipe tests had a 0.7 mm wide notch and shims were not placed in the notches to simulate a tight crack. It is noted that the connector element within ABAQUS to simulate crack face contact has some convergence issues. Finally, damage can be introduced which can model the crack growth. The use of this element is a major

improvement compared to the procedure used in past NRC/IPIRG programs using ANSYS where a series of springs and dashpots were required. Since it is a novel improvement, a thorough validation was necessary to understand the numerical behavior of the connector element before introducing it into the piping systems. This validation procedure included four cases with increasing complexity.

1. Circumferential through-wall-cracked pipe test with straight pipe sections under quasi-static monotonic bending past maximum load in displacement-controlled loading to see if the loads and remote displacements could be predicted,
2. Circumferential surface-cracked pipe test with quasi-static monotonic bending to see if the transition to through-wall crack can be modeled,
3. Circumferential through-wall-cracked pipe test under quasi-static displacement-control cyclic bending with R = -1 to see how hysteresis loops are predicted and if the low-cycle fatigue damage can be properly captured, and
4. Circumferential surface-cracked pipe test under pressure, dead-weight, and inertial bending to see how the dynamic analysis performs with hysteresis loops.

In this validation effort, a series of FE analyses were conducted and the predicted results were compared with experimental measurements to thoroughly understand the elastic, plastic, and damage behavior of connector element. These efforts were completed prior to examining the JNES tests.

3.3.1.1 Circumferential through-wall-cracked pipe simulation

The test specimen chosen for this simulation was a section of 914-mm (36-inch) nominal diameter cold-leg pipe obtained as part of the Degraded Piping Program[14]. The experiment number was 1.1.1.28. The test specimen had a circumferential through-wall crack and was loaded in four-point bending as shown in Figure 13. The bimetallic welds were fabricated by first buttering the bevel of the carbon steel pipe with two layers of Inconel 182 weld rod and then completing the weld using a shielded-metal-arc weld (SMAW) process using In182 weld rod. This was a cold-leg pipe from a cancelled nuclear plant back in the 1980's. The crack tips were located such that they followed the fusion line at the interface of the carbon steel pipe and the In182 weld metal. The outer diameter of the pipe was 921 mm, wall thickness was 85.7 mm, crack length/pipe circumference was 0.359 and test temperature was 288°C (550°F). The outer span and inner span of the 4-point bending were 11,580 mm and 3,350 mm. There are only 21 beam elements for this model.

Figure 14 shows the comparison of moment versus rotation-due-to-the-crack from the test data and the ABAQUS response using the "connector element." The black curve represents the test data and it is the connector element property input for the ABAQUS validation. The FEA prediction is the solid fine (pink) line in Figure 14. The small load drop past maximum load occurred in the experiment due to the crack suddenly growing into the ferritic material. Both data sets are close to each other and indicate that ABAQUS can simulate the crack loading and damage behavior accurately. Figure 15 shows the comparison of the load and remote displacement from test measurements and FEA prediction. (Note, in the experiment the pipe specimen was unloaded a few times to mark the crack growth. That unloading was not included in the FE analysis.) The simulation and measurements give very similar maximum loading levels. After passing the maximum loading point, the FE analysis predicted a slightly higher load or shift in the displacement predictions. This could be due to the simplicity of the model. Overall, both experiment and FEA results show similar trends that are acceptable, but could be slightly improved.

(a) Four-point bend testing

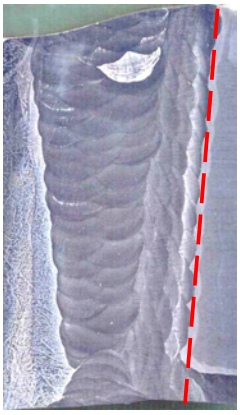

(b) Crack location thru the thickness

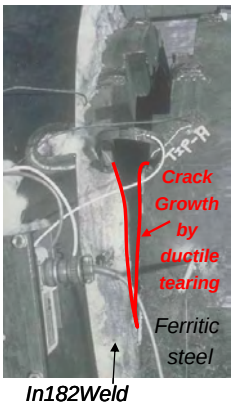

(c) Crack growth

Figure 13 Photographs of pipe specimen for Experiment 1.1.1.28, the crack location in the weld and the circumferential crack growth from one crack tip

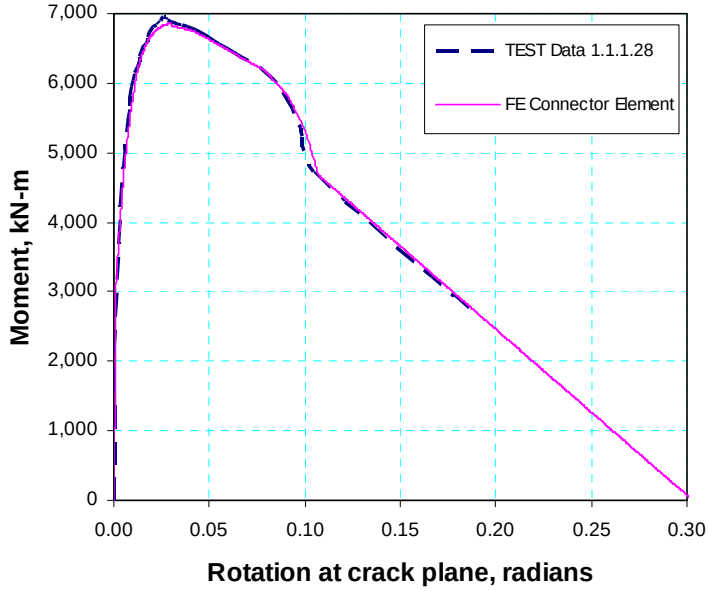

Figure 14 Moment versus rotation-due-to-the-crack comparisons between ABAQUS and test for Experiment 1.1.1.28

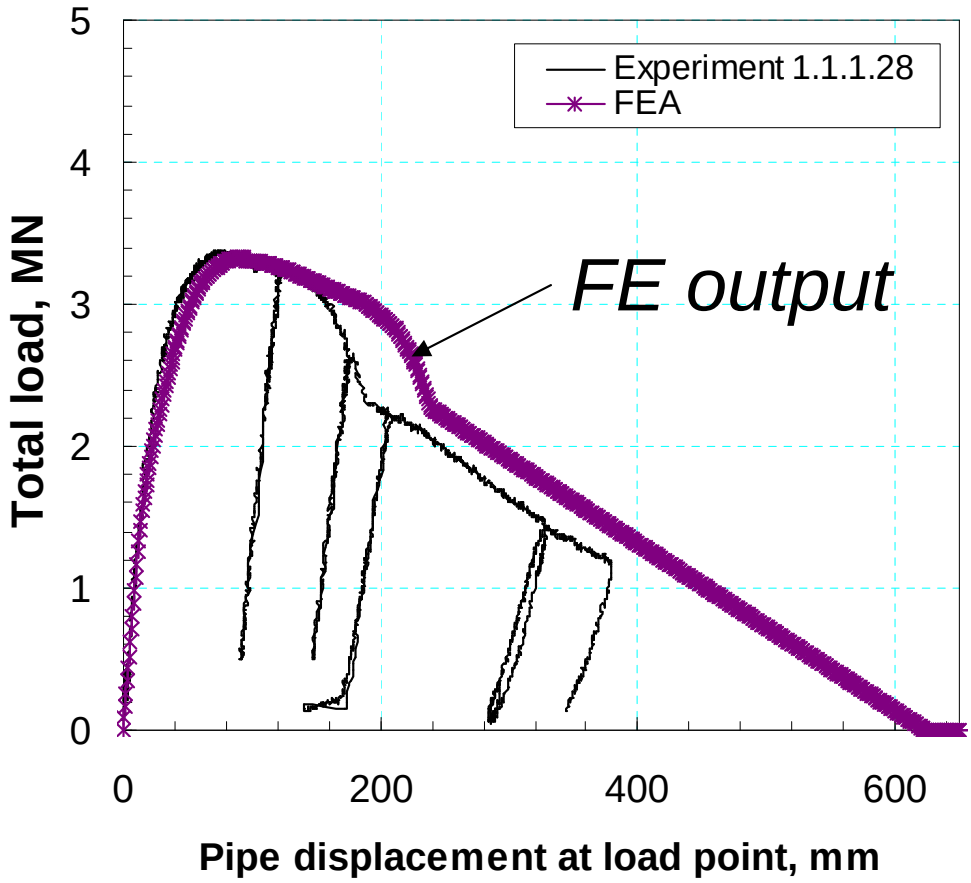

Figure 15 Comparison of applied load and far-field displacements between ABAQUS and test data from Experiment 1.1.1.28

3.3.1.2 Circumferential surface-cracked pipe simulation

For this simulation, Experiment 1.2.1.3 was chosen from the NRC Degraded Piping Program, as shown in Figure 16. The test specimen was fabricated from a 6-inch (152-mm) nominal diameter Schedule 120 stainless-steel pipe. The test specimen had a circumferential surface crack on the inside surface and was loaded in four-point bending without internal pressure. A schematic of how a circumferential surface crack grows to become through-wall crack is shown in Figure 17. The wall thickness of the pipe was 13.6 mm, crack length/pipe circumference was 0.518 and test temperature was 288°C (550°F). The outer span and inner span of the 4-point bending were 1,524 mm and 609.6 mm, respectively.

In this study, the moment versus rotation-due-to-the-crack curve for a connector element to simulate the circumferential surface crack to through-wall crack and finally break of the pipe has to be carefully defined. The FEA input of the moment versus rotation-due-to-the-crack curve was marked as the dashed line with black color in Figure 18. This black curve includes two parts: one is the EPFM fracture mechanics prediction of a circumferential surface-cracked pipe in bending (EPFM predictions made using the NRCPIPES code with the SC.TNP1 J-estimation scheme option for a circumferential surface-cracked pipe) and gives the maximum load capacity and rotations due to the surface crack in the pipe. The other part of the complete moment versus rotation-due-to-the-crack curve is from a circumferential though-wall crack EPFM analysis. The circumferential through-wall-cracked pipe analysis used the NRCPIPE code

with the LBB.ENG2 J-estimation scheme option. The SC.TNP1 and LBB.ENG2 J-estimation schemes were found to give the most accurate predictions of all the EPFM analyses investigated during the NRC pipe fracture programs[2]. The sudden decrease in load represents the transition from surface crack to through wall crack. It should be pointed out that the experiment to FE predictions using the "connector element" (and only 20 pipe beam elements) starting with J-estimation scheme predictions of the moment versus rotation-due-to-the-crack were from a fundamental start, i.e., no pipe test data used to guide input.

Figure 19 shows the comparison of moment-versus-rotation curves for ABAQUS "connector element" response and the input curve. The FEA prediction is marked in solid red line in Figure 19. Since there is a sudden decrease of moment from the surface-crack to through-wall-crack transition region, there is a slight difference in the numerical analyses results. ABAQUS still provides appropriate simulation of the crack loading and post-maximum load behavior (damage region for the connector element). Figure 20 shows the comparison of the load and load-line displacement curves from NRCPIPES and FEA prediction along with the experimental measurement values. (The occasional unloading during the pipe test was not modeled in this FE analysis.) Overall, for these analyses and experimental values, the trends are similar. The maximum load was predicted well. The applied load was under-predicted (conservative) during through-wall crack growth. The FEA displacement prediction is lower than the experimental values. This may be because the inputted moment-rotation curve is a combination of surface crack and through-wall crack curves from the J-estimation schemes, while in the experiment the load did not drop to the predicted value.

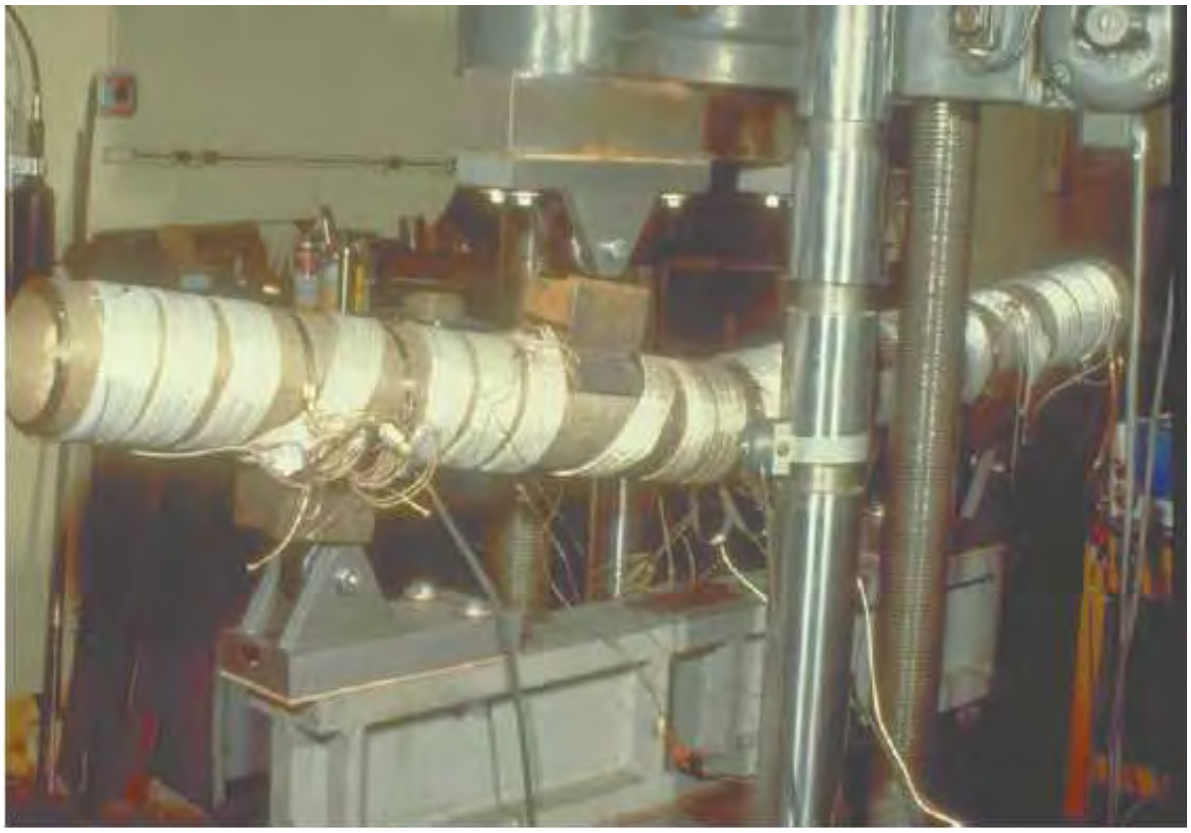

Figure 16 Post-test photograph of pipe specimen for Experiment 1.2.1.3

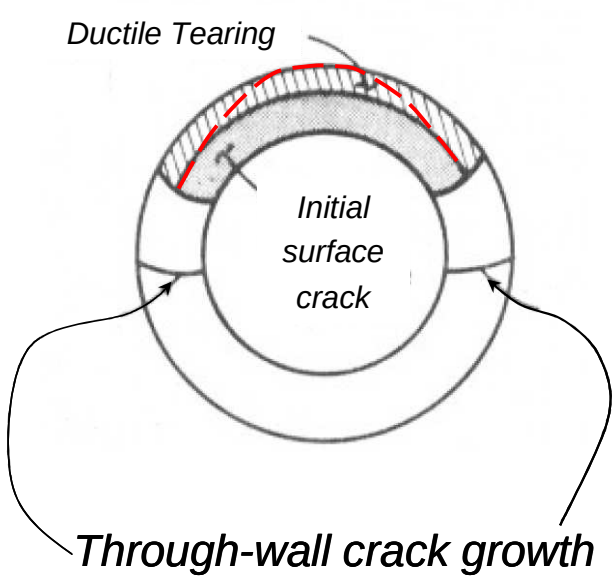

Figure 17 Illustration of crack growth for circumferential surface cracks

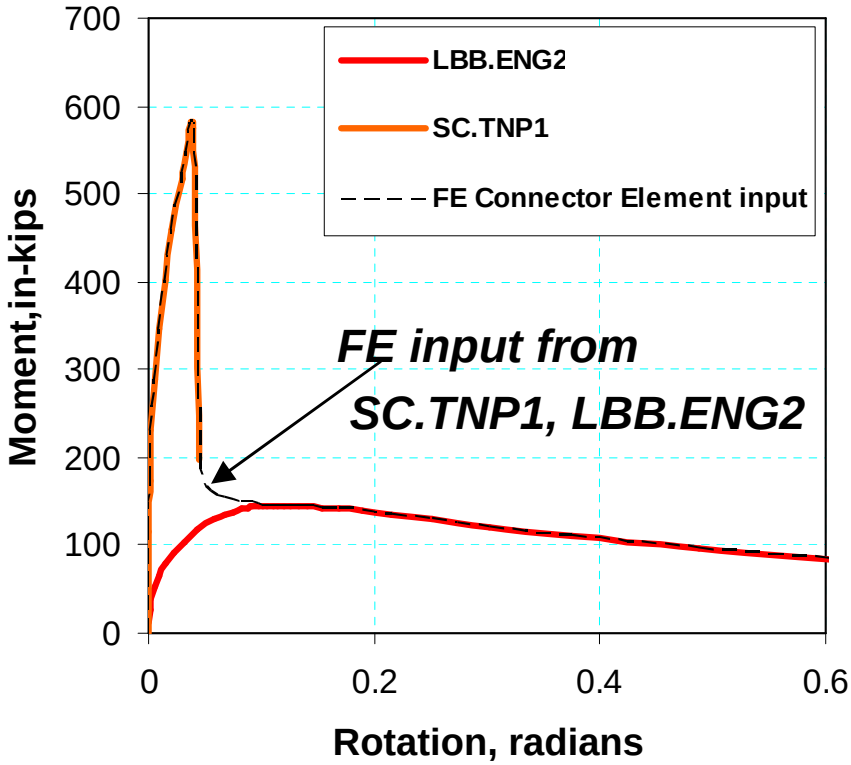

Figure 18 Moment-rotation input curve for Experiment 1.2.1.3

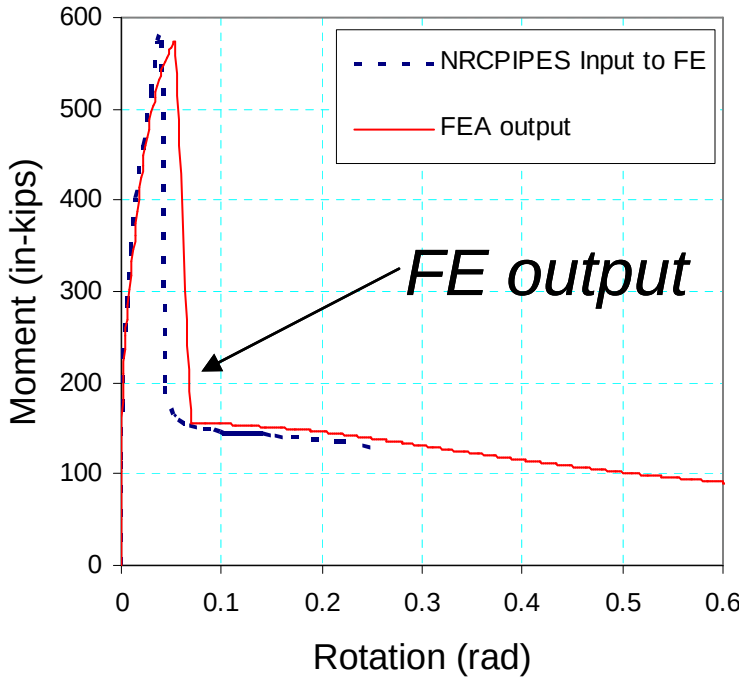

Figure 19 Moment versus rotation-due-to-the-crack comparison between ABAQUS and test results from Experiment 1.2.1.3

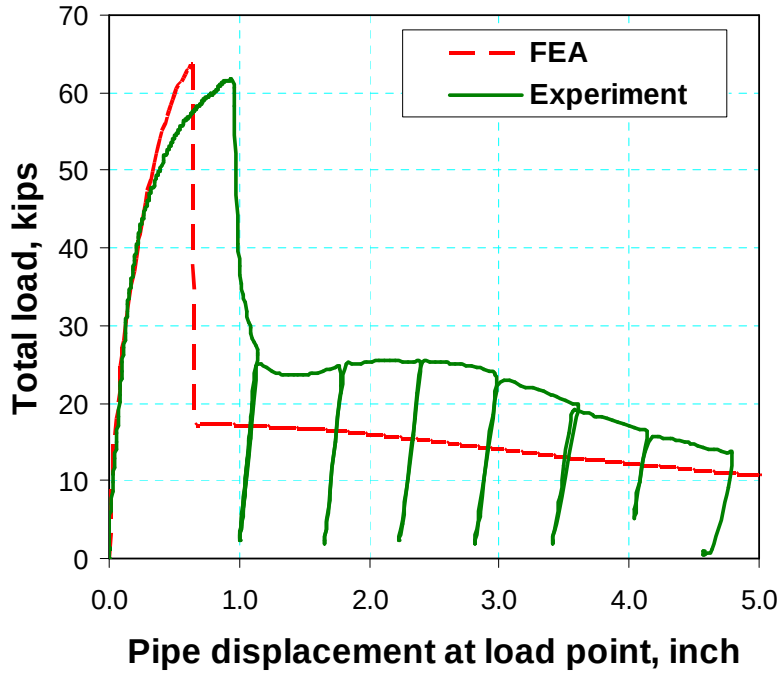

Figure 20 Applied load versus load-line displacement curve comparison between ABAQUS and test results from Experiment 1.2.1.3

3.3.1.3 Quasi-static circumferential through-wall-cracked pipe simulation

For this simulation, a circumferential through-wall-cracked pipe test was loaded by quasi-static displacement-control fully reversed cyclic bending (R = -1). The objective of the validation effort was to see how hysteresis loops and low-cycle fatigue crack growth are predicted. The test was chosen from a test record book entry from the NRC Degraded Piping Program, Experiment 1.2-5, as shown in Figure 21. Figure 22 is a schematic of the test apparatus. This experiment evaluated the fracture initiation and propagation behavior of a 152-mm diameter, Type 304 stainless steel pipe under cyclic quasi-static four-point bending. The loading cycle for this experiment consisted of loading the four point bend specimen into tension by a known displacement, recording the load at that point, then loading the specimen into compression equal to the tension load (i.e., R = -1). The test specimen was fabricated from a 168.5-mm (6.6-inch) outside diameter SA-376 TP304 stainless steel pipe (outside pipe diameter was slightly machined to get a constant thickness specimen). The wall thickness was 14.2 mm, crack length/pipe circumference was 0.37 and test temperature was 288°C (550°F). The outer span and inner span of the 4-point bending were 1,524 mm and 610 mm, respectively.

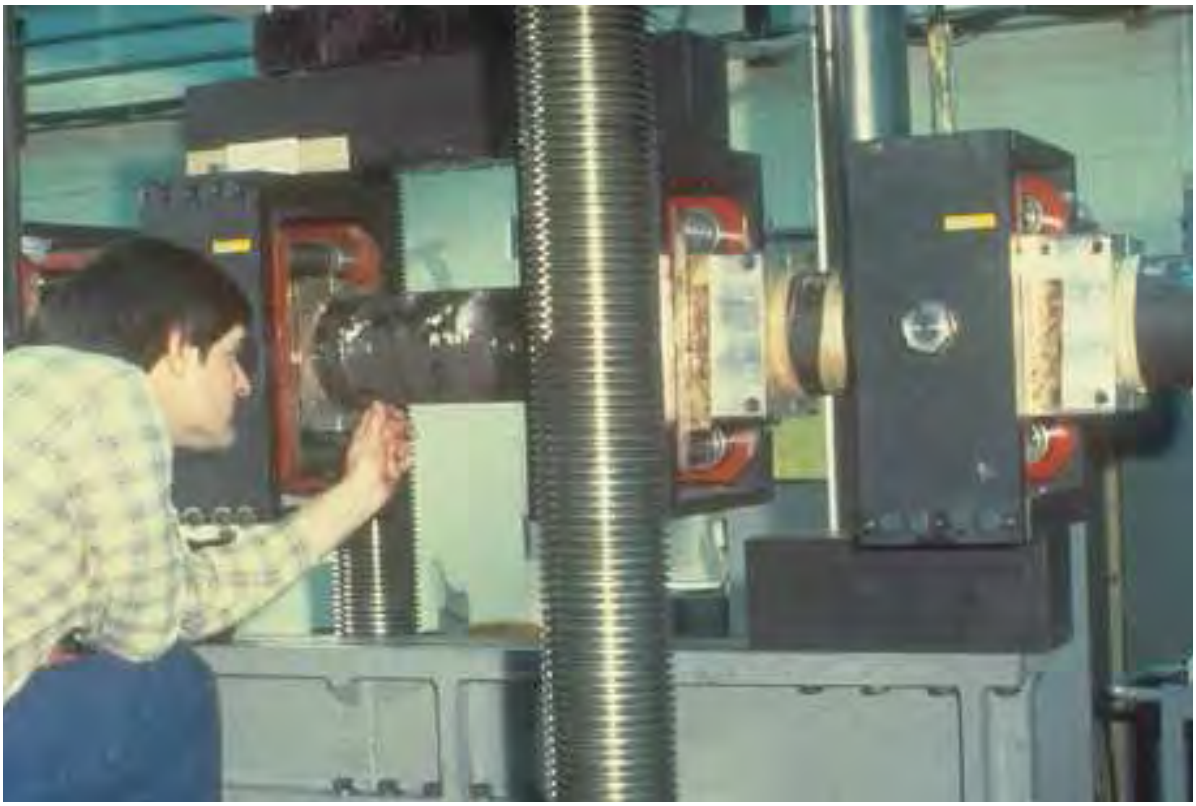

Figure 21 Photograph of pipe specimen for Experiment 1.2-5

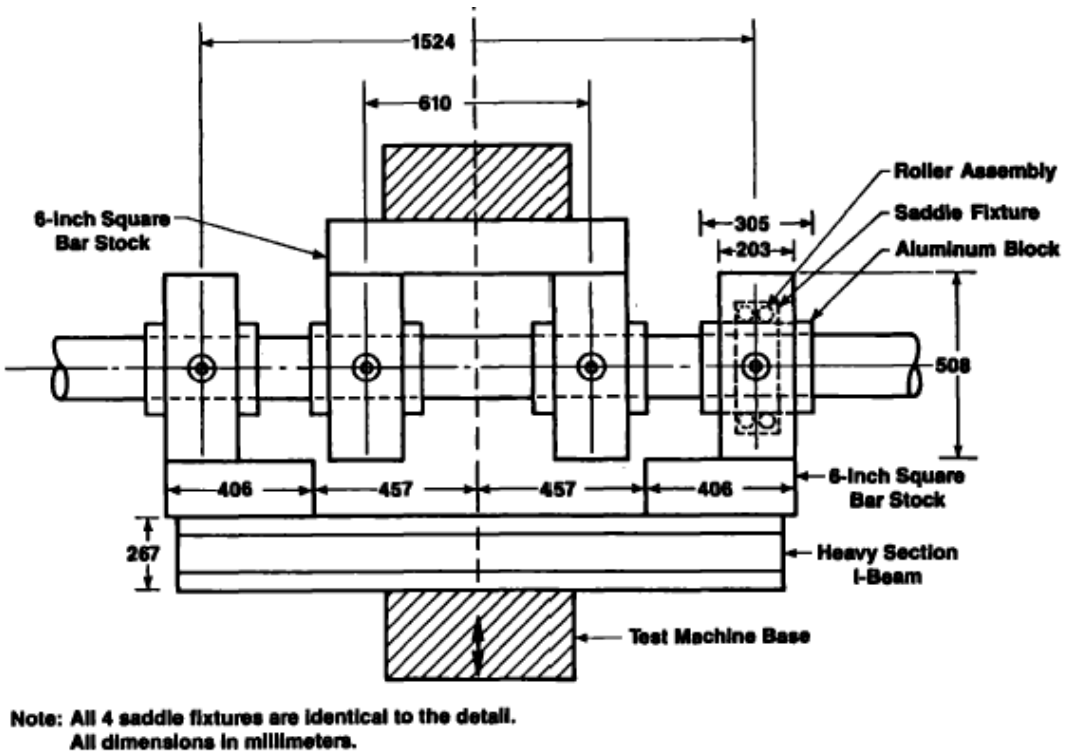

Figure 22 Schematic of test apparatus for Experiment 1.2-5

In this analysis, the moment versus rotation-due-to-the-crack curve for a connector element to simulate the cyclic behavior of a circumferential through-wall cracked pipe needs to be defined. The finer curve of Figure 23 is the moment-rotation history from experiment. The upper envelope of the experimental data was used as moment-rotation input for the connector element, i.e., the FEA input data of the moment-rotation curve is the black dashed line in Figure 23. It should be noted that the data acquisition failed to collect some data for this test and all fully reversed cyclic loads were actually applied by computer control during the test (observe missing data near maximum load in Figure 23). This simulation started using the experimental moment-rotation (near crack) upper envelope curve as input. The purpose was to see how hysteresis behavior was predicted (kinematic-hardening rule used) by the connector element.

Figure 24 shows the comparison of moment versus rotation-due-to-the-crack curves for the ABAQUS response and the inputted curve. The ABAQUS output gave more rotation than the inputted value and slightly over-predicted the displacement as shown in Figure 25. Why the input and output did not match is a question being asked of ABAQUS staff at this time. Even though there are some differences between the input and output data, the overall trends are still similar. Further, it is interesting to see if the moment-rotation changes, i.e., reducing input rotation by a factor (70%) so output moment-rotation curve is in agreement compensating for ABAQUS connector element (kinematic hardening used), what kind of load-displacement history can be obtained. Figure 26 shows the comparison of input and output moment-rotation curves, which are in agreement. It is observed that the load versus load-line displacement is slightly conservative for R = -1 loading, see Figure 27.

From this analysis, it can be seen that the connector element can capture the hysteresis behavior of a crack at a reasonable accuracy level under static cyclic loading condition, but the input and output moment-rotation values need to be checked carefully until ABAQUS comes up with a solution to this observed problem.

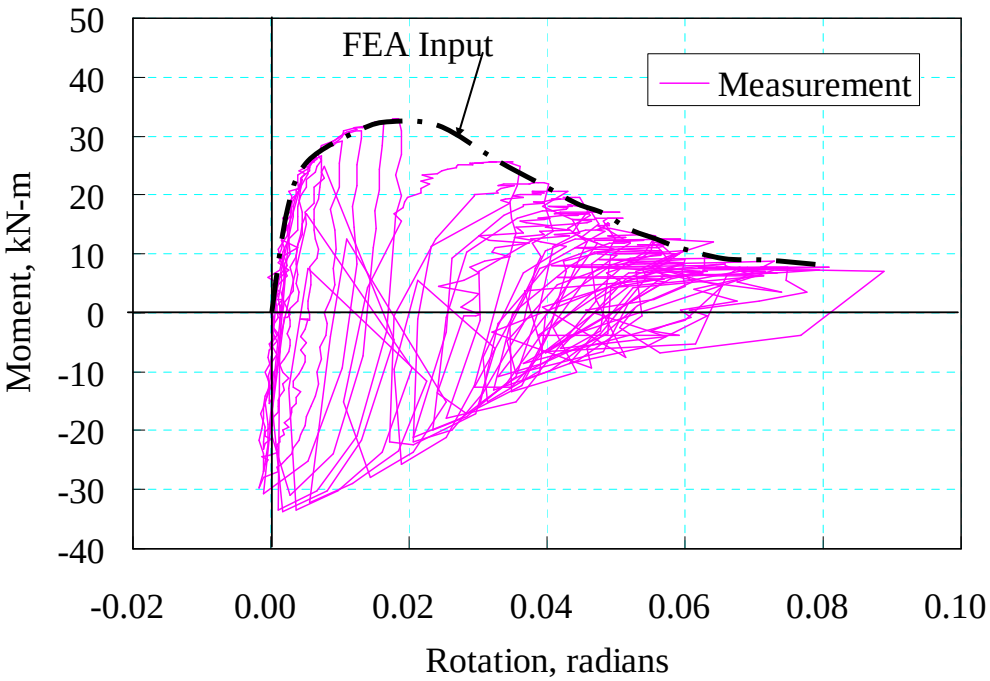

Figure 23 Upper envelope to cyclic experimental moment versus crack rotation-due-to-the-crack data from Experiment 1.2-5

(Note, the data acquisition system failed to take some of the cyclic data that was actually applied in this test.)

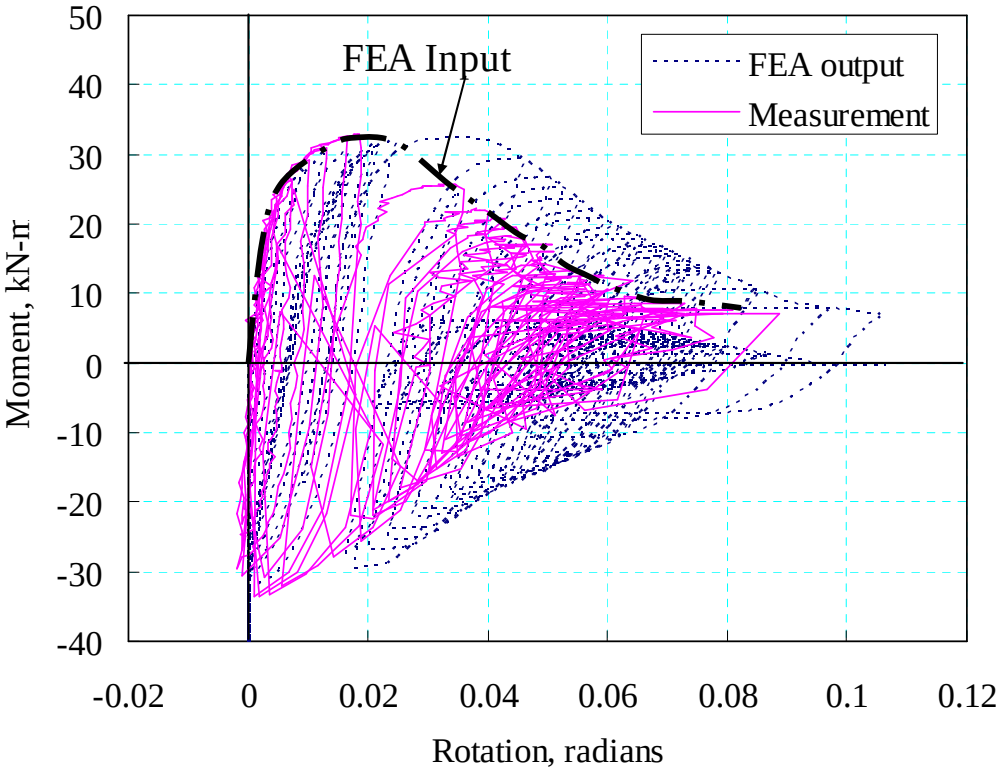

Figure 24 Comparison of moment versus rotation-due-to-the-crack from the FEA and measurements for Experiment 1.2-5 (from inclinometer readings)

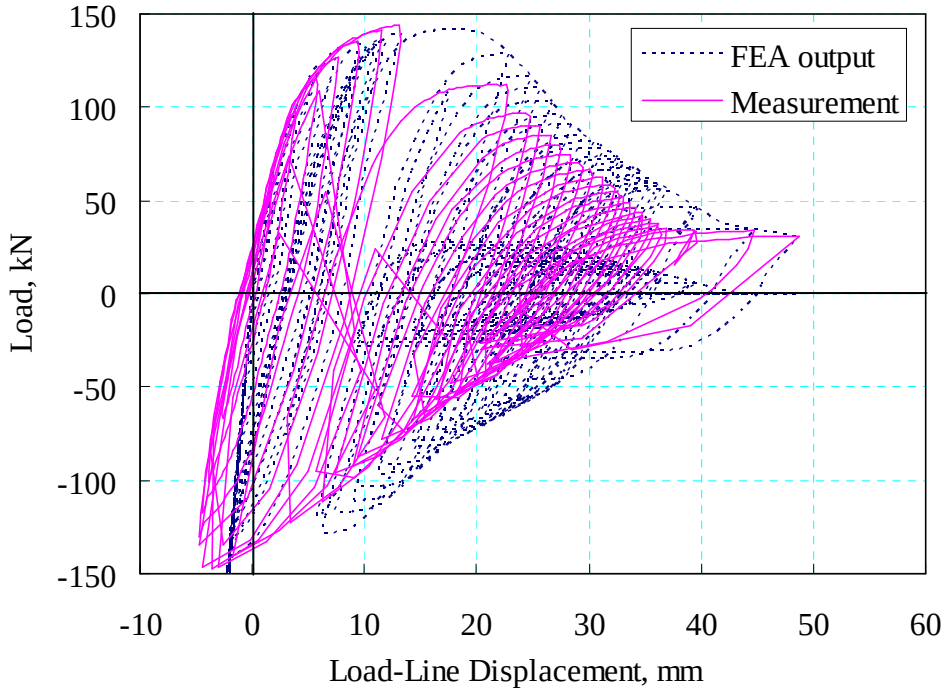

Figure 25 Load versus load-line displacement history by FEA and measurement for Experiment 1.2-5

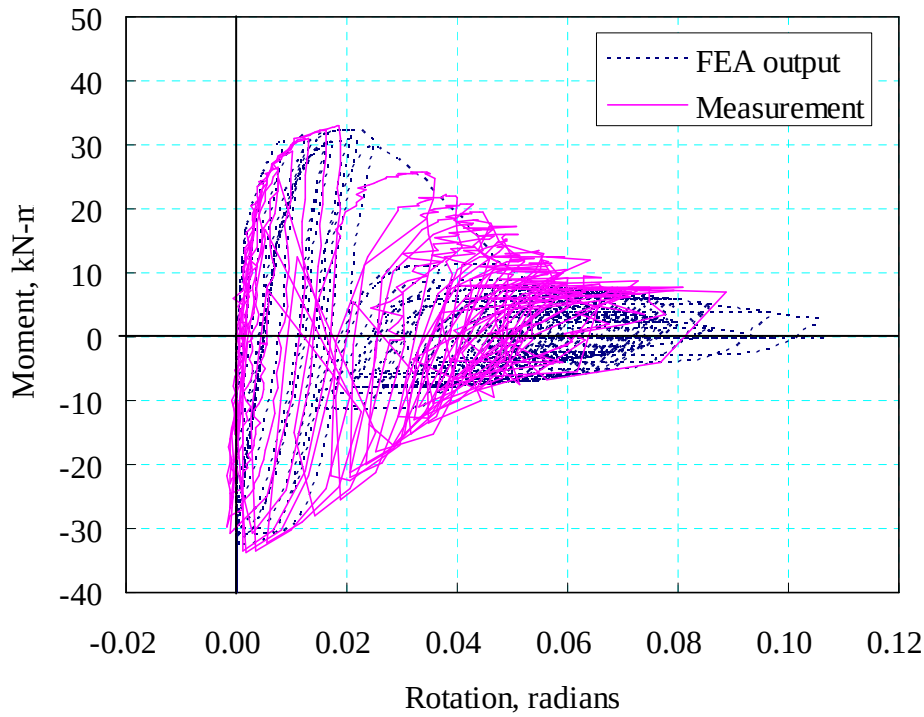

Figure 26 Comparison of moment versus rotation-due-to-the-crack curves from the FEA (with 70% reduction factor) and measurement for Experiment 1.2-5

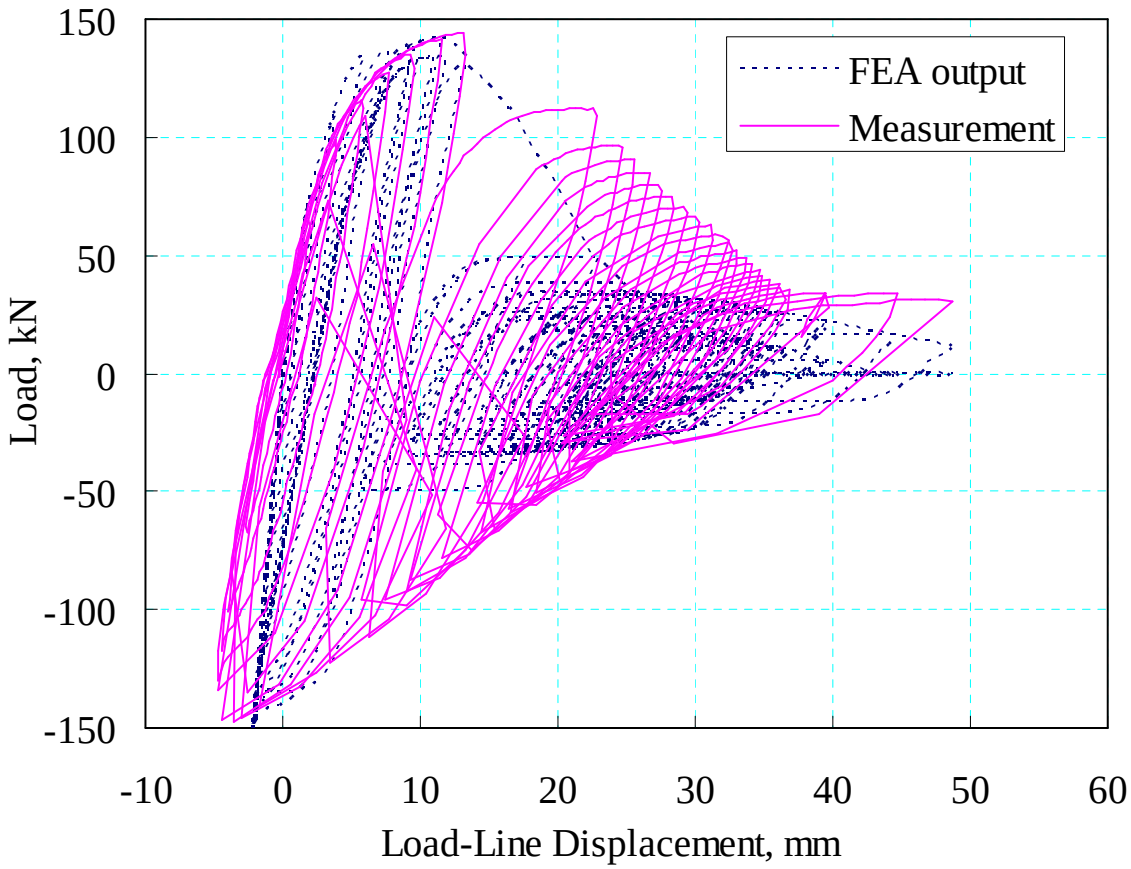

Figure 27 Comparison of load versus load-line displacement curves from the FEA (using 70% reduction factor) and measurement for Experiment 1.2-5

3.3.1.4 Dynamic simulation of circumferential through-wall -cracked pipe under cyclic loading

The objective of this analysis was to evaluate if the connector element can be used to simulate the response of a circumferential through-wall-cracked pipe test under predominately inertial stresses and see how hysteresis loops are predicted. The test was chosen from a test record book entry from the IPIRG-1 Program, Experiment 1.1-3, as photographically shown in Figure 28. Figure 29 is the schematic of test apparatus. The material used for this experiment was seamless, schedule 120, SA-376 TP304 stainless steel pipe. The pipe outside diameter was 169 mm (6.65 inch) with a 14.0-mm wall thickness. The test specimen length was 457 mm and, due to close tolerances maintained by the mill for this particular piece of pipe, required no additional machining to maintain roundness and constant thickness. A circumferential through-wall crack was machined into the specimen using a band saw. The tips of the saw cut were sharpened using a 0.13-mm thick jeweler's saw. The total crack length was 37 percent of the pipe circumference. The test temperature and pressure were 288°C (550°F) and 15.5 MPa, respectively. Figure 30 is the post-test photograph of the specimen. Figure 31 shows the load-line displacement of actuators.

Figure 28 Post-test photograph of pipe specimen in Experiment 1.1-3

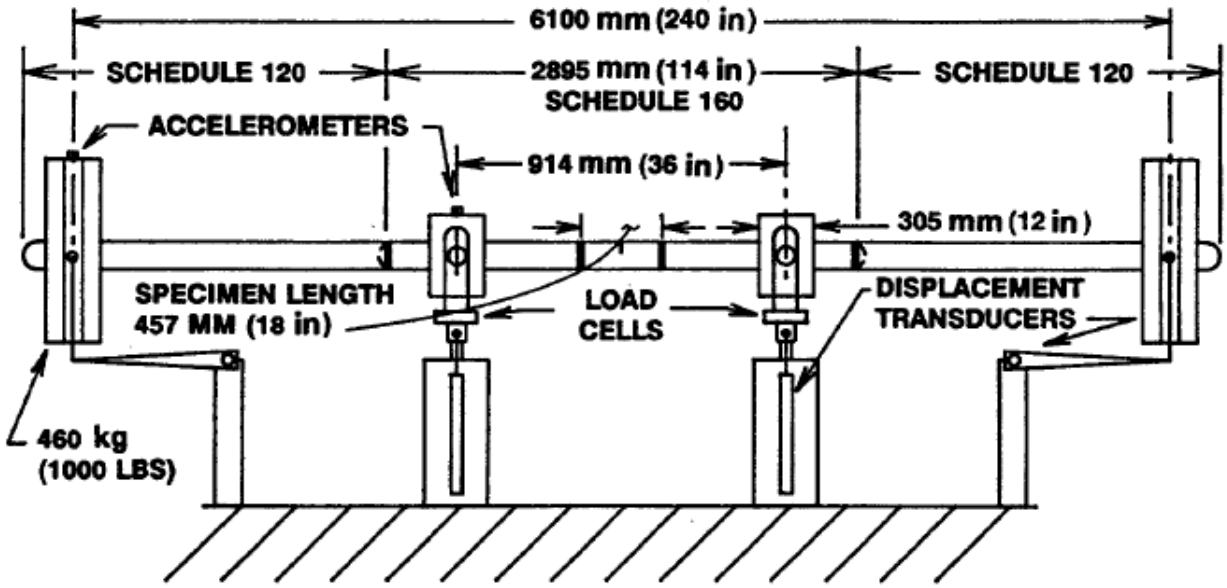

Figure 29 Schematic of overall test setup showing dimensions and major transducer locations for Experiment 1.1-3

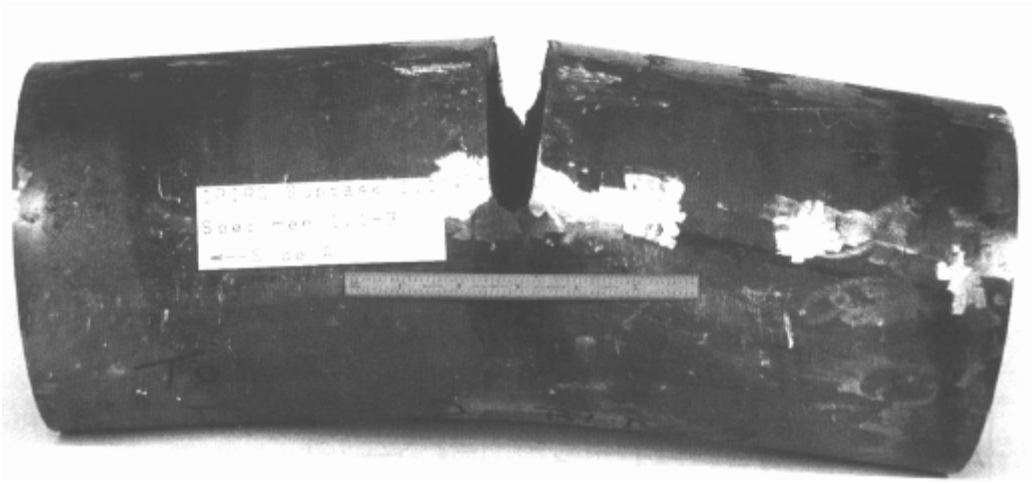

Figure 30 Post-test photograph of specimen 1.1-3

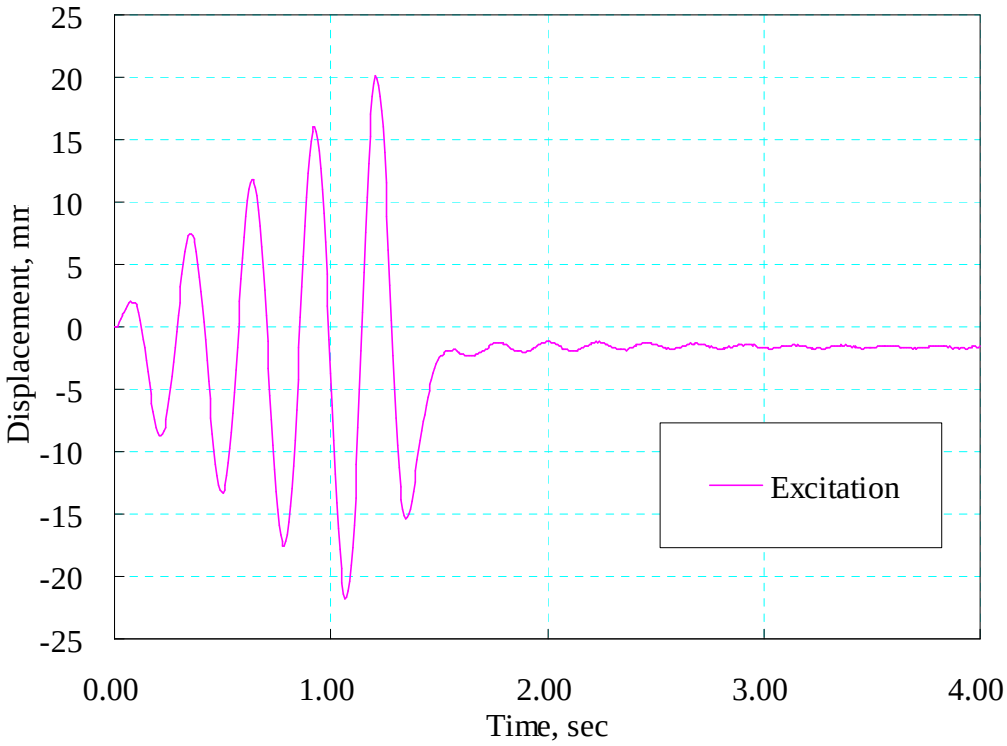

Figure 31 Plot of load-line displacement for actuators as a function of time for Experiment 1.1-3

Similar to the third validation case, the moment-rotation curve for a connector element to simulate the cyclic behavior of a through-wall crack needs to be defined. The black cyclic curve of Figure 32 is the moment-rotation history from experiment. The upper envelope data curve in the lighter color was used as moment-rotation input for the connector element, i.e., the FEA input data of the moment-rotation curve is in dashed line in Figure 32. Note that here, the surface crack broke through to a through wall crack during a re-load cycle so the drop off seen in Figure 10 is not always seen.

Figure 33 shows the comparison of moment-versus-rotation curves for ABAQUS (using kinematic-hardening rule for connector element) response and the inputted curve. Figure 34 presents the displacement history comparison between FEA (kinematical hardening rule) and measurement for Experiment 1.1-3. It was observed that the output moment-rotation was close to input curve; experimental compressive loads were greater than ABAQUS prediction; hysteresis loops were slightly larger and the displacements of end-mass were close to the measurement. Another set of comparisons was made by using the isotropic-hardening rule for the connector element. Keep in mind that the frequency of the system changes as the crack grows and crack tip plasticity changes damping. Figure 35 shows the comparison of moment-versus-rotation curves for ABAQUS (using isotropic-hardening rule for the connector element) response and the inputted curve. Figure 36 presents the displacement history comparison between FEA (isotropic hardening rule) and measurement for Experiment 1.1-3. With isotropic hardening, the connector element results showed that the output moment versus rotation-due-to-the-crack curve grew progressively off. The experimental compressive load was closer to the measurement, and end-mass displacement slightly deviated from the measurement at termination of test. There was almost no hysteresis loop during unloading. This study showed that the kinematic-hardening rule of the connector element was better overall than isotropic-hardening rule for capturing the cyclic plasticity. In reality, the fracture response could be between kinematic and isotropic hardening rule, but that effort was outside the scope of this study.

In summary, these four sets of validation investigations permit the conclusion that the connector element approach can reasonably simulate the crack response from elastic, plastic, and damage until break. Numerical comparisons between FEA predictions and experimental measurements show, in general, a *well-defined* connector element can capture the static and dynamic behavior under monotonic and cyclic loading. Moreover, the connector element approach to represent a “cracked-pipe element” is more efficient with reasonable accuracy. For all of the above simulation models, there are only about 20 beam/pipe elements plus one connector element, whereas full 3D simulations with sufficient mesh refinements for fracture analyses would require about 15,000 elements per crack location. This approach to making multiple crack simulations and crack growth analyses during dynamic seismic loading is very time efficient, while a three-dimensional model including one crack is very time consuming and multiple crack analyses would present an even greater challenge. Additionally, a detailed 3D mesh refinement would require the crack to be grown and additional remeshing during the seismic loading, making the 3D FE analyses prohibitively expensive in computation time and labor hours.

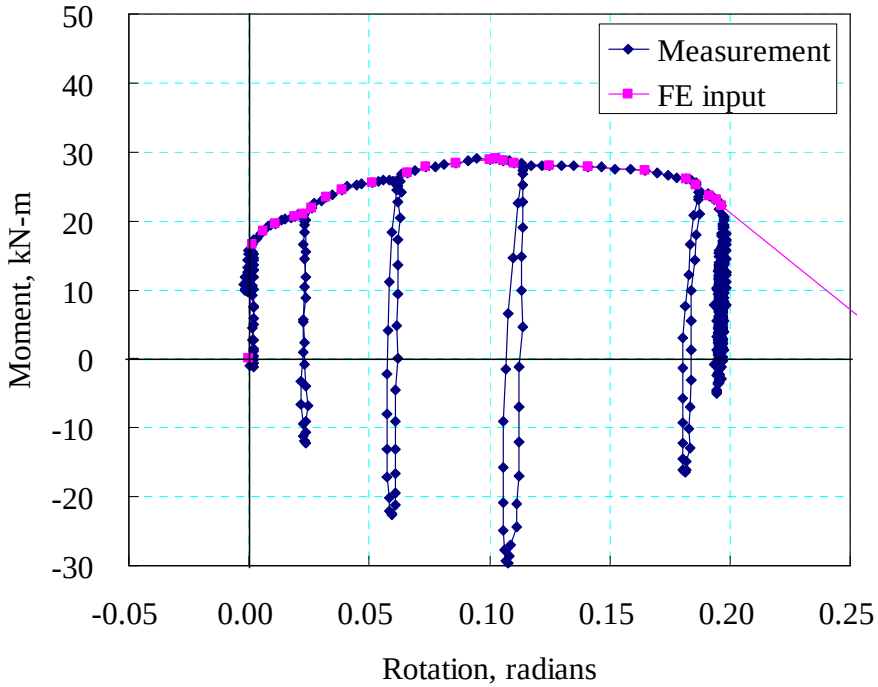

Figure 32 Moment versus rotation-due-to-the-crack curve from Experiment 1.1-3 and upper envelope used for the FE input

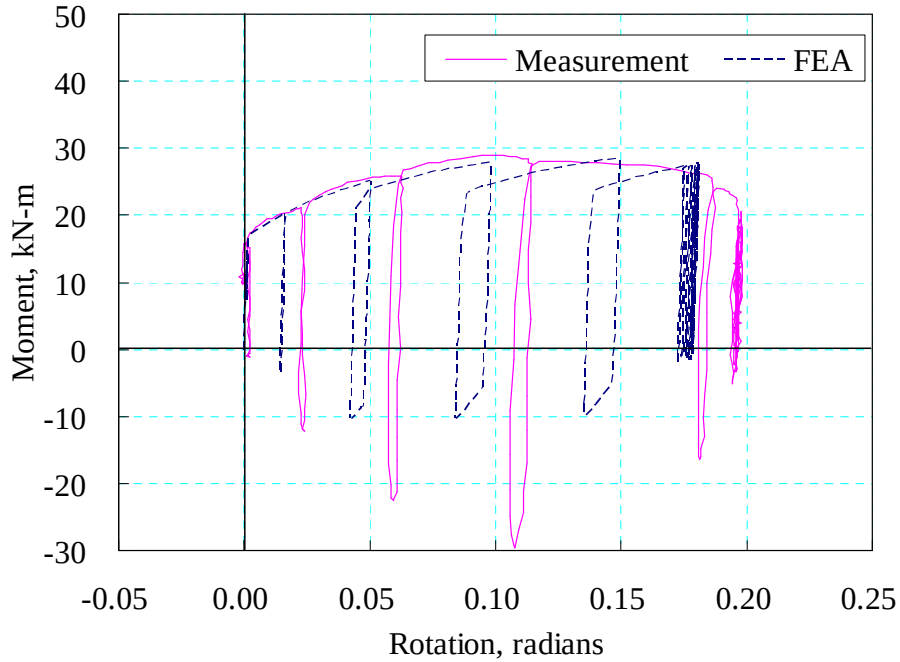

Figure 33 Moment versus rotation-due-to-the-crack comparison between the FEA output (*kinematic hardening* rule) and measurement for Experiment 1.1-3

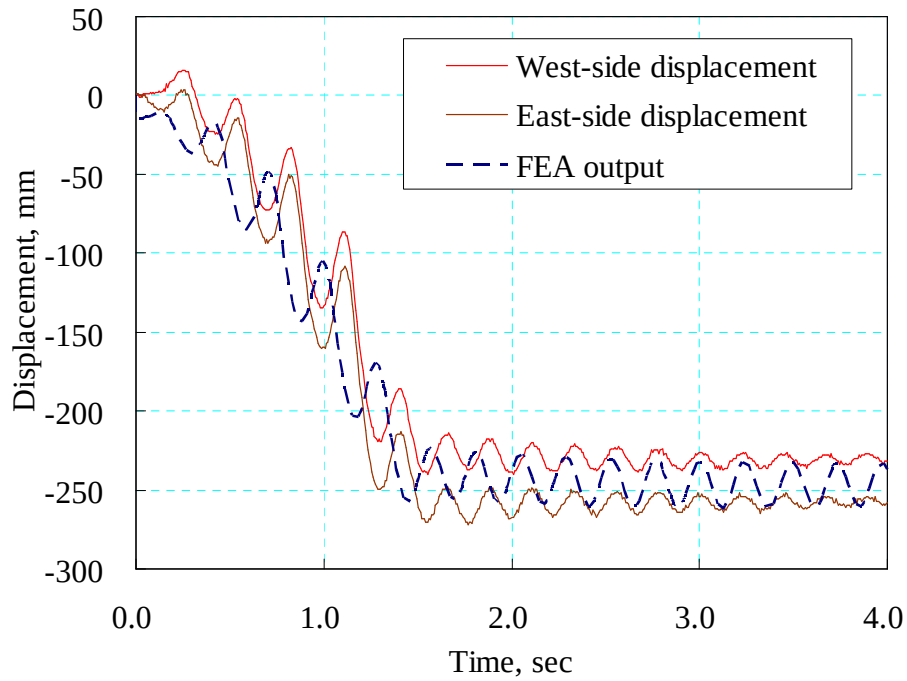

Figure 34 Displacement at the ends of the pipe masses versus time comparison between the FEA (*kinematic hardening* rule) output and measurements for Experiment 1.1-3

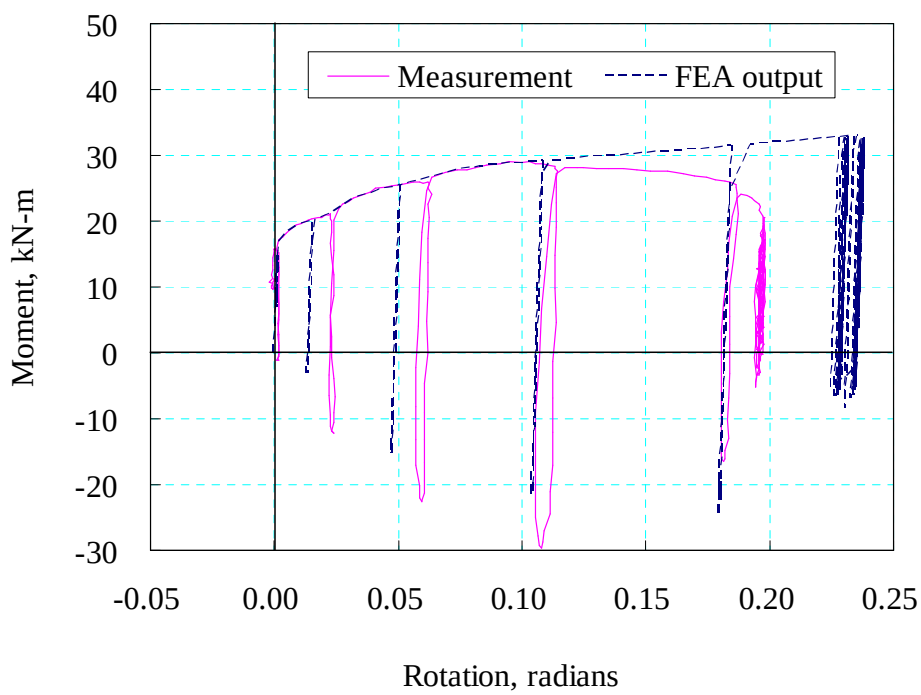

Figure 35 Moment versus rotation-due-to-the-crack curve comparison between FEA (*isotropic hardening* rule) output and measurements from Experiment 1.1-3

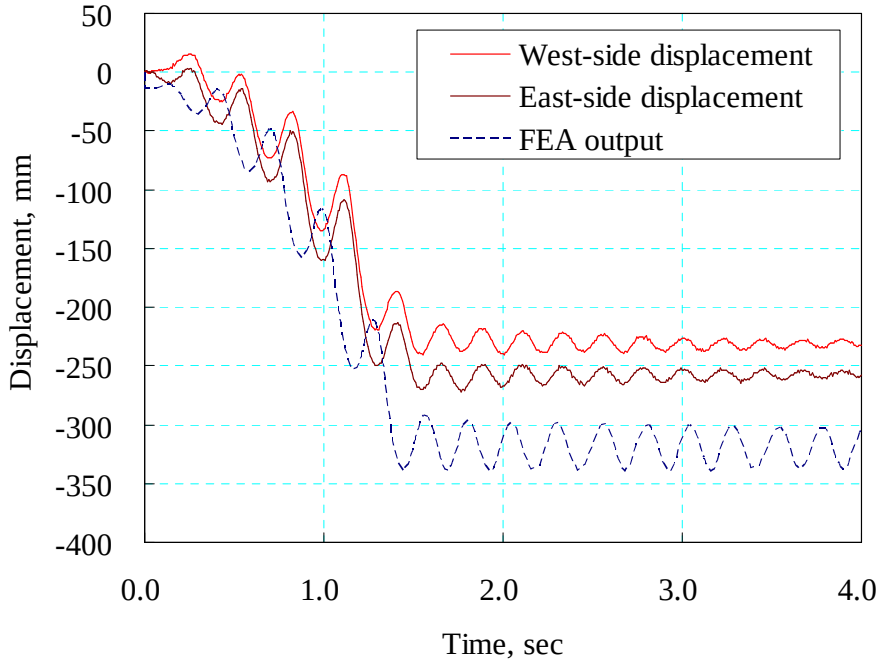

Figure 36 Displacement at the ends of the pipe masses versus time comparison between the FEA (*isotropic hardening* rule) output and measurements for Experiment 1.1-3

3.3.2 Additional Comments on Modeling Low-Cycle Fatigue Damage

Low-cycle fatigue damage can be modeled several different ways. The "cracked-pipe element" approach used in this report is one that facilitates the calculation of the low-cycle fatigue crack growth so that it is automatically accounted for during the dynamic FE analysis in a very efficient manner. Two different ways to model low-cycle fatigue analyses are discussed below.

One of the more fundamental ways to model low-cycle fatigue crack growth is by looking at the change in the crack-driving force during the cyclic loading. To understand this, first high-cycle fatigue crack growth is briefly discussed. In high-cycle fatigue a parameter called the "stress intensity factor" (K) is used so the change in the crack driving force is ΔK, where K is a function of the applied load, crack size, type of loading (tension, bending, etc.), and geometry of the part. In high-cycle fatigue, the stresses are elastic, so that linear elastic fracture mechanics analysis (LEFM) is used to characterize the crack growth. There are many handbooks on stress-intensity factors for cracks in different geometries and loading conditions[15]. High-cycle fatigue crack growth usually follows a relationship called a Paris Law, or

$$da/dn = C(\Delta K)^m \qquad (1)$$

where,

- a = crack length
- n = number of cycles
- C = an empirically measured constant
- m = an experimentally measured parameter
- K = stress intensity factor = $F*\sigma a^{0.5}$
- σ = far field stress
- F = a geometric function related to the crack size, loading direction, and geometry of the component (from stress intensity handbook solutions)

For high-cycle fatigue there are actually many advanced forms of Equation (1) that account for load ratio effects, mean stress, crack closure, among other factors. Here we use the Paris law, which is typically used for high-cycle fatigue analysis. For low-cycle fatigue, plasticity occurs and the LEFM stress intensity factor cannot be used. An alternative nonlinear fracture mechanics parameter is called the J-integral[16]. In linear elastic behavior J is related to K by $J = K^2/E'$, where $E' = E/(1-\nu^2)$ for plane strain and E for plane stress. The applied crack-driving force in nonlinear analysis is $J_{applied}$ and theoretically it is used only for monotonic loading, not cyclic loading. An empirical approach proposed for low-cycle fatigue is the Dowling ΔJ parameter[17]. Since an experimental measure of the J-integral is a factor times the area under a load-displacement curve (energy measure), Dowling explored using that definition for low-cycle fatigue testing. However, he found that when there was reverse or compressive loading, then the crack faces will contact each other (called crack closure), and the area of the load-displacement curve to be integrated needs to include the compressive loads down to the crack closure behavior, see Figure 37. Once the crack growth per cycle for the ΔJ value applied is determined, the ΔJ could be converted to ΔK and the results follow the same log-log scale plot (Equation 1) for high-cycle fatigue crack growth[18]. The difficulty with this analysis approach is that for a seismic loading event as was applied in the JNES tests, each cycle needs to be analyzed in the manner illustrated in Figure 37. This tedious exercise is not easy to automate within the dynamic FE analysis.

The alternative low-cycle fatigue analysis approach that is convenient for automatic implementation in the "cracked-pipe element," is to consider the nonlinear loading as interrupted cyclic tearing, i.e., the load-displacement (or moment-rotation) curve follows the curve for ductile tearing under monotonic loading. A significant amount of effort was conducted in the IPIRG programs[5,6] to assess if this could be done. If the reverse loading had the minimum cyclic load close to zero load or greater, then this simple method works quite well. During the positive loading, the tensile stresses in front of the crack tip produce voids at the inclusions. However, if there is fully reverse loading, then the corresponding compressive stresses ahead of the crack can flatten voids. Then during the subsequent tensile load, the 'flattened' or sharp voids may break and link, leading to additional crack growth[19]. (This is somewhat analogous to repeated bending of a steel hanger in an effort to break it. The more one fully bends it the easier it is to break it). This causes a local drop in the material fracture resistance, so that if there was constant cyclic loading of this magnitude and the crack was always growing in that damaged region, then the apparent material tearing resistance (J-R curve) is reduced. For fully reversed loading, a lower yield strength material may experience a drop in the J-R curve by a factor of four. Pipe tests and laboratory specimen compact tension (CT) tests were conducted with this reverse cyclic loading to come up with approximate methods to predict how the J-R curve changes with the cyclic loading. Guidance is provided in Reference 2. Generally, materials with lower strength are more sensitive to the degradation of the J-R curve under fully reverse cyclic loading, while higher strength material and welds are not.

For the purpose of the "cracked-pipe element" applications, one would first determine the moment versus rotation-due-to-the crack starting with the standard monotonic J-R curve. Next, that moment-rotation curve would be implemented as a "cracked-pipe element" into the FE mesh of the pipe system, and the seismic load would be applied with all the other normal operating loads. One would examine the moment-rotation behavior at the cracks to determine the magnitude of the compressive loading, and then use the IPIRG guidance to adjust the monotonic J-R curve for cyclic loading. The cyclic moment-rotation curve is then used to recalibrate the "cracked-pipe element," and with the seismic loading applied, the cyclic moments are then examined again to see what the magnitude of the compressive loads are. Typically, this only takes one iteration step to get to the proper cyclic-adjusted J-R curve. Hence, one key aspect of the "cracked-pipe element" is that it needs to properly predict the magnitude of the compressive cyclic loading. As was seen in the earlier comparison with the cyclic loaded pipe test with a circumferential through-wall crack, isotropic hardening behavior better captured the compressive loads, while kinematic hardening better captured the upper envelope shape and the hysteresis loops. Real behavior is somewhere between the two hardening laws. Until the proper hardening relationship for

cyclic loading is worked out (it is probably material sensitive), the seismic loading with the initial "cracked-pipe element" calibrated with the monotonic J-R curve should be conducted using both kinematic and isotropic hardening to assess the low-cycle fatigue corrections needed. Fortunately in the JNES tests, the crack is in a higher strength weld metal, so the detrimental effect of the cyclic loading on the J-R curve are minimal.

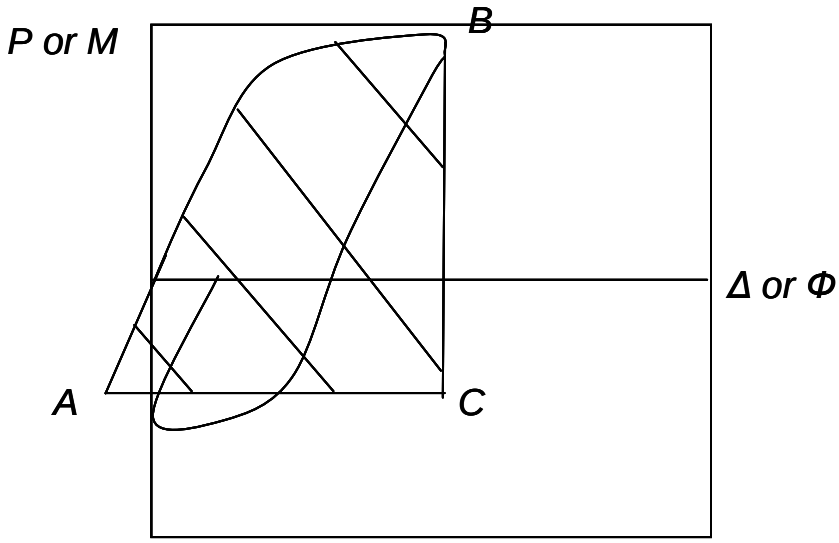

Figure 37 Schematic of area under load-displacement curve to calculate ΔJ during low-cycle fatigue with compressive loading

3.3.3 Validation of Fracture Analysis in Component Systems

The elbow and reducer components were tested under quasi-static displacement-control monotonic and cyclic loading conditions. These tests were conducted to evaluate the ultimate strength of cracked components and to determine the corresponding margin of the safety. Figure 1 (in the Introduction Section) shows a schematic overview of the component test program for degraded PLR piping. Two types of tests were conducted using the reducer and elbow components containing simulated cracking (Figure 1). The component test specimens (reducer and elbow) were designed to have a simulated circumferential crack made by electronic discharge machining (EDM) in the welded joints. Two types of cracks were considered, named Type A and Type B in Figure 5. The base metal was stainless steel (316L) and the test specimens were pressurized to 8.1 MPa. This study focused on the analysis and validation of the reducer and damage response of the Type A crack.

Figure 38 shows the geometric dimensions and a schematic view of the crack. The stress-strain curve of a typical base metal was provided by JNES and is shown in Figure 39(a). The J-resistance curve was not available from JNES so it was obtained from past NRC project efforts, and is shown in Figure 39(b). The stress-strain curve, in conjunction with the J-R curve, was used to calculate the moment versus rotation-due-to-the-crack curves for the initial surface crack using J-Tearing methods. These curves are also used for the circumferential through-wall crack having the same length as the initial circumferential surface crack using J-Tearing theory. Figure 40 gives the moment versus rotation-due-to-the-crack curves for a circumferential surface cracked pipe and a circumferential through-wall cracked pipe separately. In reality, the crack will grow from surface, become a through-wall crack, and then completely break. Therefore, a combination curve of surface to through-wall crack is defined as in Figure 41(a), which is used as input for FEA analysis.

JNES[1] conducted component tests for cases EM-1 to EM-4 for both the elbow and reducer under monotonic loading. Since the present study was focused on the Type A crack for the reducer, EM-3 test data were used to compare and validate the FEA results. Figure 42 shows the results of ABAQUS and the measurement data for the load-displacement history. The black triangle-marked curve is the test data named as EM-3, while the square-marked curve shows the ABAQUS predicted load-displacement history under this monotonic loading with the assumed J-R curve. The ABAQUS prediction was higher than the experimental load. This may be due to lack of an actual J-R curve for crack resistance of the weld metal (recall that we used a J-R curve from the past NRC testing work), or variability of the strength of the stainless steel materials in this test. The coupons were apparently cut from a pipe segment with D_o=216.3 mm and t=12.7mm. The test coupons had a diameter of 4 mm.

Therefore, a reduction factor was applied to the J-R curve to match the actual load displacement curve of the experiment. (Cracks in other components may change slightly due to the statistical variability of these properties too.) The diamond-marked curve in Figure 42 shows predicted results with the 85% reduction calibration of the maximum load and the measurement and FEA prediction match well.

The moment-rotation curve calculated from the calibrated J-R curve was also used for the reducer test ES-1 under cyclic loading. This curve is shown in Figure 41(b). In JNES test ES-1, a reducer element was tested under sinusoidal loading, in which the surface crack grew through the thickness and leaked on the 29th cycle. Figure 43 shows the load-displacement history from the measurement in the ES-1 test and from the ABAQUS prediction using the same "cracked-pipe element" moment versus rotation curve shown in Figure 41(b). They are in good agreement and the calibrated J-R curve will be used to calculate moment-rotation curves for all cracks in the combined-component testing, i.e., the PLR scaled piping systems, presented in the next section. However, note that the behavior is in the very small-scale plasticity region at this load level. The "connector element" is behaving almost elastically at this load level, so it will not capture the low-cycle fatigue growth with this small-scale plasticity. A separate Dowling ΔJ analysis would be needed for this low-cycle fatigue analysis. With the EDM machined notch, there may also be some cycles to initiate a fatigue crack from the notch, so the crack growth in the test may not be indicative of a sharp crack in service.

The results discussed above present a thorough validation of both the NRC, IPIRG and the JNES component tests, and show that the connector element approach is an efficient way to simulate crack growth under static and dynamic loading condition, with reasonable accuracy. For very small-scale plasticity a separate low-cycle fatigue analysis is needed using Dowling approach (Section 3.6). Even though the weld metal properties for the JNES weld material were not available, the "cracked-pipe element" moment-versus-rotation curve used was calibrated by comparisons with component test data. It is possible to make reasonable nonlinear predictions with low-cycle fatigue crack growth and hysteresis loop (energy damping) using the simple "cracked-pipe element" in the FE model, i.e., using one connector element and 20 to 25 pipe beam elements. Multiple crack growth simulation in the piping system is possible by using this novel feature of the connector element in comparison to the more conventional fracture analysis, which requires a very fine mesh for modeling one crack (frequently up to 15,000 elements per surface crack) for proper mesh refinement of a surface crack for fracture mechanics analyses. The efficiency of this "cracked-pipe element" approach allows for completion of multiple crack analyses compared with the extremely time consuming full model solution normally needed for this type of analysis. Additionally, if a full 3D model was used, it would be necessary to have a crack growth criteria and possible re-meshing during the seismic test simulation. This greatly complicates the analysis, whereas the "cracked-pipe element" is capable of automatically capturing low-cycle fatigue damage (with large-scale plasticity), ductile tearing, and the ultimate failure of the material during the simulated seismic loading if the loading is close to failure. If the loading is very low and in the elastic region or small-scale plasticity region, the "cracked-pipe element" is not capable of capturing the fatigue damage. Calculation

of the high-cycle fatigue or low-cycle fatigue damage with small-scale plasticity can be done outside of the dynamic analysis since there would be no interaction between the elastic behavior of the crack and the elastic loading of the pipe system. As an additional note, a blunt EDM notch may also take some cycles to initiate a fatigue crack from the EDM notch.

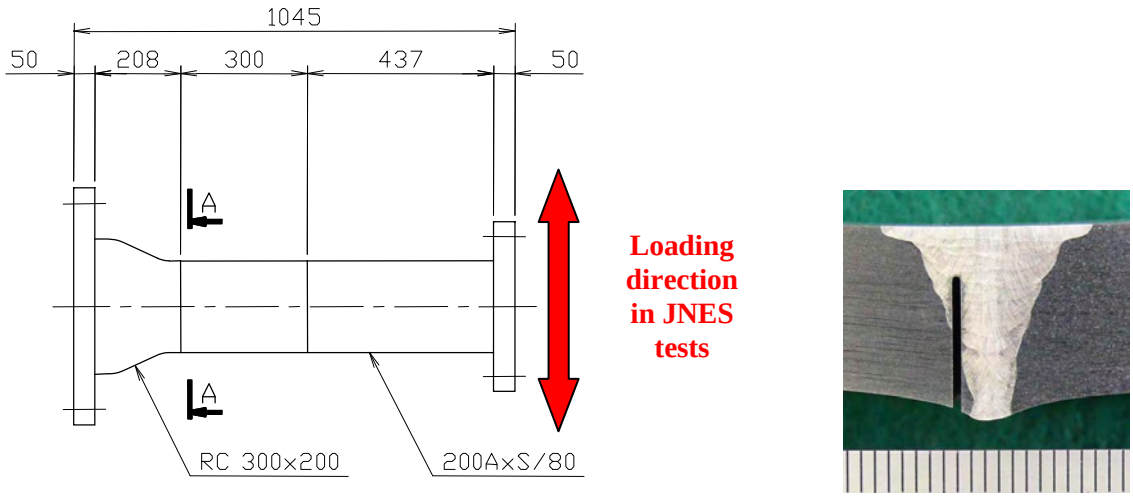

Figure 38 Dimension of reducer, the schematic view of crack and testing setup

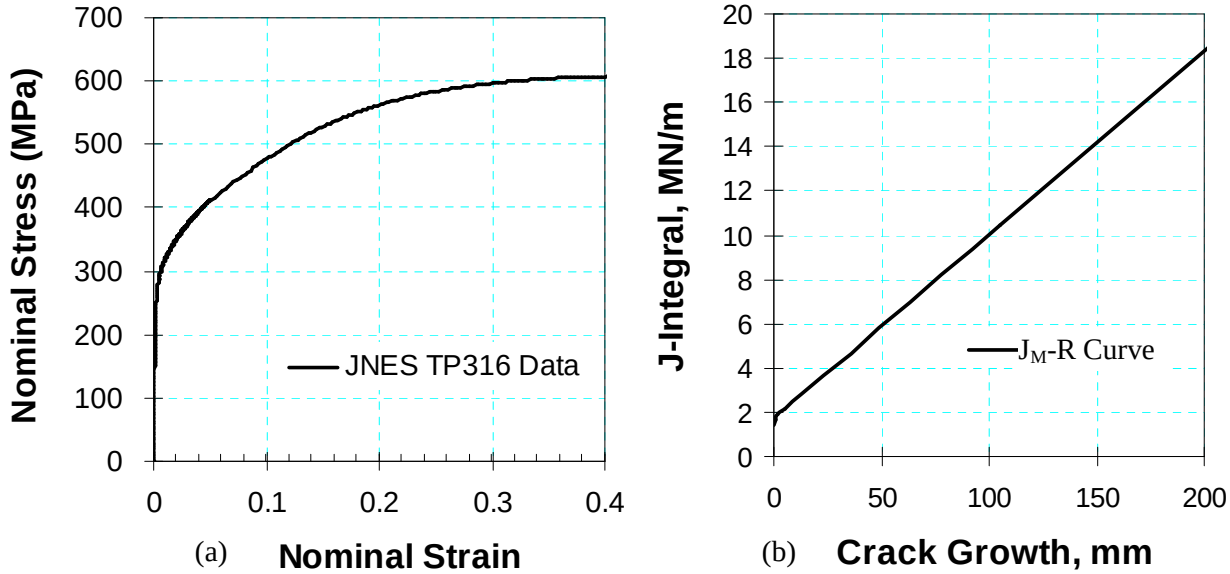

Figure 39 Stress-strain curve (from JNES) and J-R curve for TP308 TIG weld at 20°C used for initial estimate of toughness of GTAW

(Note, the J-R curve shown is the Modified J-R curve or J_M-R curve, where past experience[2] has shown it is more accurate for predicting large crack growth for circumferential through-wall-cracked pipes.)

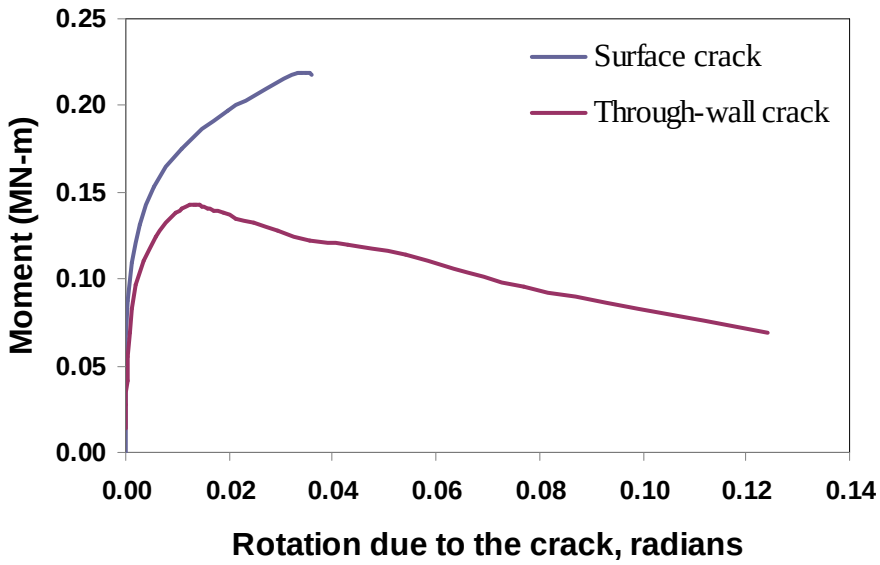

Figure 40 Moment versus rotation-due-to-the-crack curves for circumferential surface and through-wall cracks in pipes under bending with internal pressure (Type A surface crack in 203-mm (8-inch) nominal diameter TP316 stainless steel pipe and girth weld)

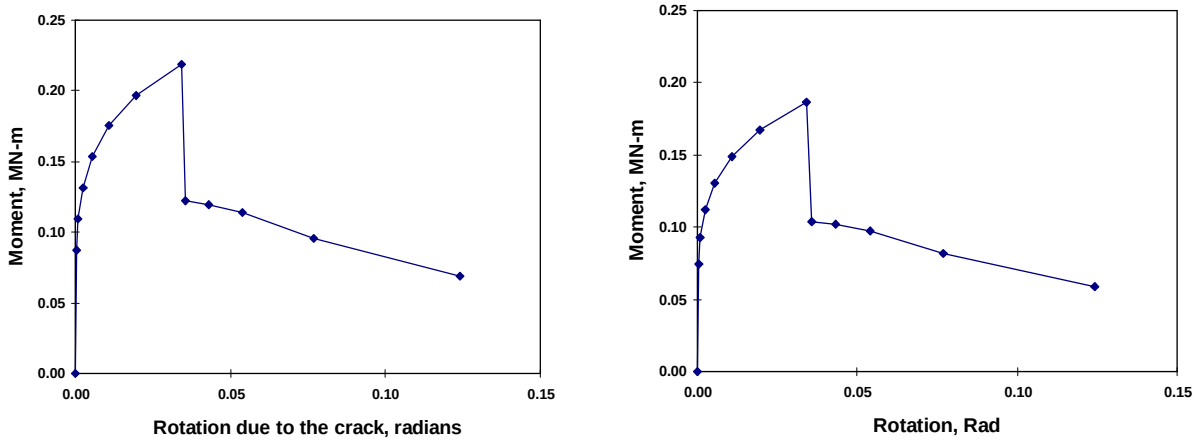

(a) Using assumed J-R curve from other NRC programs and JNES stress-strain curve

(b) with load reduced by 85%

Figure 41 Moment versus rotation-due-to-the-crack curves from circumferential surface to through-wall cracks. Case (b) represents the moment-rotation curve produced using an 85% reduction of the load obtained from past NRC programs. The "cracked-pipe element" for the JNES combined-component test analyses used the Case (b) curve.

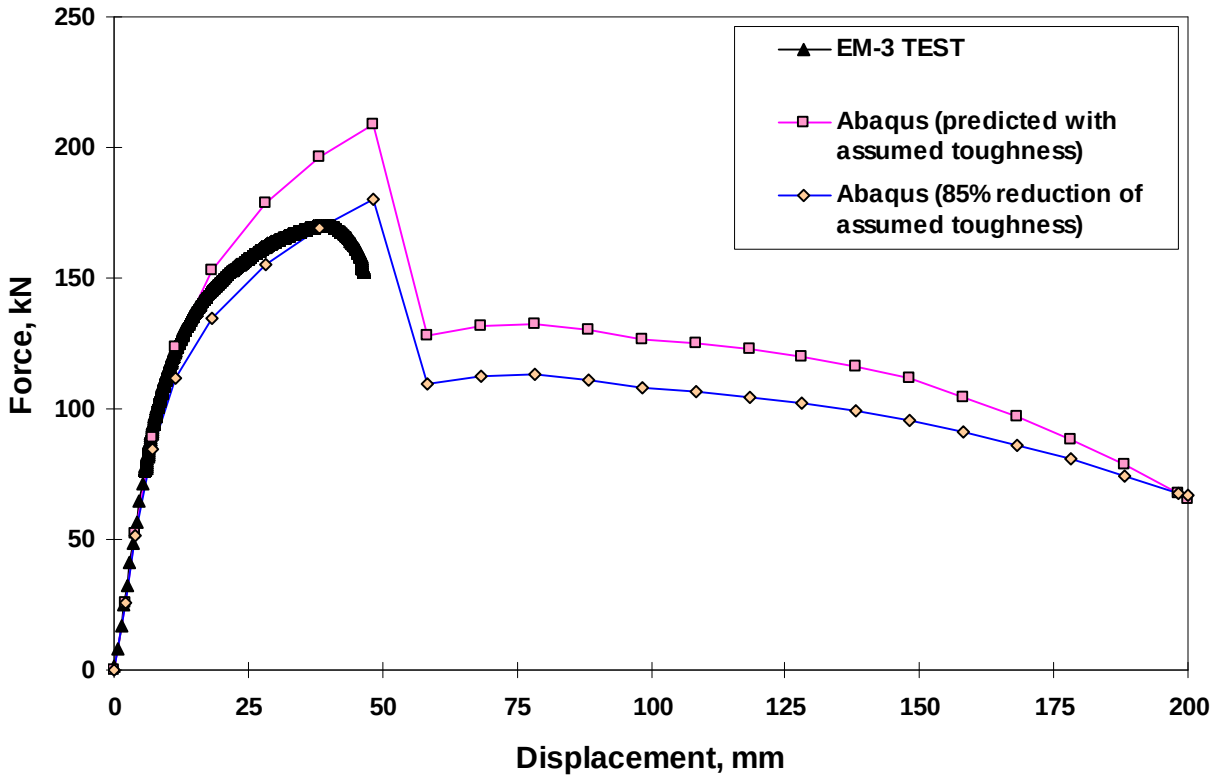

Figure 42 Load versus load-point displacement history for JNES Test EM-3 and ABAQUS predictions

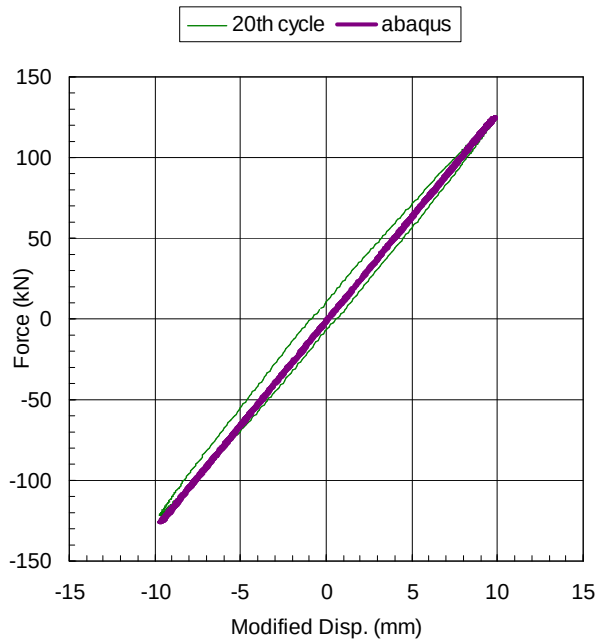

Figure 43 Load versus load-line displacement history from JNES Test ES-1 data and ABAQUS predictions for cyclic loading

3.4 Analysis of JNES Pipe System Test

The main purpose of this program was to conduct detailed analyses of JNES degraded piping system tests with circumferential surface flaws under seismic loading to gain insights on how the results might assist NRC efforts that consider seismic effects on degraded nuclear piping. The modeling can provide important information on; (1) seismic LOCA analyses for Transition Break Size development, (2) margins in pipe flaw evaluation procedures, (3) better understanding of Leak-Before-Break behavior, and (4) seismic design stress rule changes. Most past work for circumferential cracks in welds between straight pipes in nuclear piping systems was not prototypical of plant installations. The JNES case involves a more prototypical pipe system, and cracks at more prototypical locations, i.e., in girth welds by nozzles, at elbow girth welds, and tee girth welds to straight pipe.

Referring to Figure 1 and Figure 7 presented earlier, the nominal outer diameter of the main pipe diameter in the 1/3-scaled PLR system is 216 mm (8.5 inch) and the thickness is 12.7 mm; the outer diameter of a branch pipe in the scaled PLR system is 114 mm and the thickness is 9 mm. The mesh and three crack locations are shown in Figure 44. The three cracks are located at a tee connection, a reducer, and an elbow.

The circumferential surface flaws were electronic discharge machining (EDM) notches and no shim was put in the notched area to take compressive loads. The shims would be used to model crack face contact and closure for a tight crack subjected to cyclic loading during compression portions of the cycle. The crack orientations are shown in Figure 45. In order to study the growth of simulated cracks under seismic loading conditions, JNES conducted a series of experiments labeled FTP-1, FTP-2, FTP-3 and FTP-4. This study focused on the analysis of FTP-4 since this is the only test that led to a leak. The simulated seismic loading was generally more than 1.5 times of the Japanese S2 level (the original plan was $1.5 \times S2 \approx 1.5$ g, while the actual measurement at the shaking table top was about 2 g), and leakage occurred in the last of the 6 large seismic loading series for FTP-4. There are six consecutive acceleration-time histories applied to the base of the shaking table: CO-30 through CO-35 and the final case (CO-35) led to a through-wall crack and leakage. Actually, there were other acceleration-time histories applied to the FTP-4 system that were of lower magnitude. These were not considered here since these loading blocks cannot induce crack growth. Three of the important applied acceleration histories (CO-30, CO-33, and CO-35) are shown in Figure 46 and magnified views at different intervals are shown in Figure 47. It is seen that shaker table acceleration-time histories for CO-30 to CO-35 are almost identical. Using a correction procedure that involves Lagrange multiplier based minimization, the measured acceleration-time histories were corrected so that the model system would not drift off in space at the end of the analysis due to minor noise in the measurements.

For a dynamic analysis, it is necessary to include a damping coefficient in simulations. For this study, the damping coefficient follows the Rayleigh damping model as described in ASME N-1232.1. The selected damping ratio was based on experimental damping estimates at the first mode and adjusted by case studies to consider the damping effects of plasticity in elbows and cracked sections. As shown in previous sections on the validation of component tests (both JNES and the NRC tests), in order to simulate the crack behavior, it is necessary to have a moment versus rotation-due-to-the-crack curve for each crack location. Therefore, as discussed above the stress-strain curves of materials and proper fracture toughness (J-R curve) are necessary to calculate moment-rotation for the "cracked-pipe element." Typical stress-strain curves for the pipe materials were supplied by JNES. However, no fracture toughness (J-R curve) or weld metal stress-strain curves were available. The variability of these properties was unknown, but some statistical data is available for probabilistic analyses being conducted for the NRC[20]. The moment versus rotation-due-to-the-crack curves for the flaws in the main pipe and branch pipe were obtained at room temperature (Figure 48) and 288°C (550°F) (Figure 49). These

analyses will give insight into the crack response at both room temperature and high temperature. This is important since the margins might be different at actual BWR and PWR nuclear plant operating temperatures.

Referring again to Figure 44, there were three cracks in the JNES test piping system. Crack 1 is in the girth weld between the elbow and straight pipe region. Crack 2 is located at the reducer, and Crack 3 is near the Tee junction in the smaller-diameter branch pipe. It turns out that Crack 2 began to leak during application of the final acceleration-time history (CO-35). From the J-tearing analysis discussed earlier concerning Figure 42 and Figure 48, the moment versus rotation-due-to-crack curves were obtained. This moment-rotation curve was then input to the finite element model as 'cracked-pipe element' to model the response of the crack in a convenient, albeit simple, fashion. From the fracture mechanics analysis used to develop the cracked-pipe moment-rotation curve, the surface crack was predicted to initiate in the main pipe when the moment reaches a level of 0.181 MN-m. However, when the load reaches 0.181 MN-m, and the crack begins to grow, the cracked pipe response will reflect this in the form of moment-rotation response. However, the major affect is when a surface crack breaks to a through-wall crack, which was not predicted here. Interestingly, it will be seen that the moments produced at the crack locations from the acceleration-time histories (CO30 – CO35) have a maximum value of about 0.145 MN-m during the CO-35 test. More will be discussed about this later after showing results of the cracked-pipe analyses.

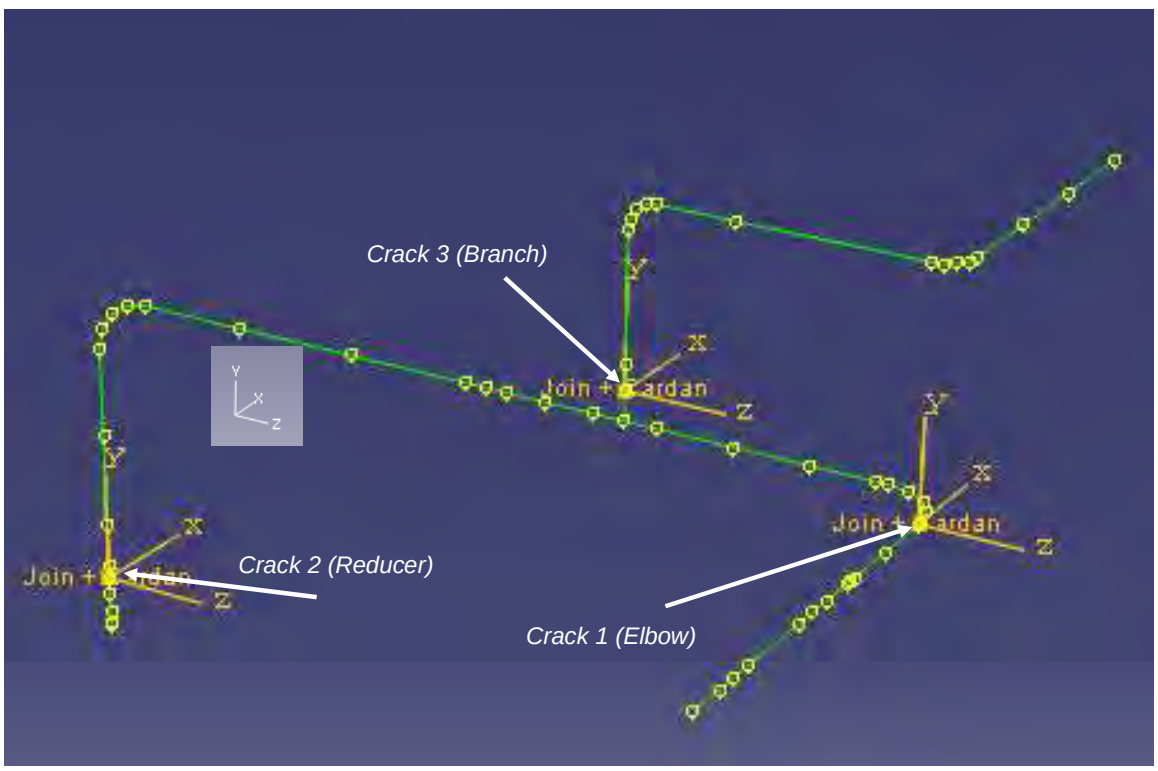

Figure 44 Mesh and crack locations of the scaled PLR system (Test FTP-4)

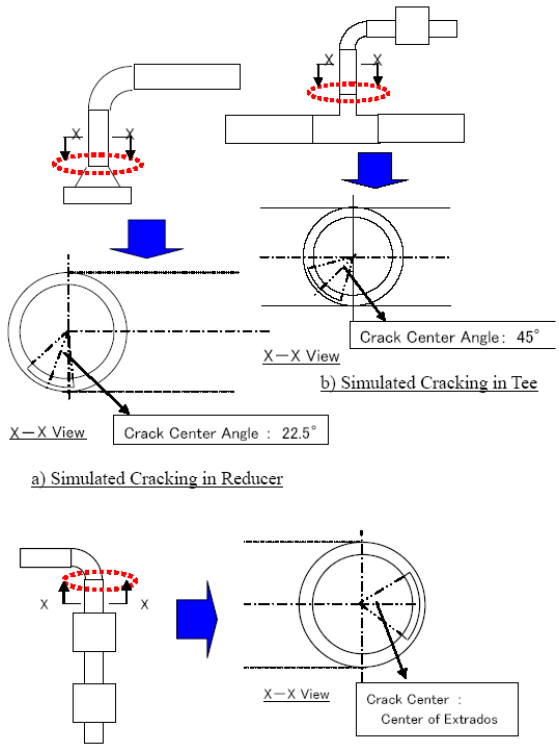

Figure 45 Location and directions of simulated cracking of Type A for test FTP-4

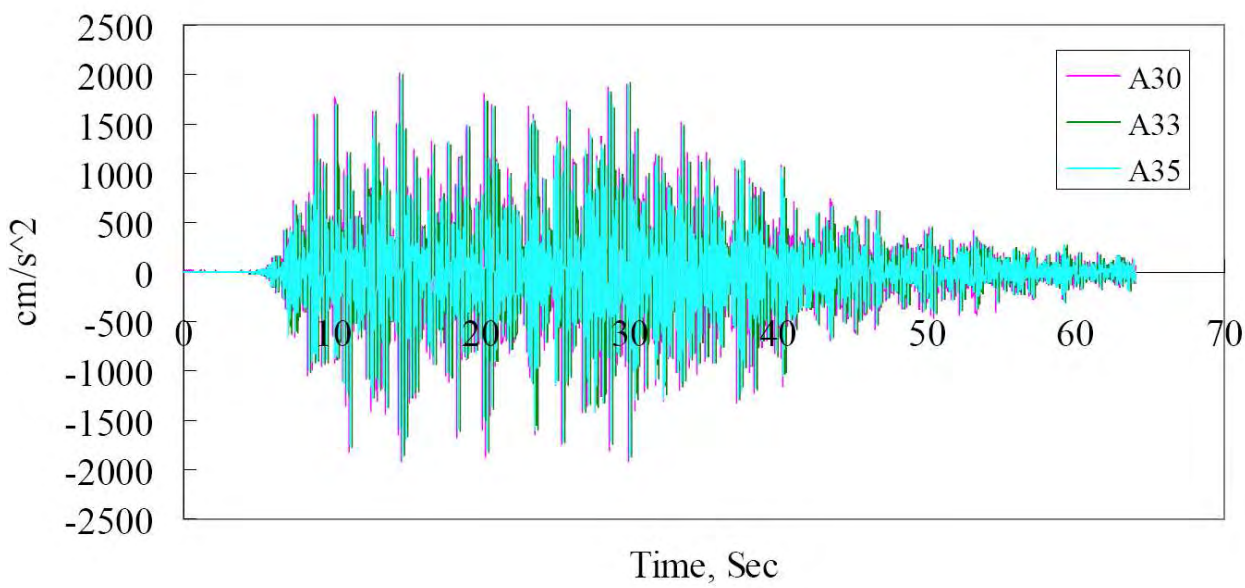

Figure 46 Applied acceleration histories for PLR system in Test FTP-4 (Load blocks CO-30, CO-33, and CO-35)

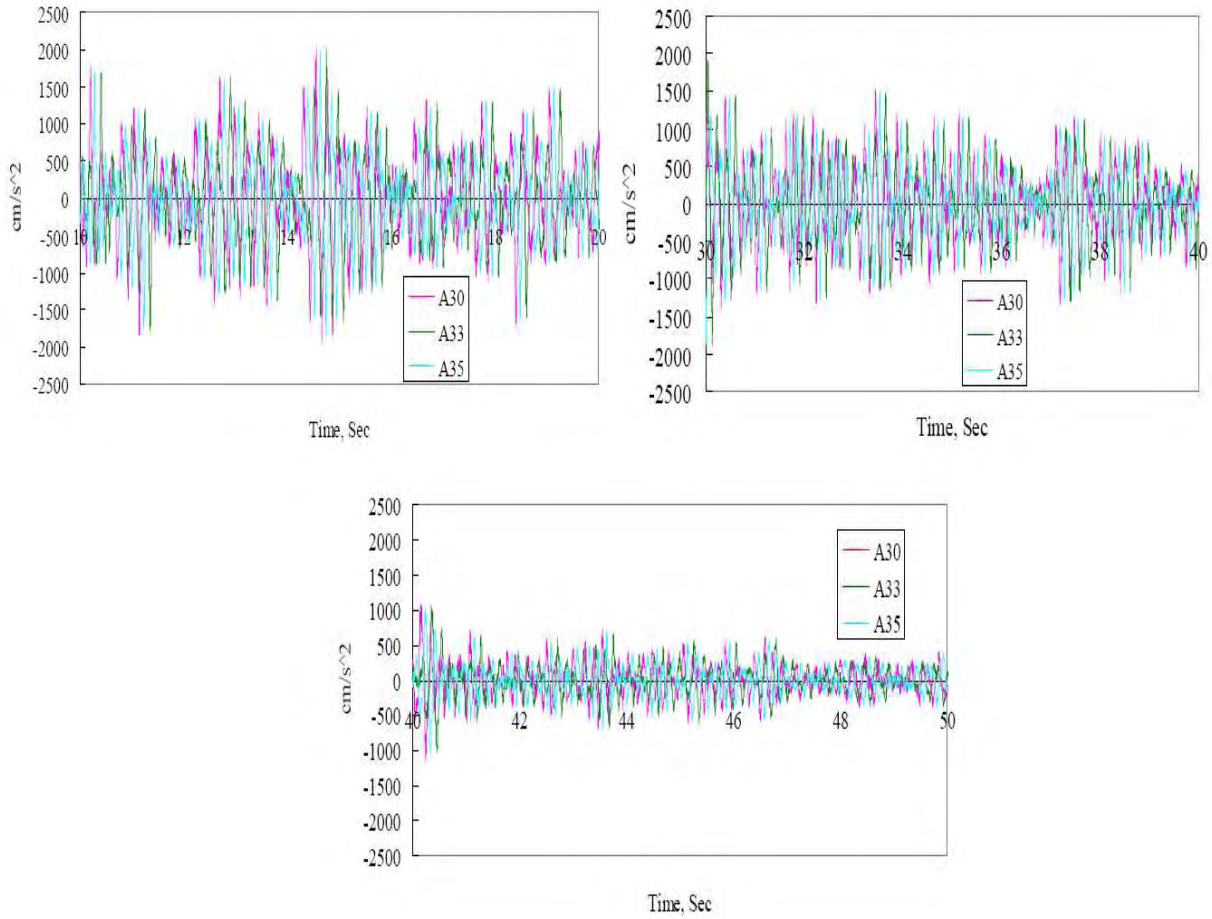

Figure 47 Different intervals of applied acceleration histories for PLR system (Test FTP-4, load steps CO-30, CO-33, and CO-35)

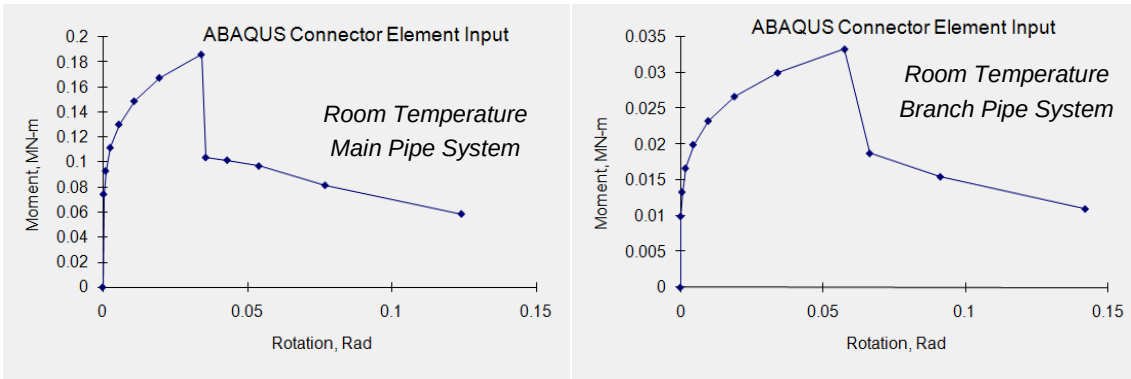

(a) (b)

Figure 48 Moment versus rotation-due-to-the-crack curves for Type A flaws in the main pipe and branch pipe flaw locations at room temperature

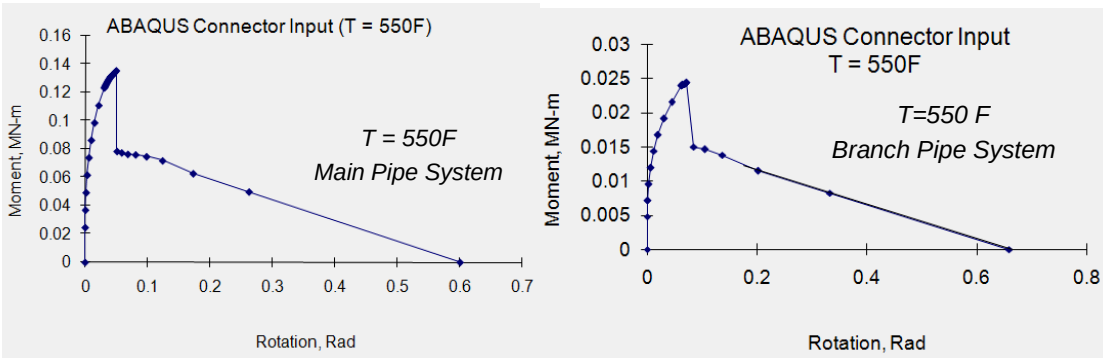

(a) (b)

Figure 49 Moment versus rotation-due-to-the-crack curves for Type A flaws in the main pipe and branch pipe flaw locations at high temperature (288°C, 550°F)

3.4.1 Damping Considerations

Several analyses were made using different damping coefficients. Proper damping can play a key role in the accuracy of the solutions. Figure 50 shows the plasticity contour plot of PLR with no damping and it is found there was about 16% plasticity around the elbow area. A typical damping factor may be 3% to 5% for elastic design purposes. The IPIRG piping system, which likewise considered seismic loading of a cracked-pipe system[12], had experimentally measured damping of 0.5%. For this study of C0-30 to CO-35 series test, the calculation of the damping coefficients follows the Rayleigh damping model as the ASME N-1232.1 procedure, i.e., α = 1.148 and β = 1.157E-04 for 2% damping specified at 5 Hz (first mode) and 50 Hz. For the case of high temperature, the same damping coefficients were used due to lack of experimental information. This should have a small effect on the predictions for the higher temperature case, shown later. However, in this report the viscous damping was also kept the same when increasing the amplitude of the acceleration to predict failure in one loading block.

The D01 displacement location of Figure 51 is one location for measuring displacement history near the reducer crack. Figure 52 shows the comparison of measured and predicted displacement history at location D01 when using 2% damping. The overall trend and magnitude of Figure 52(a) compares well with the test measurements. Figure 52 (b) shows the comparison for times between 335 and 345 seconds.

The comparison is good although the predictions are higher than the measurements in the time period 335 to 345 seconds. Figure 53(a) and (b) show comparisons at different time intervals. In general, measurement and predicted data are similar except between time 340 and time 345. It should be noted that the D01displacement responses are much smaller than D07.

Displacement comparisons were also made at the simulated pump location (D07) shown in Figure 51. Figure 54(a) gives the overall comparison between the measured and predicted displacement results and Figure 54(b) through Figure 54(d) are the magnified views at different intervals. Overall magnitude and trend are agreeable, while predicted data is a little larger than the measurements over some time durations. This could be due to the simplified model assumptions where pipe and beam elements are used rather than full three-dimensional elements. However, the agreement between prediction and experiment is considered remarkable given the model simplicity. Since displacements are in good agreement, this validates that 2% damping assumption is reasonable.

Six seismic loading cases (CO-30 through CO-35) were analyzed for the FTP-4 case . In reality, there were additional seismic loading cases applied to this system prior to loading block CO-30, which apparently did not produce any damage (except perhaps high-cycle fatigue damage). The modeling procedure developed here can account for incremental low-cycle fatigue damage that occurs due to prior load history. For instance, if some low-cycle fatigue crack growth and cyclic plasticity damage occurred during load case CO-30, this nonlinear damage would serve as the starting point for load case CO-31, and so on. In other words, the history of nonlinear damage development can be properly accounted for with the "cracked-pipe element" analysis approach (using restart option in ABAQUS). However, because the seismic loading was not large in the JNES tests, no noticeable nonlinear damage occurred between each test. The comparisons of displacement predictions between considering and neglecting history effects for CO-35 showed very little difference. If the seismic loading were higher, and damage occurred during each load case, there would be clear differences in the predictions, and damage history effects would show clear differences. The effects of torsion on crack growth are not considered with this model. Fortunately, mode II fracture, which would be driven by torsion, is normally not a key driver in fracture and mode I typically dominates.

By using validated moment versus rotation-due-to-the-crack behavior for the "cracked-pipe element" and damping parameters, it is possible to evaluate the cracked piping system under seismic loading (CO-30 through CO-35). In addition, it is possible to predict low-cycle fatigue crack growth if large-scale plasticity happens. Figure 55, Figure 56 and Figure 57 are the moment histories in the plane of the crack at the crack locations by the elbow, reducer, and branch pipe at room temperature under loading blocks CO-30 through CO-35 shaking accelerations. Note that each loading block lasted for about 65 seconds. Therefore, loading block CO-30 was from time 0 to 65 seconds, loading block CO-31 was from time 65 to 130 seconds, and so on until loading block CO-35 which is from about time 325 to 390 seconds. According to Figure 55, the maximum moment value over the whole history of loading at the elbow is about 0.147 MN-m, while the maximum moment at the damage point for the "cracked-pipe element" is about 0.185 MN-m, see Figure 48(a). The safety margin in terms of reaching the maximum moment is about 1.26. According to Figure 56, the maximum applied moment value over the whole history at the reducer is about 0.15 MN-m, while the maximum moment-carrying capacity of the cracked section is about 0.185 MN-m (nearly the same as elbow because these two cracks are in the main pipe with the same size). Notice that the magnitudes of the calculated moment for the elbow and reducer cracks are similar. However, the reducer crack sees more cycles of higher moments compared to the elbow (compare Figures 55 and 56). Therefore, the reducer is the critical crack location as observed in the test results. According to Figure 57, the maximum applied moment over the whole time-history at the tee-to-pipe girth weld for the branch section is about 0.015 MN-m, while the maximum moment capacity [Figure 48(b)] is about 0.033 MN-m. The safety margin in terms of the applied to the maximum moment capacity is about 2.20.

Additional analyses were conducted to assess what would have happened if these JNES tests were conducted at 288°C (550°F). (Thermal expansion stresses were not included in this analysis, but could be done, as well as seismic anchor motion stresses.) The properties of the piping and the "cracked-pipe-elements" were changed to represent operating condition at 288°C (550°F), and then the FTP-4 CO-35 loading block was applied again. Figure 58, Figure 59 and Figure 60 are the crack moment histories at elbow, reducer, and branch pipe at high temperature. The margins of the applied moments to the maximum moment-capacity at the reducer was 1.19 at 288°C (550°F). Again, the margins are calculated for moment by comparing the maximum predicted moment with the input maximum moment capacity at high temperature (Figure 49). Figure 61 shows the history of the moment versus rotation-due-to-the-crack curve at the reducer crack location at room and high temperature (288°C, 550°F). The ratcheting behavior during the loading and unloading period is also presented in Figure 61. It is clear that more damage is predicted at high temperature compared with the low temperature results, which is expected since the strength and toughness of stainless steel drops with increasing temperature.

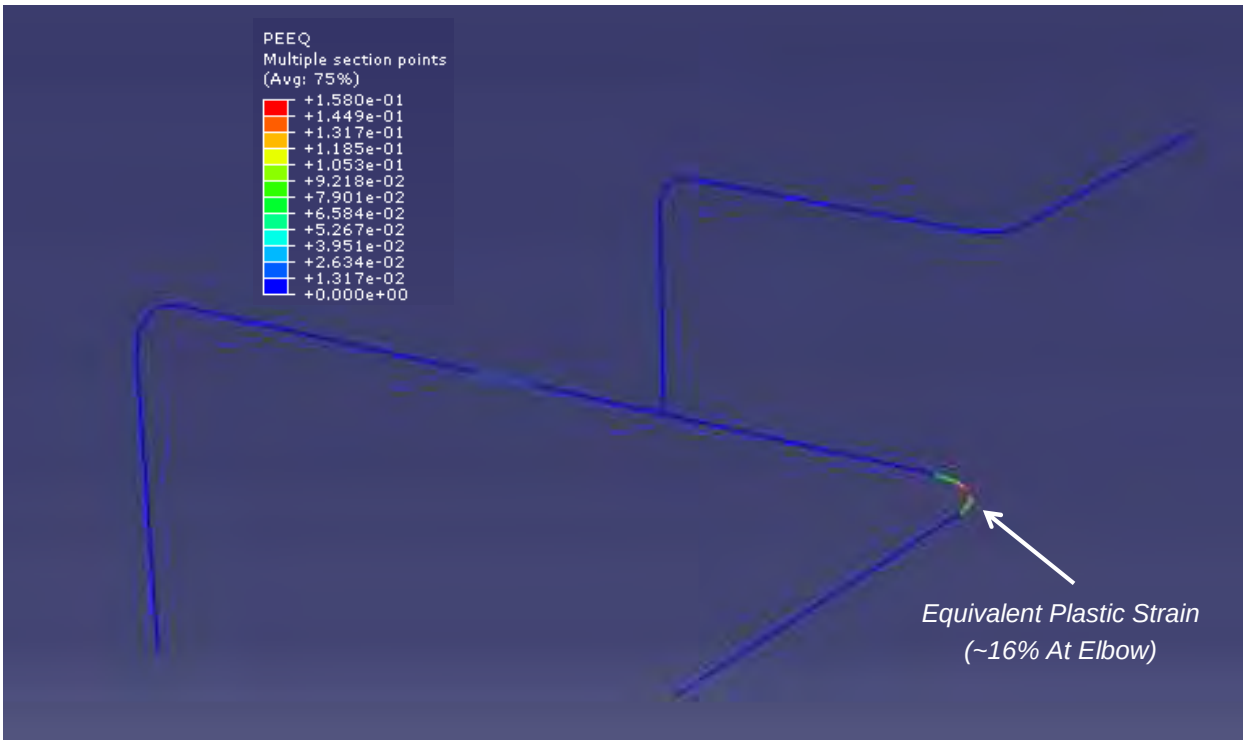

Figure 50 Plasticity contour plot of FTP-4 test system with no damping

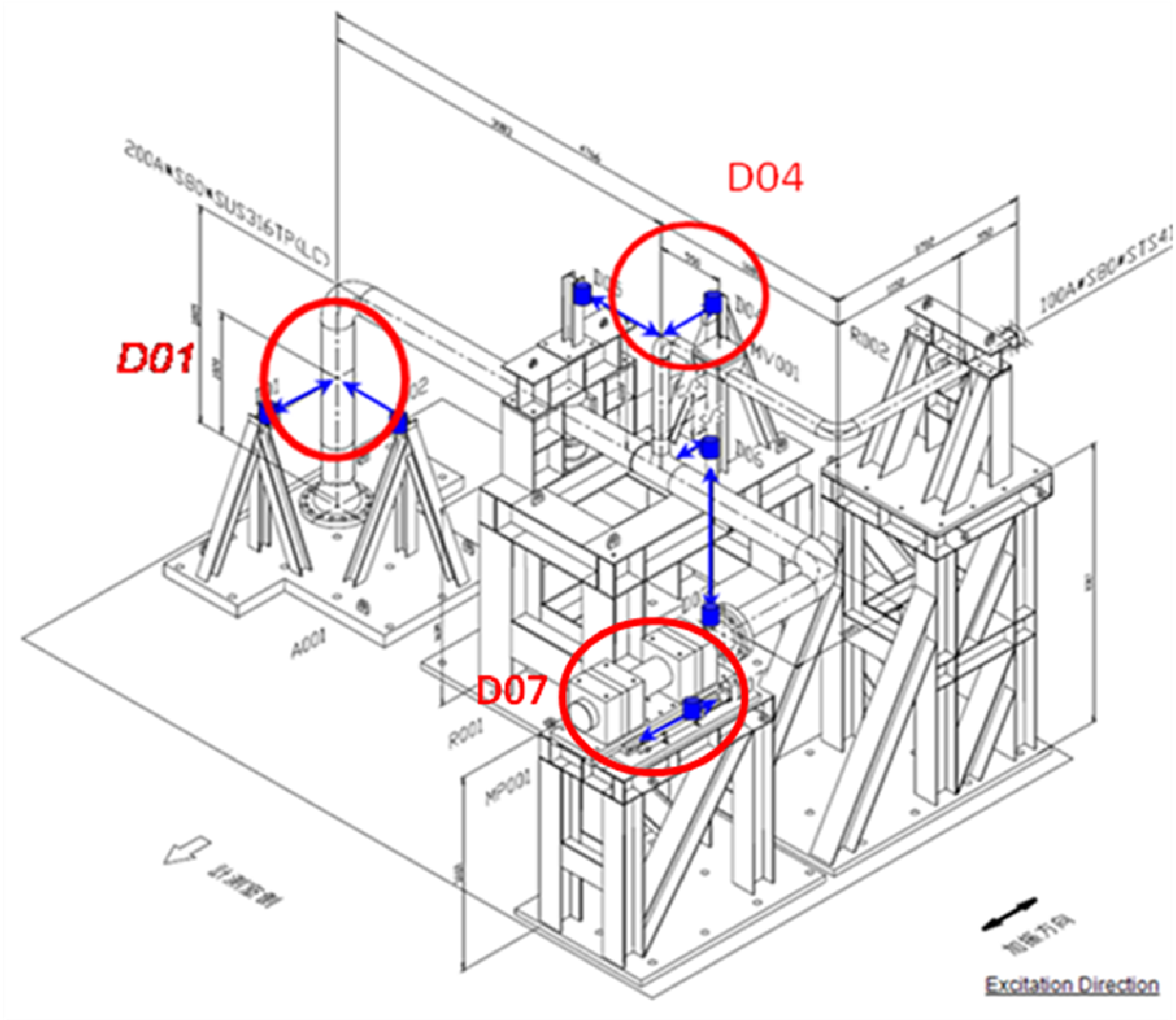

Figure 51 Displacement measurement locations DO1, DO4 and DO7 for FTP-4 test system

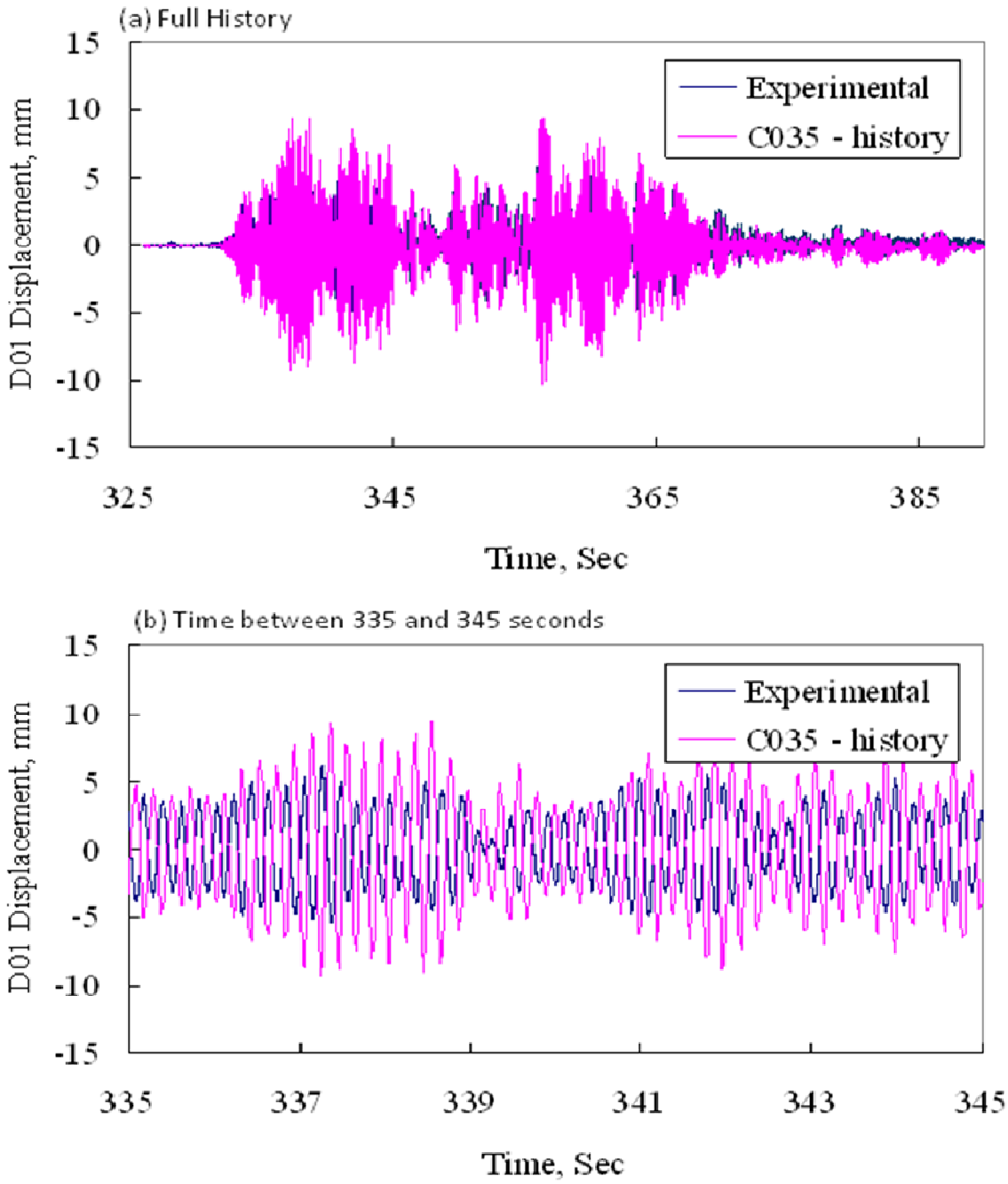

Figure 52 Comparison of displacement history between the measured and predicted values at Location DO1

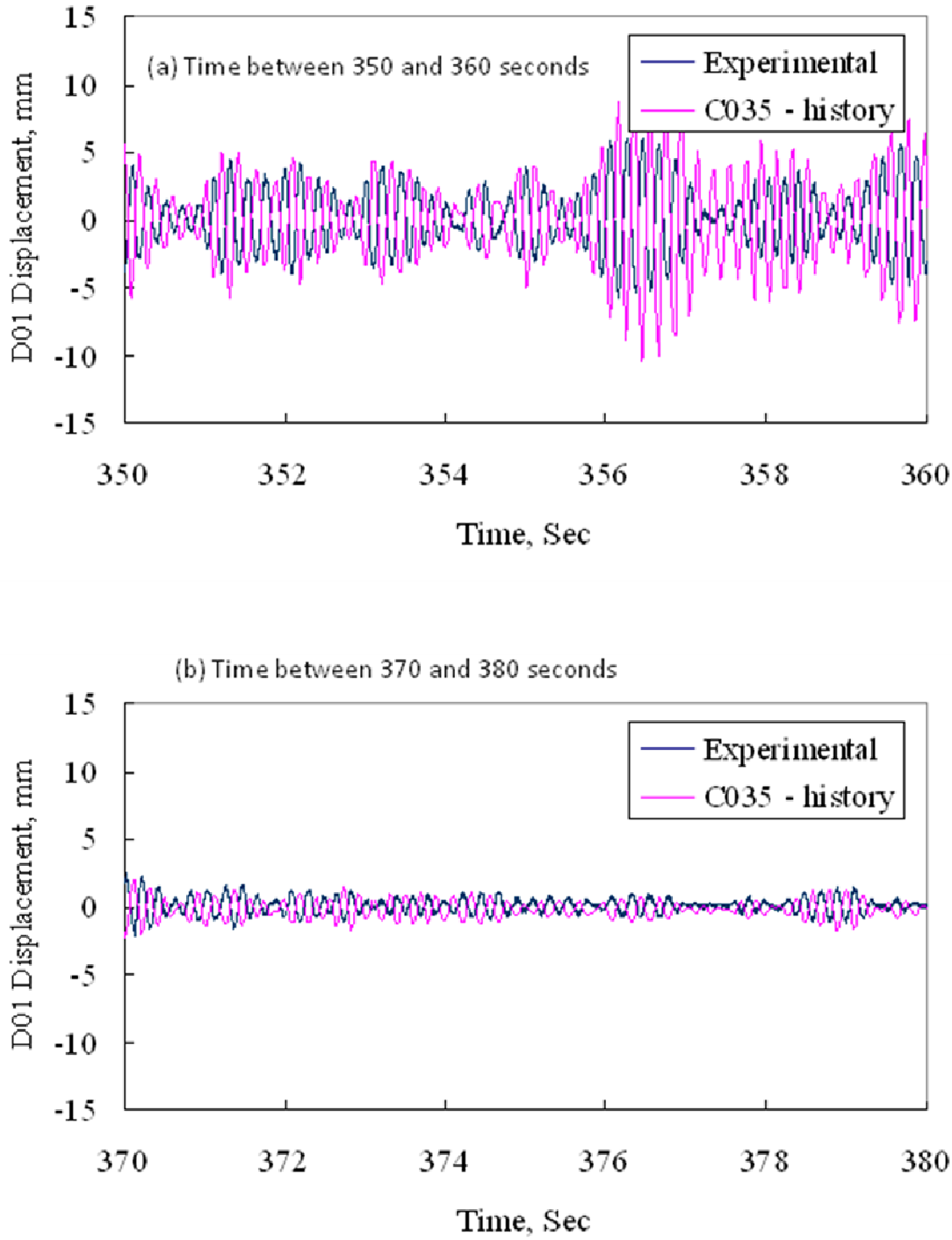

Figure 53 Comparison of displacement history between the measured and predicted values at Location DO1 at different times

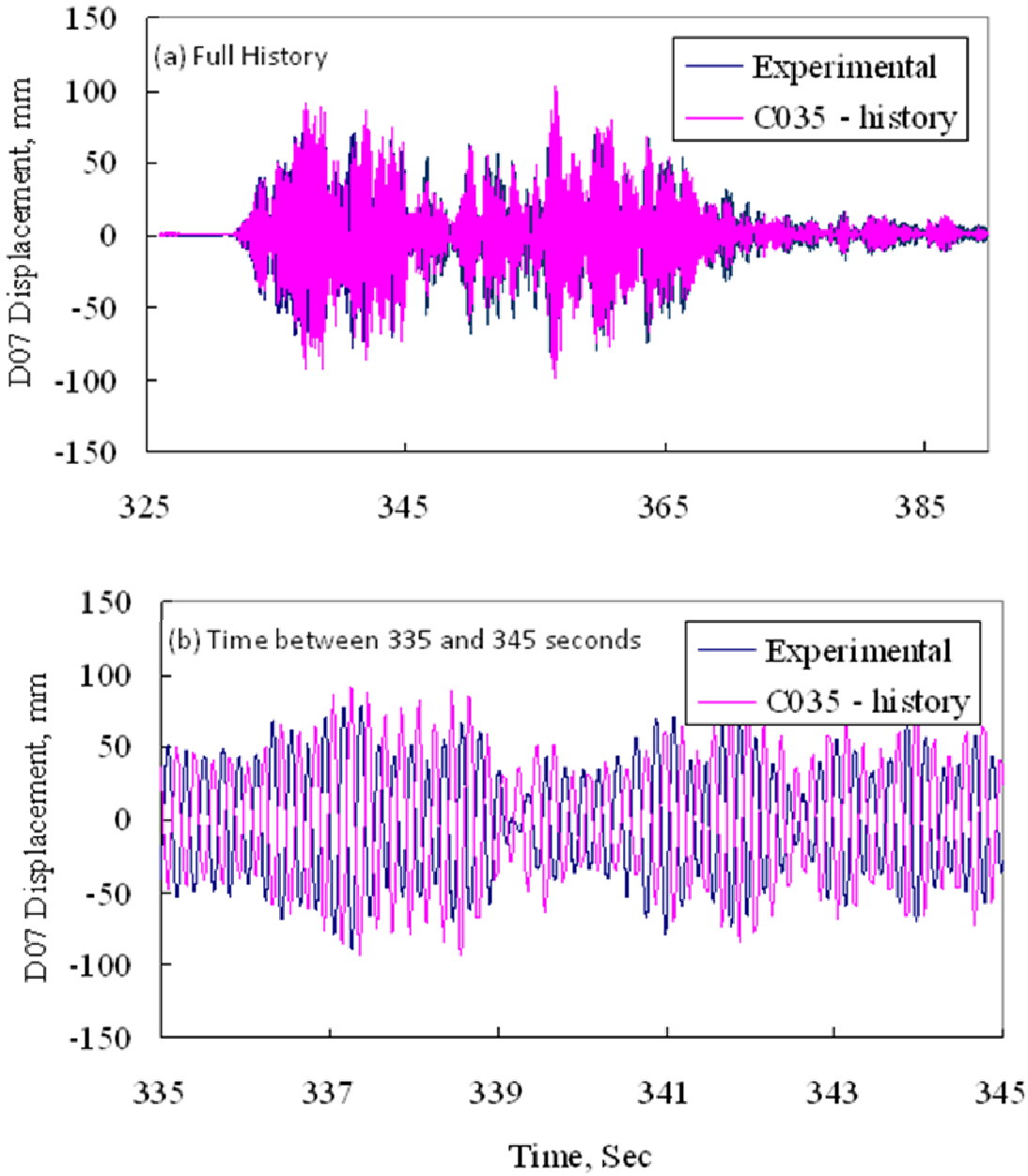

Figure 54 Comparison of displacement history between the measured and predicted values at Location DO7

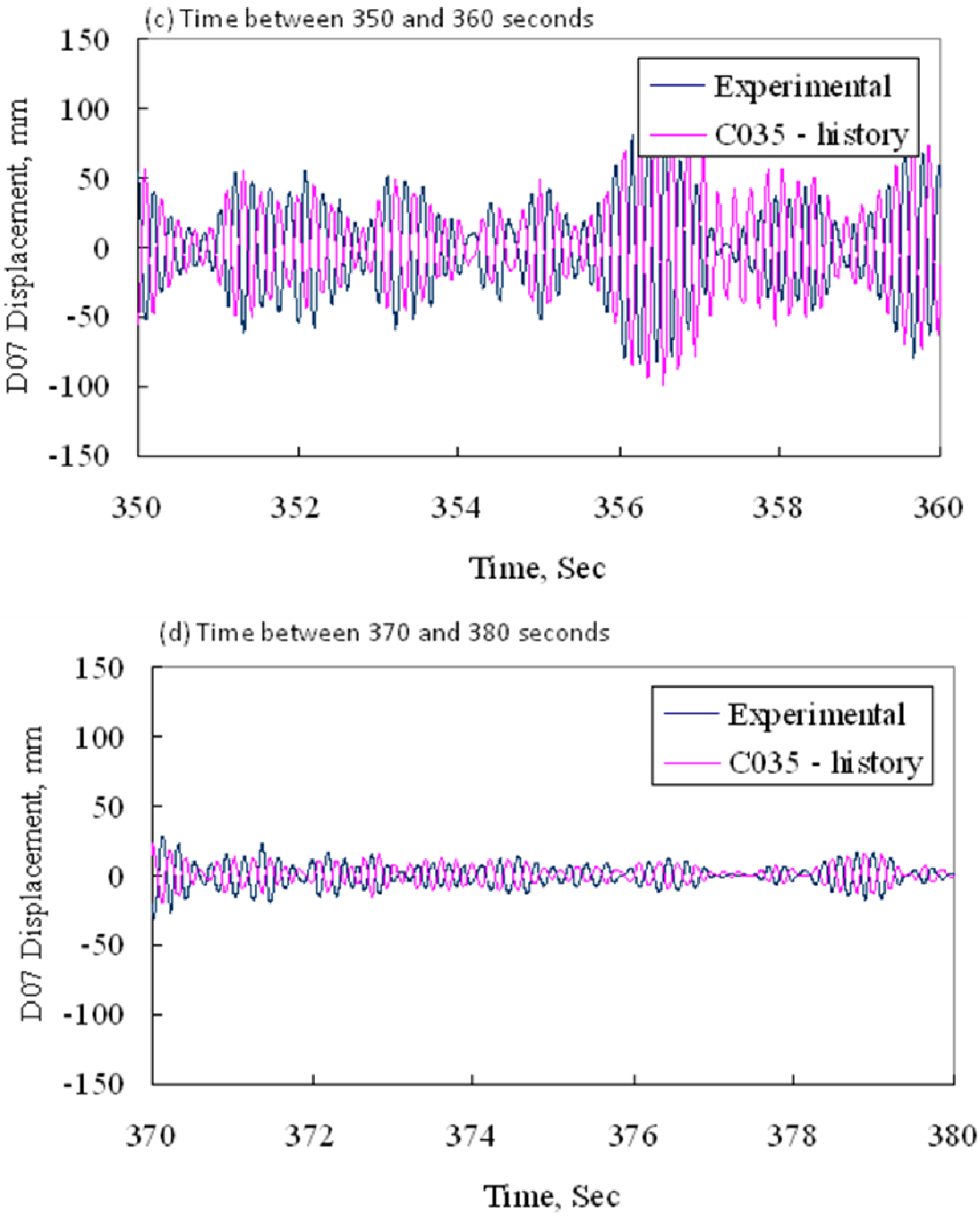

Figure 54, continued Comparison of displacement history between the measured and predicted values at Location DO7

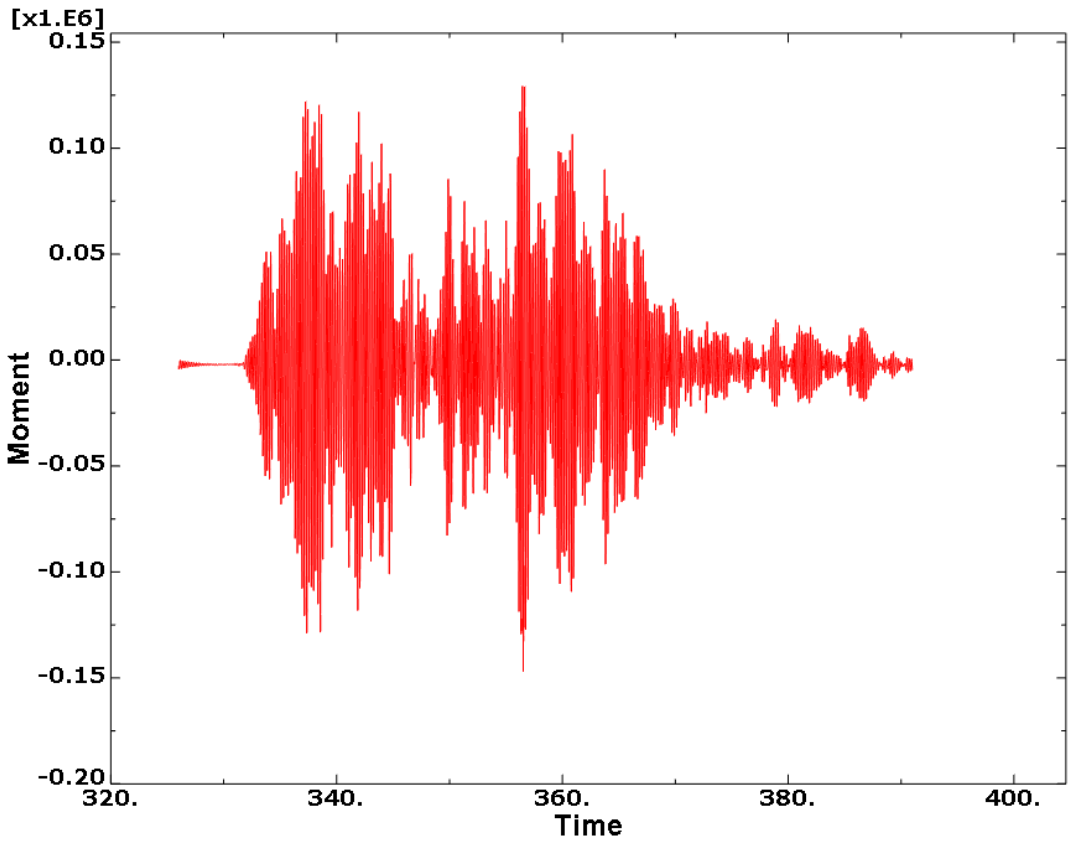

Figure 55 Calculated applied moment (MN-m) at elbow crack location at room temperature for loading block CO-35

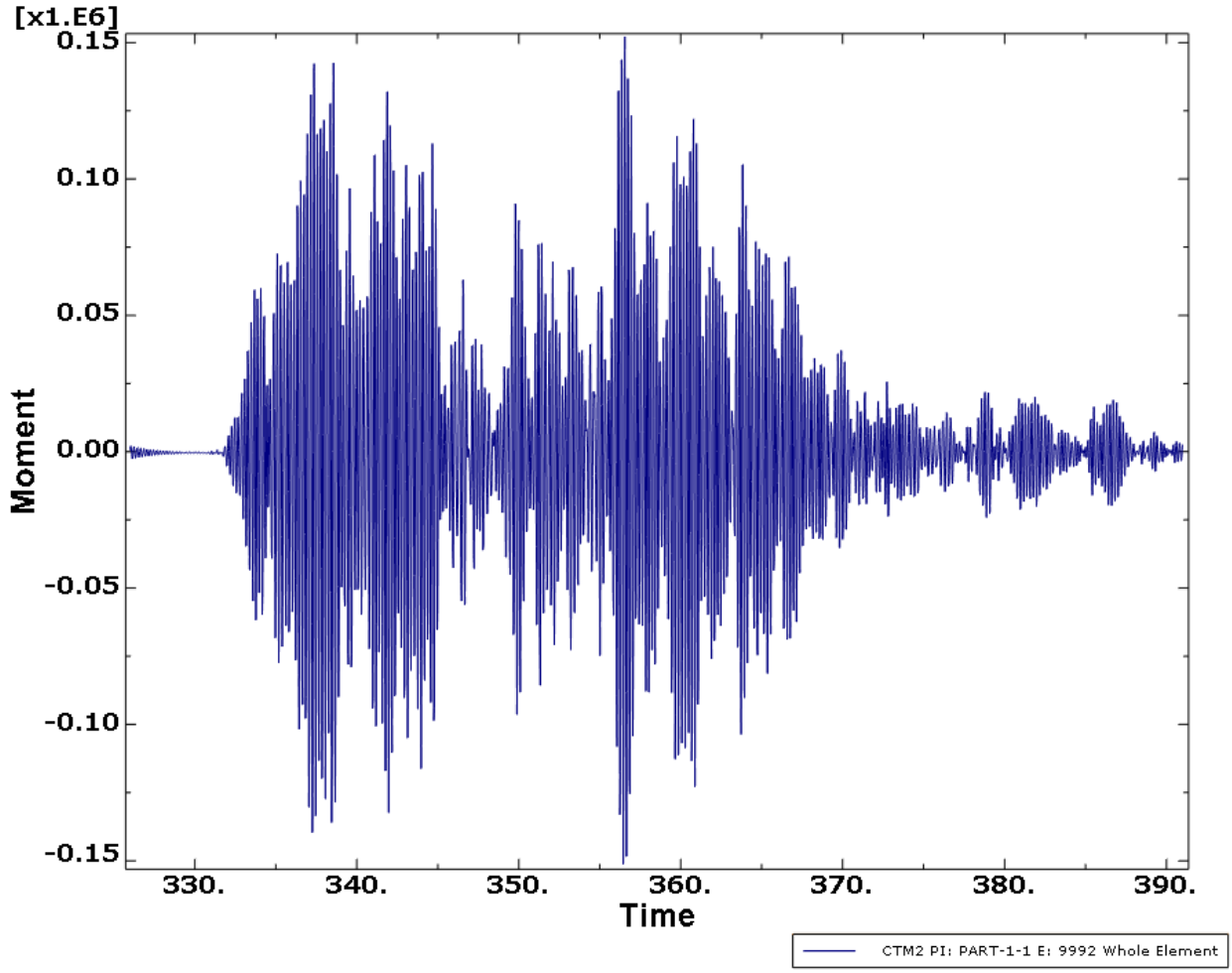

Figure 56 Calculated applied moment (MN-m) at reducer crack location at room temperature for loading block CO-35

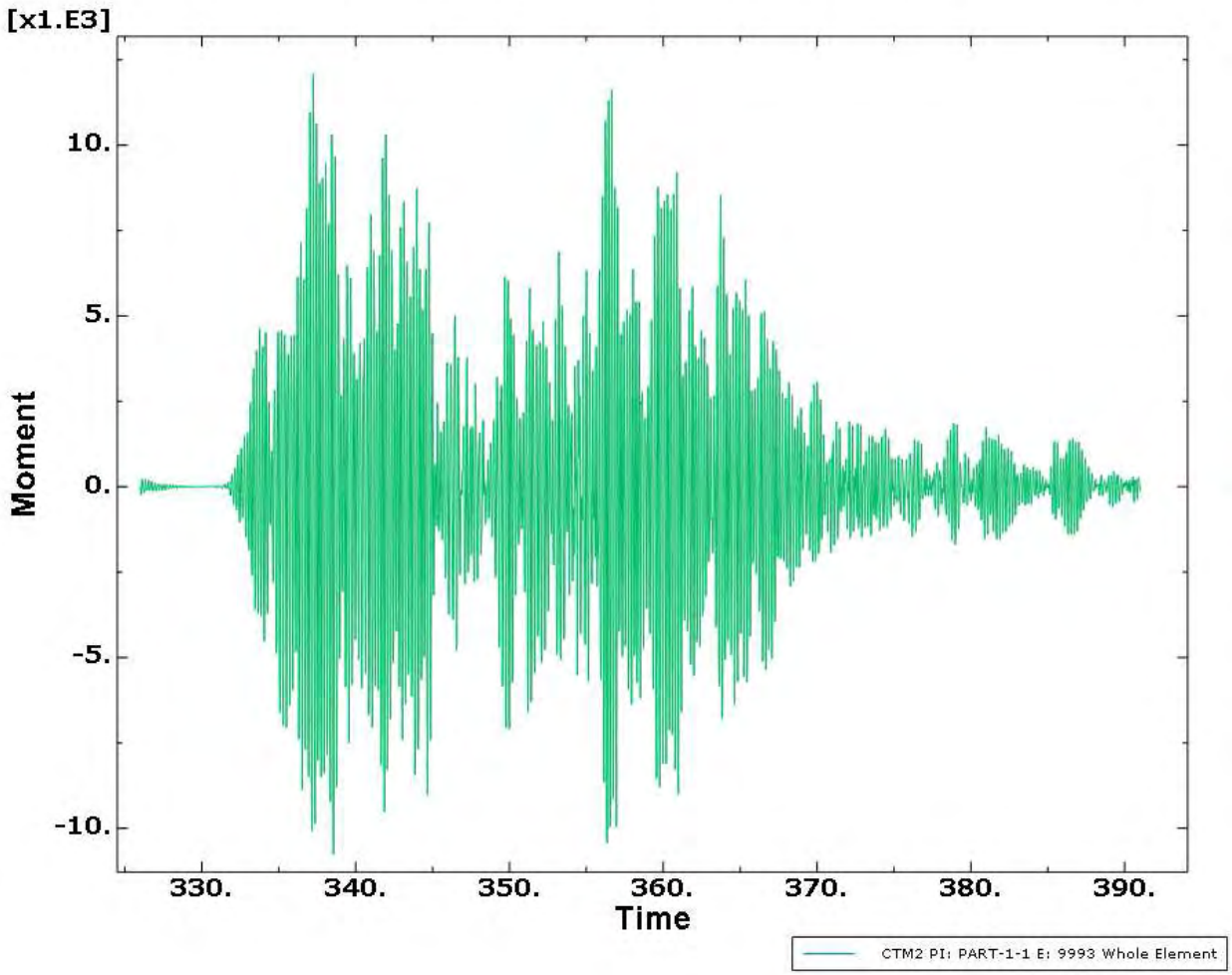

Figure 57 Calculated applied moment (KN-m) at branch connection crack at room temperature for loading block CO-35

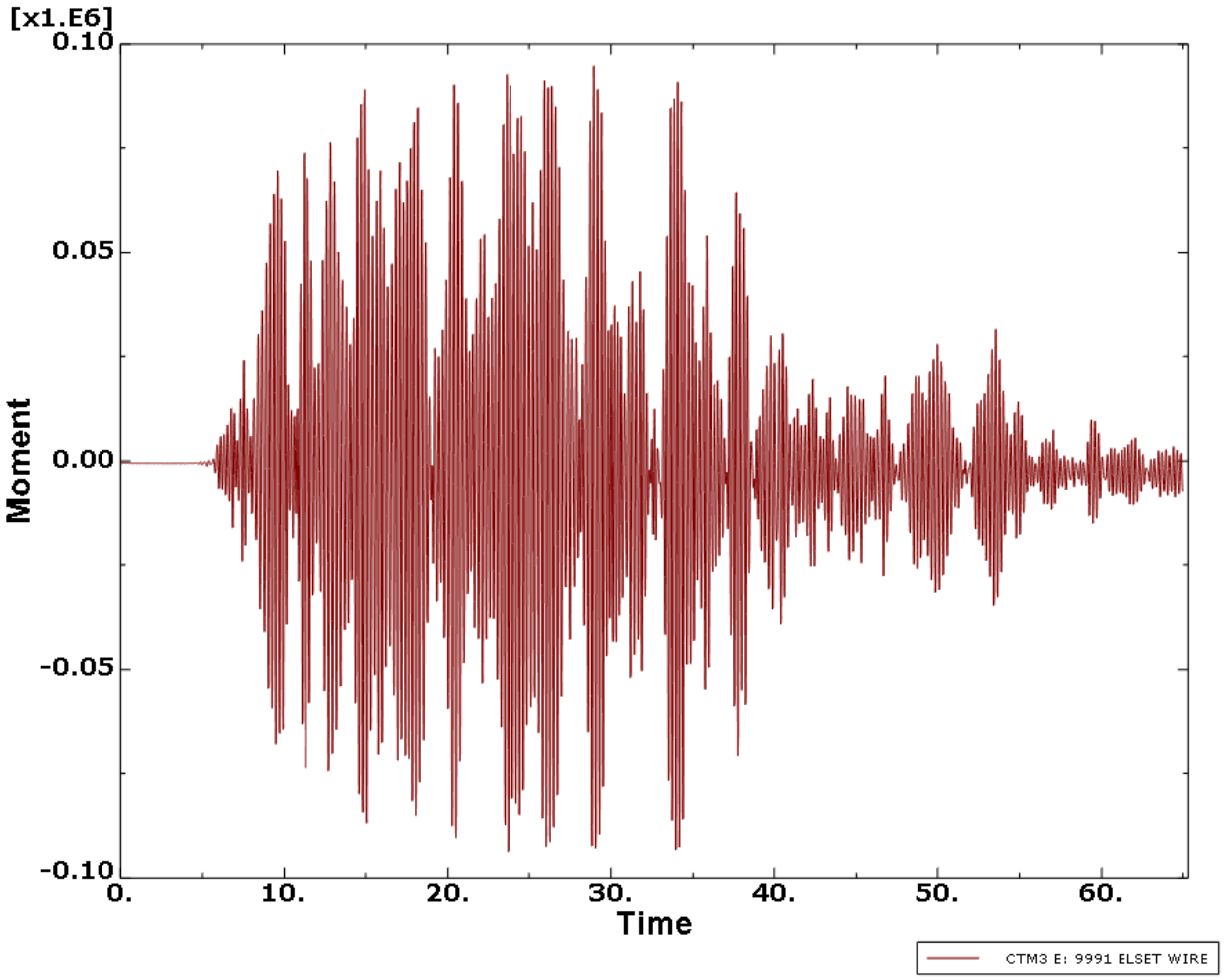

Figure 58 Calculated moment (MN-m) at elbow crack location at high temperature (288°C) using loading block CO-35

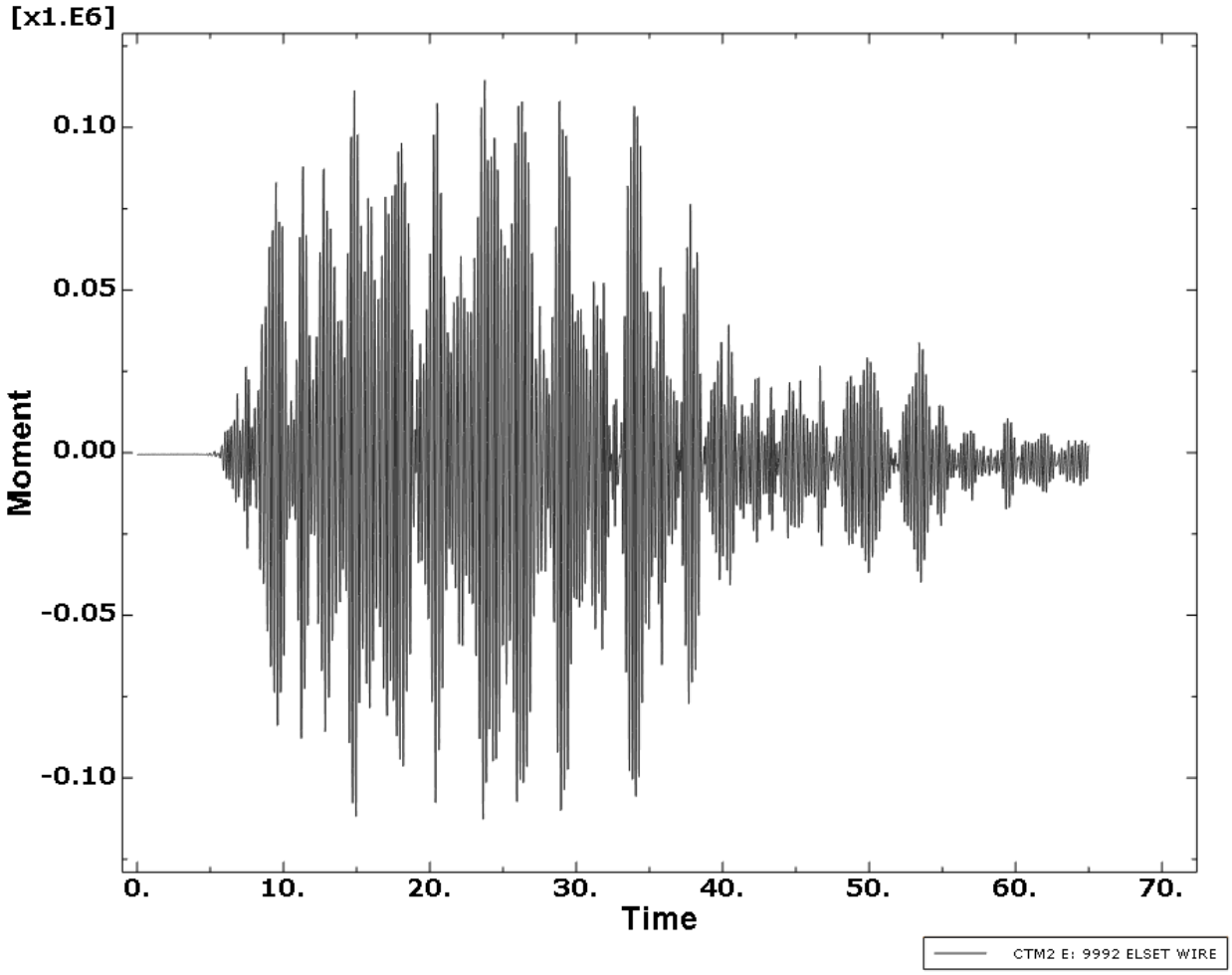

Figure 59 Calculated moment (MN-m) at reducer crack location at high temperature (288°C) using loading block CO-35

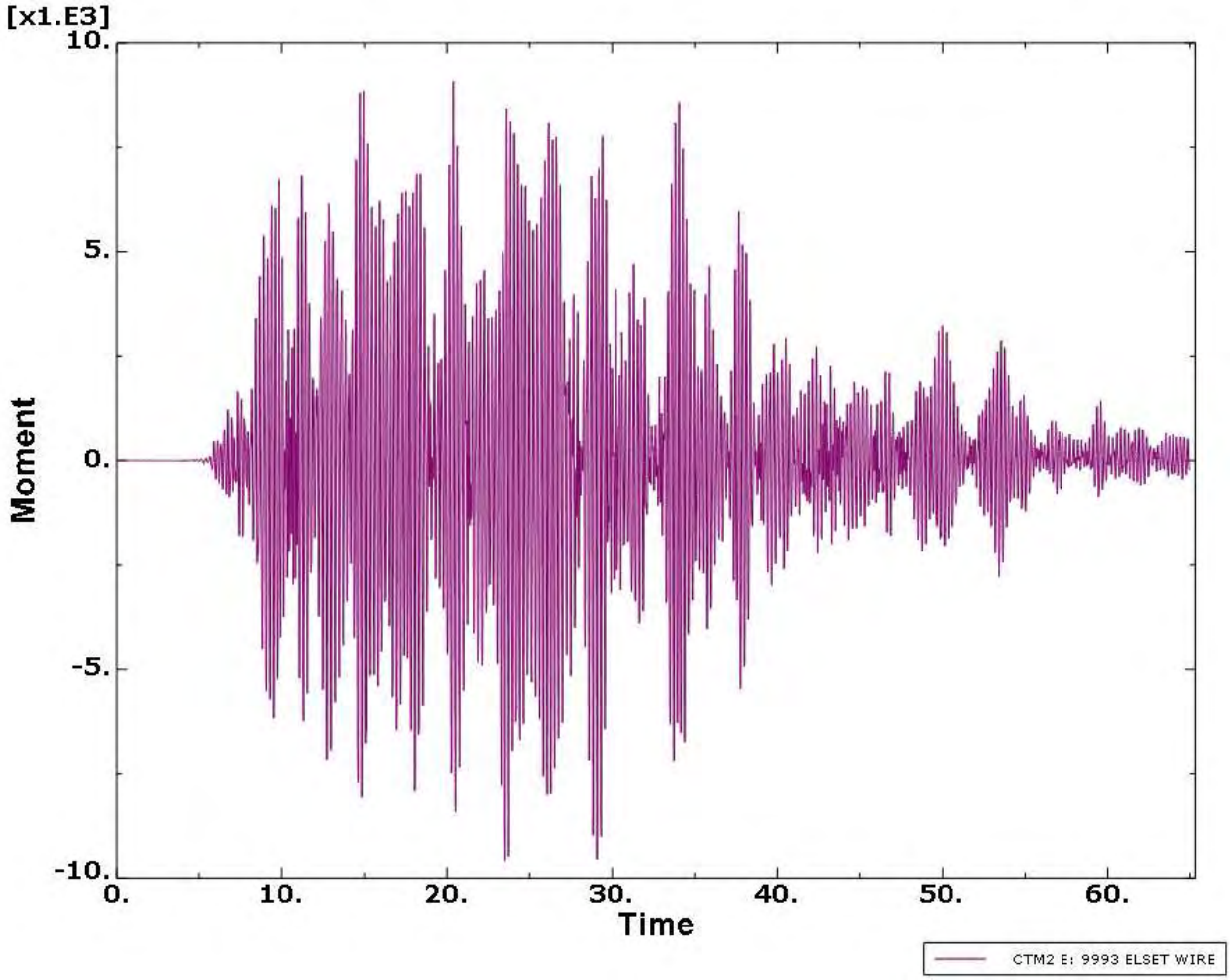

Figure 60 Calculated moment (kN-m) at branch crack location at high temperature using loading block CO-35

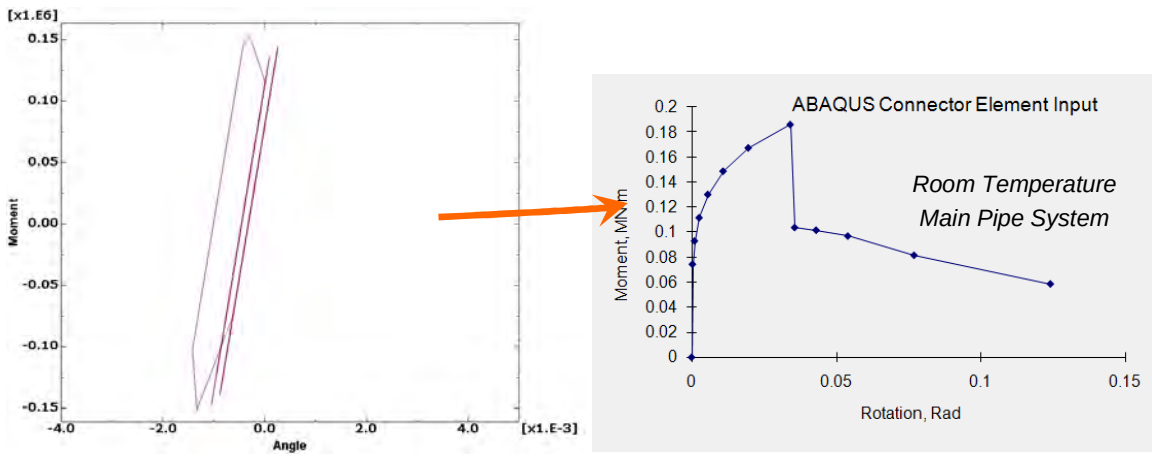

(a) Room Temperature

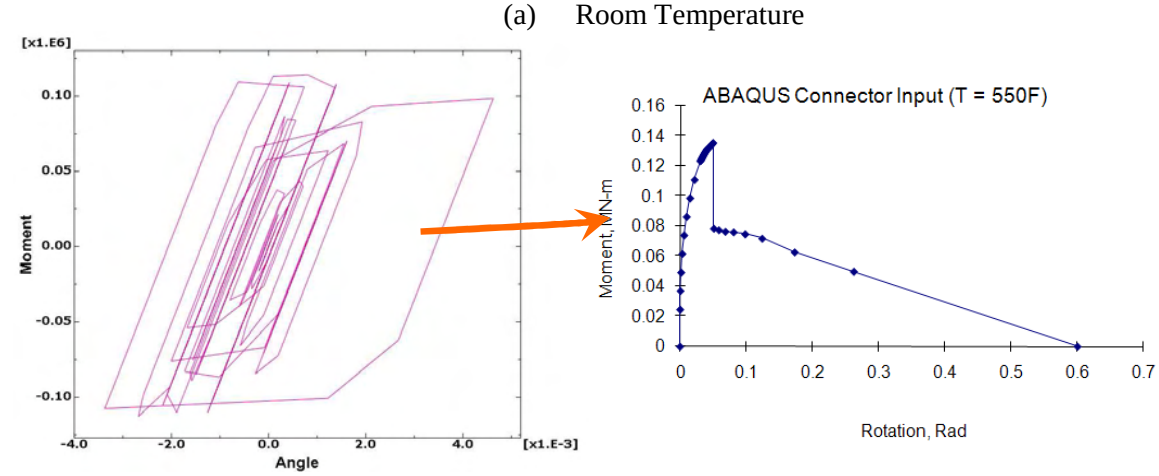

(b) T = 288 C

Figure 61 Calculated moment versus rotation-due-to-the-crack history at reducer crack at high temperature during loading block CO-35

It is clear that the nonlinear damage introduced by the seismic-load histories applied to the FTP-4 test system at room temperature is negligible and mainly elastic perhaps with some local small-scale plasticity. The margin on predicted maximum moment capacity to the maximum applied moment that can be accommodated by the crack element is 1.26. The margin calculated by moment is very conservative since the pipe system can still perform past maximum load and to get to this maximum moment the damping of the uncracked part of the pipe system should increase. However, after pipe pressure is lost, the system probably cannot perform its cooling function. After the surface crack breaks through the pipe wall, the crack will begin to leak, but the through-wall crack may not completely tear into two pipe pieces (e.g., double-end break) for some additional number of cycles. In addition, it may simply remain a leaking pipe, which does not break fully. This behavior can be predicted using the methodology presented here.

It is also clear that at higher temperature, the margins are lower (in the range of 1.19 on the maximum moment capacity compared to the applied moments). Moreover, from Figure 61, it is seen that a very small amount of nonlinear cyclic damage is occurring in the CPE. However, the seismic loading is small so that the cracked pipe will still not become a TWC due to the applied low-cycle fatigue with just this applied loading block.

The following analyses consider another, and perhaps more important, measure of the margins in the JNES tests, i.e., the margins on the applied acceleration amplitude to the multiplier needed on the acceleration amplitude to get the pipe to break.

3.5 Determining Margins on Acceleration Amplitudes for Pipe Break

In this section, margins created by applying a factor to the seismic acceleration block (CO-30 to CO-35) are examined. This is perhaps a more important measure of the margins as it directly addresses the main objective of this program. In order to accomplish this evaluation, sensitivity analyses were conducted to determine the increase in the seismic amplitude needed to "break" the pipe. In this series of analyses, the scaled amplitudes were only applied on a single block of seismic excitation (CO-35 level) to obtain the surface crack penetration in one seismic event by ductile tearing rather than high-cycle or low-cycle fatigue with small-scale yielding. The procedure for determining the margin on seismic loading follows. A factor of 2 was applied to the applied acceleration versus time history shown in Figure 46. The analysis was performed, and it was determined if any of the surface cracks became through-wall cracks and then completely broke. If the surface crack did not grow to a through-wall crack, then the multiplier was increased to three and the analysis performed again, and crack failure was again checked. This procedure was continued until one of the cracks failed. For this analysis, the viscous damping is kept as 2% and the entire pipe system (especially the elbows) is allowed to experience cyclic plasticity. Again, pressurized water at 8.1 MPa was included in the piping system.

Figure 62 shows the FE model with the calculated pipe break location from the room temperature loading analyses, and Figure 63 is the calculated pipe break FE model from the high temperature (288°C, 550°F) loading. The scale factor on the amplitude of the CO-35 acceleration time-history to break the pipe at room temperature was 5, and the scale factor for amplitude of the CO-35 acceleration to break pipe at high temperature was 3. It was found that the reducer failed first and once the reducer fails, the tee crack (branch pipe) fails, and then the elbow crack fails for the room temperature case. Interestingly, once the reducer crack fails, the model predicts that the entire piping system fails within about 5 seconds of additional loading. This may be an important result that should be examined further since typically only one pipe break is considered in pipe flaw evaluations. However, the issue of progressive failures may not be important from a safety standpoint since the first break may lose the cooling function of the pipe. Note that when the entire system was intact, the branch connection crack had a much lower crack-driving force than the other cracks; but once the crack at the reducer broke, then the crack-driving force at the branch connection increased significantly.

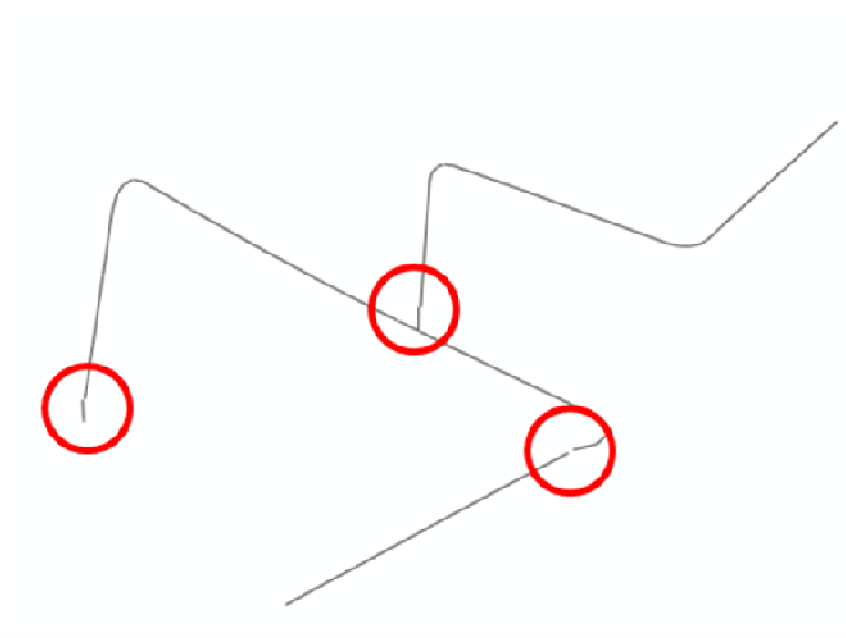

Figure 62 Broken FTP-4 combined-component system at room temperature

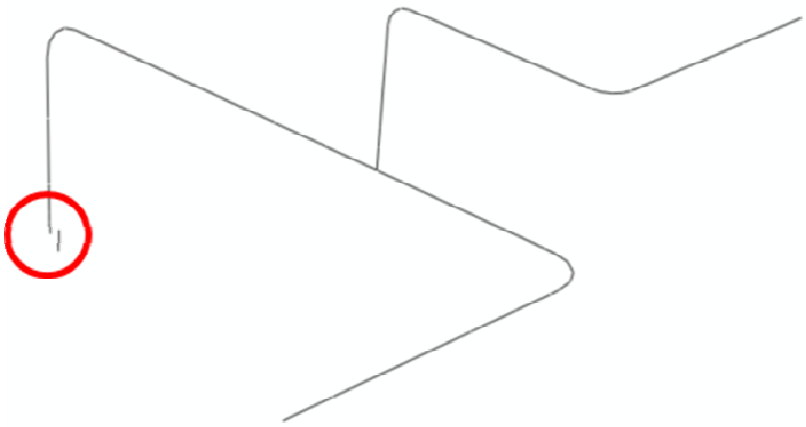

Figure 63 Broken FTP-4 combined-component system at high temperature

3.6 Low-Cycle Fatigue Crack Growth Assessment

Section 3.3.2 discussed the different types of cyclic crack growth damage that can occur in a cracked piping system that is subjected to dynamic excitation and cyclic loading. These are; (i) conducting a fatigue crack-growth analysis, and (ii) performing a "cracked-pipe element" analysis as was performed and discussed above. The excitation for the FTP-4 pipe system produced moments and forces at the crack locations which were not high enough to produce tearing or large-scale plasticity at the crack locations. Tearing of a crack can only occur if the applied loads are high enough to cause the driving force J-integral value (crack-tip severity parameter) to be higher than the J_{Ic} value (material property determining crack initiation). Here, the maximum moment predicted at the reducer crack location for all of the excitation cases was about 0.15 MN-m. The moment required to produce crack initiation was 0.181 MN-m (this value came from the J-Tearing analysis used to produce Figure 48) and the maximum moment for the surface crack in the reducer and elbow was 0.185 MN-m. Hence, based on elastic-plastic fracture mechanics analysis, the crack will not grow by ductile tearing, as was seen in the analyses discussed above.

A separate low-cycle-fatigue crack-growth assessment was made in this section to determine if the crack would grow. Equation 1 lists the classical Paris fatigue law that was discussed in Section 3.3.2. This law is usually applied when linear elastic conditions (except very close to the crack tip) prevail. For such cases, the value of ΔK is quite small and the cracked component can handle typically more than tens of thousands of cycles. Here, for the FTP-4 piping system, the loads are much higher than would typically occur in a system that is dominated by elastic crack tip and corresponding fatigue crack growth response. As discussed in Section 3.3.2, for this case Dowling developed a method to predict low-cycle fatigue crack growth. To use this method, one calculates a ΔJ value, and converts this into ΔK using $J = K^2/E'$ (where $E' = E/(1-\nu^2)$ for plane strain (plane strain dominates for the deep point of a surface crack as exists near the reducer and elbow). The technique for using this method is described fully by Wilkowski, et al.,[18] for a circumferential through-wall-cracked pipe evaluation. Here the assessment is made for the reducer circumferential surface crack only since this is the critical crack location.

The main difficulty in applying this method is determining ΔJ. The J-integral parameter is theoretically valid under proportional load conditions with the load monotonically increasing. During cyclic loading, especially if plasticity occurs, J-theory breaks down. Despite this theoretical limitation, J-theory has been used as a practical ductile fracture mechanics predictive tool in the nuclear industry for thirty years with success, although there are other alternative approaches. We use the procedure[18] discussed below to estimate J for the low-cycle-fatigue crack-growth assessment.

The value of ΔJ was estimated by using the SC.TNP J-estimation scheme. This is the estimation scheme used to obtain the cracked-pipe moment-rotation curve discussed as part of the "cracked-pipe element" analysis, and was statistically validated against many pipe fracture tests during various NRC research programs[2]. Since crack closure can play a role in low-cycle fatigue crack growth, it must be accounted for. From Reference 18 it was shown that one may write $\Delta J = \beta J$, where β is a factor that accounts for crack closure effects and is between 1 and 2. Crack closure occurs when the crack faces contact during negative, or compressive stress, portion of the loading cycle. For $\beta = 1$, $J = \Delta J$, and crack closure effects are not important (this is the case for the minimum, M_{min} to maximum M_{max} load is defined by $R \geq 0$ where $R = M_{min}/M_{max}$ loads). For full reversed loading, and no crack closure (i.e., a large notch where the crack faces cannot touch during the unload step ($M_{min} = - M_{max}$) and $R = - 1$, $\beta = 2$. For the JNES pipe system cracks, it is difficult to estimate the crack closure effect. Based on circumferential through-wall-cracked pipe tests analyzed by Wilkowski[18], it is estimated that β can range between 1.3 and 1.4. Here, the crack growth calculations were made for values of β of 1, 1.3, 1.4, and 2. For the JNES tests, since the notch for the surface flaw was introduced using an EDM procedure, the notch opening is about

0.7 mm. Prior to crack growth, the crack faces do not touch during the compressive portion of the cycle. After the crack begins to grow, the crack faces over the crack growth portion of the crack faces will contact, and crack closure is important. Hence, the experimental procedures used induced a change in the crack closure conditions as the crack growth occurs.

The procedure used to perform the low-cycle fatigue crack growth calculations is given in the seven steps below.

1. Determine the crack growth constants for Equation (1). For crack growth in meters and stress intensity factor, K, in MPa-$m^{1/2}$, the constant C is 2.75E-12 and m is 3.3. This correlation is in the ASME code, Section C 8410 of Appendix C to Section XI, and is used for austenitic stainless steels fatigued in air at room temperature. These material constants are very close to those used by Wilkowski[(18)], for TP304 stainless steel base metal and should provide reasonable fatigue-crack-growth predictions.

2. Place the moment spectrum from load cases CO-30 to CO-35 into 'load segments'. The moment load spectrum for CO-30 is shown in Figure 64(a-f) as an example. Figure 64(a) shows the predicted moments at the reducer section for time 0 to 10 seconds. It is seen that the maximum moment over this time period is about 0.7 MN-m. This level produces a ΔJ value that is so low that the crack growth for all of these cycles can be ignored. It turns out that, for these material constants of TP316 stainless steel, crack growth can be neglected for practical purposes for moment values below about 0.95 MN-m because the amount of crack growth per cycle is so small (this value was determined by including a lower load in the load segment initially (0.825 MN-m) and determining that the additional crack growth from this level is small). Figure 64(b-f) shows the predicted moments for time between 10-20, 20-30, 30-40, 40-50, and 50-65 seconds, respectively. It is seen that moments higher than 0.95 MN-m occur for the time period from 10 to 40 seconds only, all other moments can be neglected since the amount of crack growth per cycle is very small and there are not many cycles of those magnitudes for consideration for high cycle fatigue.

3. Place the load cycles into 'bins' for analysis purposes. For instance, the loads for the time periods 30 to 40 seconds [Figure 64(d)] are binned into 0.1375, 0.125, 0.112, and 0.1 MN-m moment cycles for fatigue spectrum analysis. The determination of the load bin levels is somewhat arbitrary but made to be conservative. However, one tries to determine levels where an equal number of loads are above and below the range. Moreover, when picking the levels, we conservatively place a moment in the upper 'bin level' if there is any question as to where it should be placed. From Figure 64(d), it can be seen that there are 4 x (0.125 MN-m), 2 x (0.112 MN-m), and 8 x (0.1 MN-m) cycle bins that are part of the spectrum for CO-30. This same procedure was used for all six load sets. In general, load sets CO-30 to CO-33 are similar, and CO-34 and CO-35 have higher moments that are important for low-cycle fatigue crack growth. Figure 65 shows a plot of the binned load spectra (converted to stress) that were applied for the low-cycle fatigue assessment in the AFGROW code (discussed in Step 5 below). The lines represent each important cycle within each of the blocks. The stress was simply defined as the nominal bending stress (this normalization is irrelevant as this is just used to interpolate K-values in AFGROW with user defined values) in the reducer pipe at the mid thickness based on the moment loads that were predicted, i.e., $\sigma = (M\ R_{mean/})/I$, where M is the moment from Figure 64. R_{mean} is the mean radius of 0.1017 m, and I = 4.274E-5 m^4 (here the thickness is 0.01294 at the pipe reducer section of the crack – which is slightly larger than the nominal .0127m). Note that CO-34 is more severe compared with CO-30 to CO-33, and CO-35 is the worst case.

4. The binned moment cycles are placed into spectral blocks. For this analysis, CO-30 to CO-33 are represented by one block that is applied 4 times, and the CO-34 and CO-35, which have larger moments, represents the final two blocks, with CO-35 the worst contribution to fatigue crack growth. The blocks in Figure 65 have each spectrum applying the lower loads first followed by the larger loads for each of the six spectra. If we reverse the order, with the larger loads first followed by the lower loads, the results are not affected much (this was done here). In reality, for each spectrum, the lower loads are experienced first as seen in Figure 65. The stress levels in Figure 65 are represented by the different colors. The plot, which is output from AFGROW, is somewhat deceiving in that only 4 total load levels were applied, 3 for CO-30 to CO-33, and 4 for CO-34 and CO-35. The mixed colors are an artifact of the AFGROW plotting routine.

5. The Air Force fatigue analysis code, AFGROW (Version 4), which uses a Vroman crack growth integration scheme to march through the low-cycle fatigue crack growth analysis, was used for all predictions. AFGROW is a very powerful fatigue-life estimation code used throughout the U.S. Air Force and other U.S. agencies that manage fleets of planes, and it is used in many other industries as well. This code can handle very complicated load spectra, has five different fatigue laws, numerous crack growth libraries, and a large material database and has been validated extensively.

6. AFGROW was used by inputting a user-defined spectrum (discussed in Reference 22), a user-defined Walker-based fatigue law which was simplified down to a simple Paris law of Equation 1 (constants from '1' above), and a user-defined stress-intensity-factor solution based on estimation of J-integral (discussed in Reference 18). J was calculated using the SC.TNP J-estimation method, discussed earlier. These J-values had to be converted into K in the form of an influence function table, which relates 'K' to load (or normalized stress here) for use in AFGROW. Because low-cycle fatigue crack growth based on J is nonlinear, the influence functions are actually nonlinear whereas the elastic functions are linear for high-cycle fatigue calculations. Since nonlinear influence functions are not possible with AFGROW, upper level average values were used, which cause the predictions to be slightly conservative. If failure does not occur after the entire spectrum, CO-30 to CO-35 is applied, the entire spectrum is re-applied until failure occurs.

7. It was assumed that the fatigue crack would grow immediately from the 0.7 mm wide EDM notch. In high-cycle fatigue there may be a considerable number of cycles to initiate a crack from an EDM notch, while in low-cycle fatigue the number of cycles to initiate the crack from the EDM notch significantly decreases. Hence, the low-cycle fatigue analysis here should slightly over predict the number of cycles to leakage compared to experimental results.

Figure 66 illustrates the fatigue-crack-growth predictions in the form of crack size versus load cycles. It is seen for the case of $\beta = 1$ (no crack closure) the crack does not break through the wall for the CO-30 to CO-35 spectrum application. In fact, leakage will not occur until Cycle 302, which is near the beginning of block CO-34 during the second application of this spectrum if the blocks continued to be applied (Cycle 302 represents application of the 11th total load block). (It should be noted that failure was checked for net-section collapse (limit-load failure) and elastic-plastic fracture for each case also within AFGROW). For $\beta = 1.3$, leakage is also not predicted within load step CO-35. As seen in the summary table at the bottom of Figure 66, the a/t ratio after the six spectra are applied is 0.958. If the blocks were repeated again starting with CO-30, leakage is predicted on Cycle 203. For $\beta = 1.4$, leakage is predicted at Cycle 179 within load block CO-35, which is where the experiment apparently experienced a leak. Finally, for full crack closure ($\beta = 2$), leakage is predicted near the end of load block CO-33 at Cycle 113.

Notice from Figure 65 that the crack growth for the cycles can be correlated with the load blocks with more growth predicted near the end of each block where the higher stresses were applied.

For this case, we estimate that the closure value of β should be between 1.3 and 1.4, as was observed in Reference 18. Hence, despite the assumptions made and recognizing the theoretical concerns regarding the Dowling ΔJ low-cycle-fatigue crack-growth procedure used here, the predictions compare rather well with the test measurements. It would be quite useful to develop a procedure that combined the J-Tearing based approach using the "cracked-pipe element" with the cycle-by-cycle Dowling low-cycle-fatigue analysis within the dynamic FE procedure. This could be done by developing a special user element (UMAT) for use with the ABAQUS code.

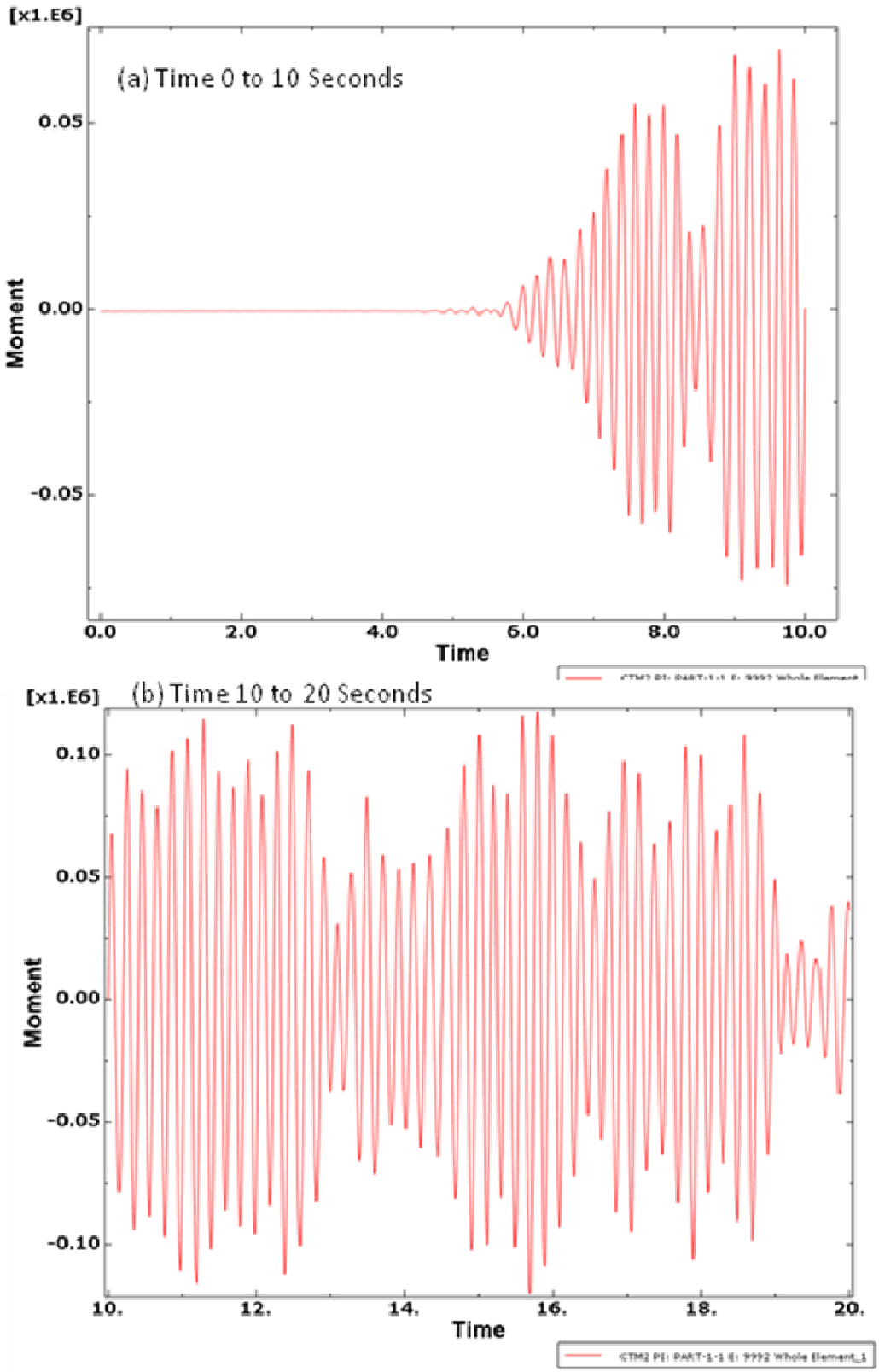

Figure 64 Predicted moment versus time history for reducer crack for spectrum CO-30

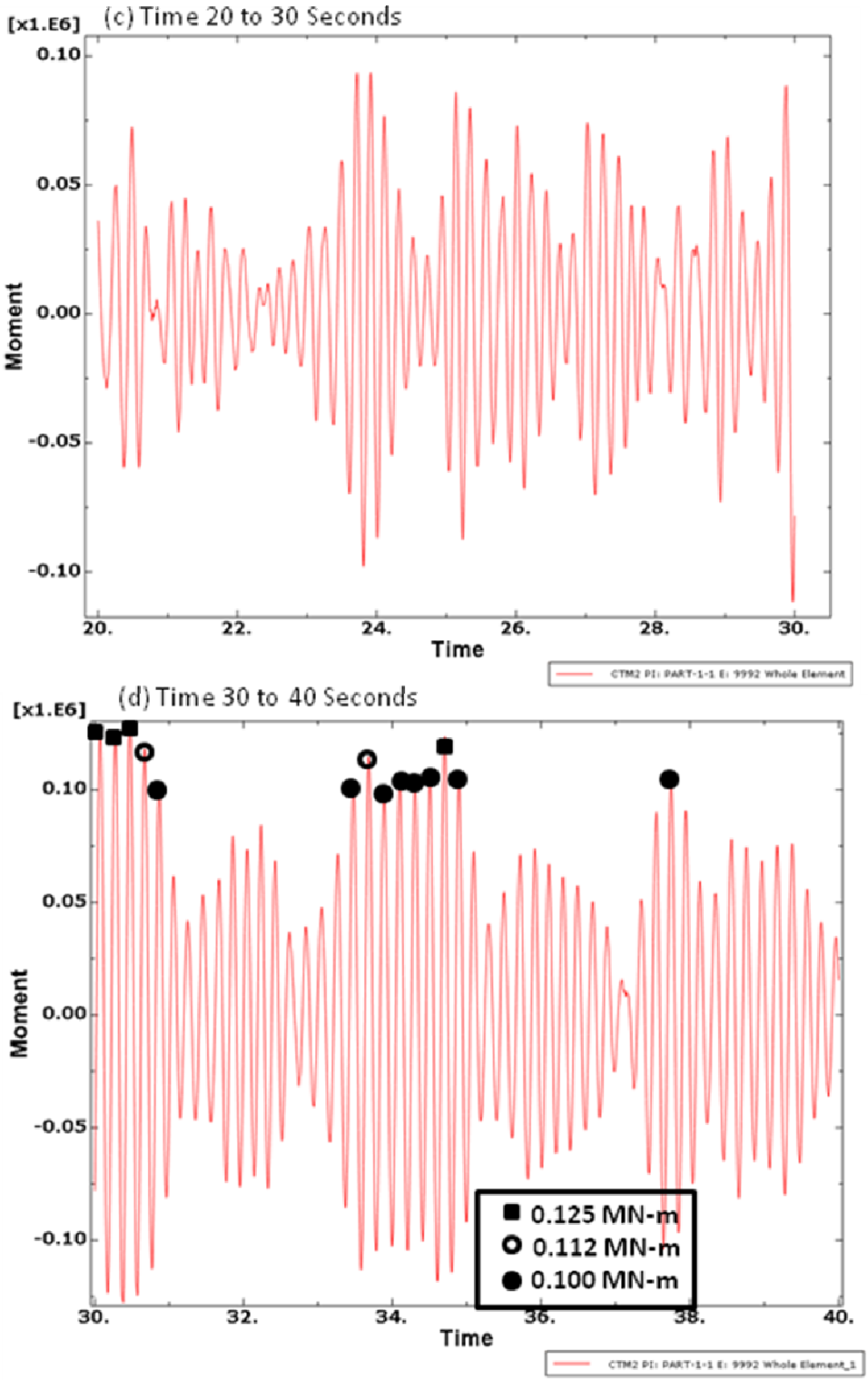

Figure 64 (continued) Predicted moment versus time history for reducer crack for spectrum CO-30

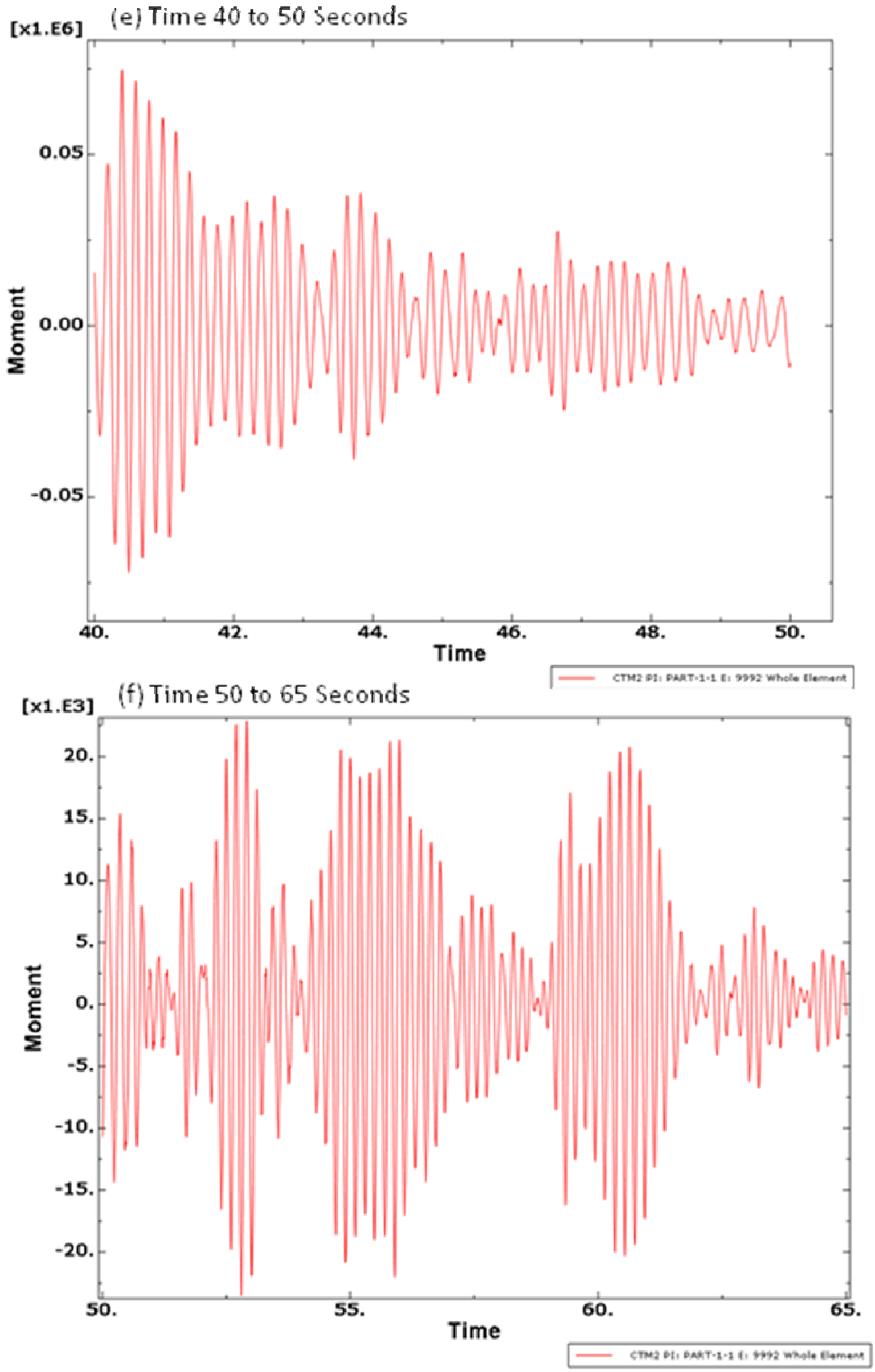

Figure 64 (continued) Predicted moment versus time history for reducer crack for spectrum CO-30

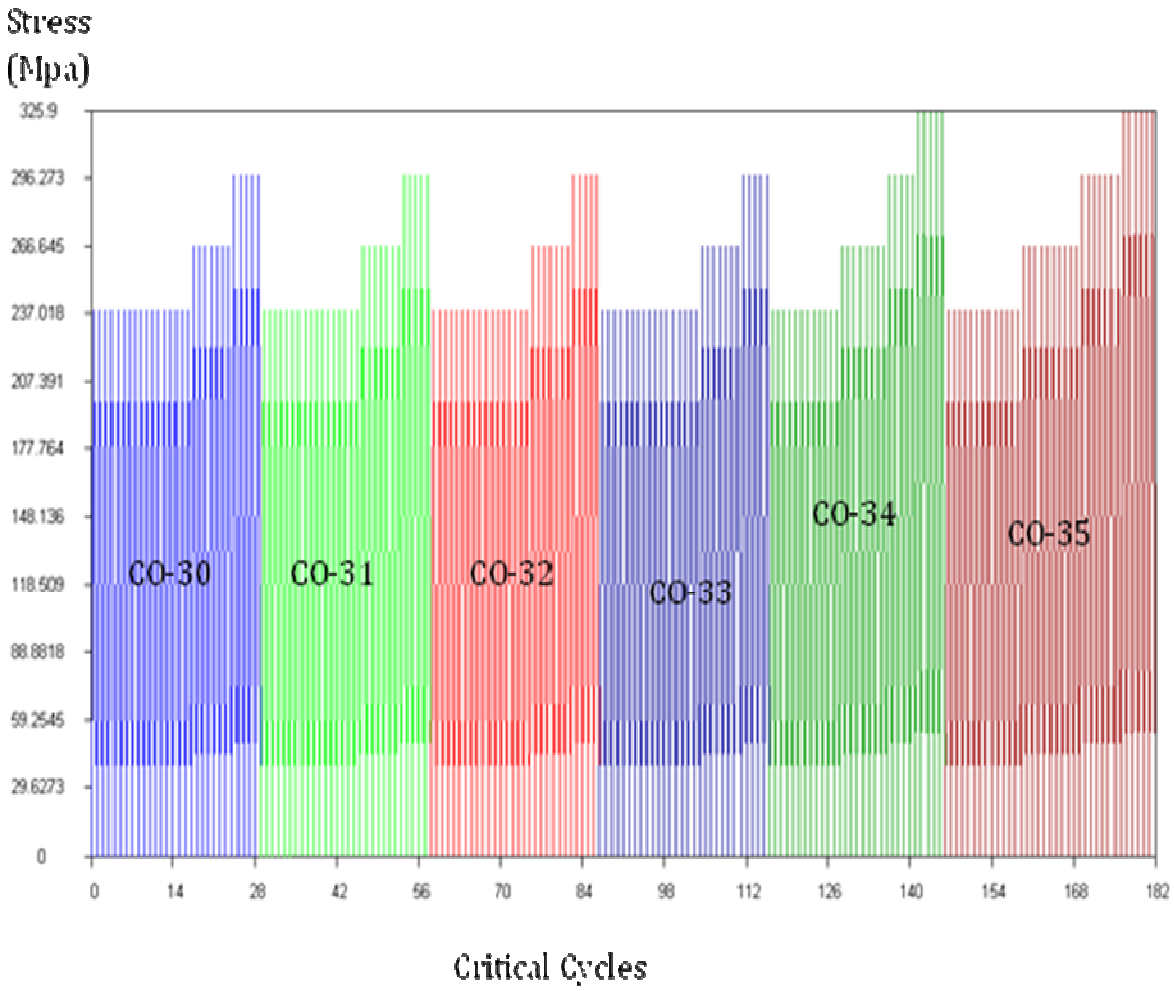

Figure 65 **Binned Stress cycles calculated from the predicted moments for all spectra (CO-30 to CO-35). σ = 138 MPa corresponds to a moment of 0.1 MN-m, σ = 155 MPa corresponds to a moment of 0.112 MN-m, σ = 173 MPa corresponds to a moment of 0.125 MN-m, and σ = 189 MPa corresponds to a moment of 0.1375 MN-m. Each 'line' represents a cycle applied.**

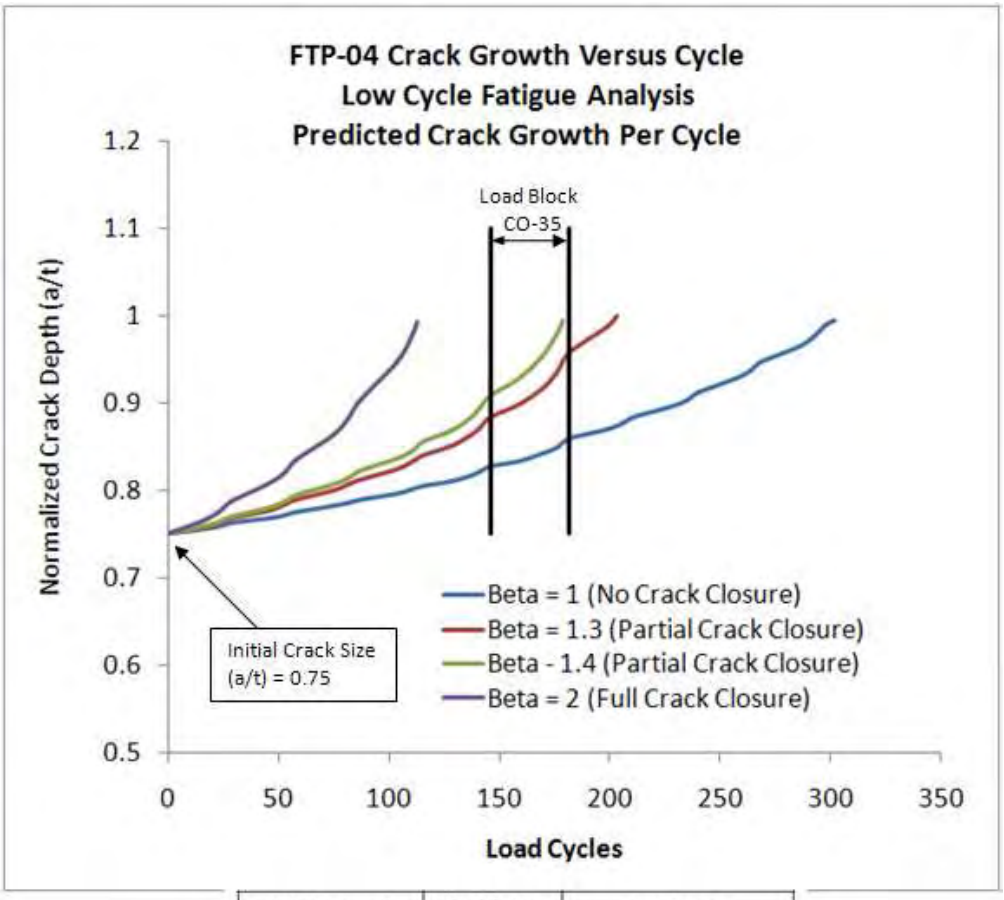

β (Closure)	(a/t) for cycle 182	Leakage
1 (no closure)	0.859	No
1.3	0.958	No (Almost)
1.4	1.0 (Leak)	Block CO-35, cycle 179
2 (full closure)	1.0 (Leak)	Block CO-33, cycle 113

Figure 66 Low-cycle fatigue-crack-growth predictions
(Ignoring number of cycles to initiate the crack from the EDM notch.)

3.7 Summary of Results

The connector element in ABAQUS has been introduced to the fracture analysis in piping systems to represent a "cracked-pipe element" (CPE). The static and dynamic behaviors were thoroughly studied and validated against a large variety of pipe experiments. This connector element can be used to simulate and automatically calculate the low-cycle fatigue crack growth during large-scale plasticity and ultimate failure under static and dynamic loading with much less computation time than full 3D FE modeling. Elastic loading where high-cycle fatigue or low-cycle fatigue with small-scale plasticity might occur is not properly modeled with this "cracked-pipe element," and currently a separate analysis is needed for such failure modes outside of the dynamic FE analysis.

Since the analysis predictions using the CPE approach did not predict leakage, this indicated that cyclic ductile tearing with large-scale plasticity was not the crack growth mode. This was evident from the tight crack at leakage in the experiment. Hence, the leakage was caused by low-cycle fatigue with very small-scale yielding, rather than by ductile tearing or low-cycle fatigue with larger plasticity that would occur if the loading were near the ultimate-load capacity of the cracked pipe. The procedure used to make predictions of low-cycle fatigue crack growth were based on the Dowling ΔJ procedure together with experience from circumferential through-wall-cracked pipe low-cycle-fatigue analysis in Reference 18.
The Dowling approach is an extension of linear-elastic-based fatigue-crack-growth methodology extended into the nonlinear plasticity regime. The predicted moments from the CPE approach were used in a cycle-by-cycle crack growth procedure. The U.S. Air Force fatigue-crack-growth code, AFGROW, was used to make these predictions. AFGROW is a completely validated code that is used by many organizations to make fatigue crack growth predictions using complicated loading spectra. The predictions using this approach compare quite well with the experimental measurements where leakage occurred during the sixth load block when using the recommendations of the β factor of 1.3 to 1.4 from Reference 18 for converting deformation plasticity J to the Dowling ΔJ, although the analysis does not account for the number of cycles that it may have taken to initiate a fatigue crack from the EDM notch. No experimental data were available to make that assessment either, however, in low-cycle fatigue there are not as many cycles needed to start a fatigue crack from an EDM notch as there is in high-cycle fatigue.

The low-cycle-fatigue-crack-growth predictions were presented in the form of crack size versus load cycles. For values of closure load expected in the JNES tests, (β = 1.3 to 1.4) leakage was predicted very near or in the sixth and final loading block, as seen experimentally. The crack growth for the cycles are examined by comparing growth per cycle throughout the loading spectra.

Margins on the applied moment to the maximum moment capacity, as well as the acceleration amplitude applied relative to the acceleration amplitude needed to fail the pipe, were determined. Table 1 summarizes these margins for different cases. For room temperature, the margin was calculated to be 1.26 for the applied moments in FTP-4 versus the maximum moment capacity of the cracked pipe. The calculated maximum acceleration level to cause a full pipe break in the FTP-4 combined-component test system was 5 times the CO-35 acceleration level. At BWR operating temperatures [288°C, (550°F], the calculated margin on the applied moment to the maximum moment capacity was 1.19, while the calculated margin on the applied acceleration to the acceleration needed to break the pipe was 3. The margins on acceleration to cause failure may be lower bounding since the viscous damping factor for the entire system may slightly increase above the 2% damping value used in these analyses. The major energy dissipation for analyses with increased excitation levels was achieved by the plastic deformation of the piping system (elbows in particular).

As a final evaluation, consideration was given to how the full-scale BWR pipe section might respond to such loading at 288°C (550°F). Although the actual full-scale model was not created in this effort, the

behavior was estimated from simple fracture mechanics considerations using an elastic-plastic fracture mechanics parameter called the Z-factor, where Z = failure stress at limit-load conditions divided by the elastic-plastic fracture mechanics failure stress (or actual failure stress). The Z-factor is a function of material, as well as the pipe diameter.

To assess the Z-factors that should be used (there are differences between the JSME and ASME Z-factors), the monotonic loaded JNES Test EM-3 that was analyzed using the "cracked-pipe element" approach in Section 3.3.3 was further analyzed. Figure 42 showed the experimental load-displacement record from that test, Figure 39 gave the stress-strain curve (flow stress is the average of the yield and ultimate strength), and knowing the crack dimensions (60-degrees and a/t of 0.75), internal pressure of 8.1 MPa, and moment arm length (~1 m) the predicted failure moment from the Net-Section-Collapse equation (used in both the ASME and JSME codes – also called limit-load) can be calculated and compared to the experimental result. This result showed that the limit-load failure stress was 1.38 times larger than the test maximum moment. That means that effectively the Z-factor was 1.38 in that test. Interestingly, from Figure 4 it was seen that for 200-mm diameter pipe the Z-factor is 1.31 for GTAW using the JSME relationship. That is excellent agreement.

As a result of the above Z-factor validation, the difference in the failure stress from a 711-mm (28-inch) diameter full-scale pipe relative to the 200-mm (8-inch) diameter pipes tested could be estimated by simply finding the ratio for the Z-factors for those two pipe diameters using the JSME Z-factor equation. That is Z(711)/Z(200) is the correction factor that could be used on the 200-mm diameter pipe test results for estimating 711-mm diameter pipe fracture behavior. This ratio is 1.48/1.31 or 1.127.

Using that Z-factor ratio, the margins on the applied moment to this reduced moment capacity for EPFM behavior at 288°C (550°F) would be about 1.06 for the 711-mm (28-inch) diameter pipe behavior. From this load level, the margins on the applied accelerations were roughly estimated to be 1.92 to 2.39 by scaling with the other analysis results. Again these are slightly conservative estimates of the margins since the damping could slightly increase as excitation level increases. A constant viscous damping ratio of 2% was used for these analyses. It would be instructive to actually run the full-scale case with the "cracked-pipe element" analysis (including thermal expansion stresses). Similar results for a PWR primary pipe loop system would also be instructive. The above calculated margin values are given in Table 1.

In conclusion, these analyses showed large margins for the acceleration to cause failure relative to the typical design PGA values. These margins are lower bounding since the viscous damping could slightly increase as the excitation increases, and are qualitatively instructive in understanding the safety factors that might actually exist under seismic loading. In the NRC's Transition Break Size seismic considerations analyses[(3)], it was known that such margins might exist between elastically calculated seismic stresses for beyond design basis earthquakes, and nonlinear fracture behavior. A correction factor of 1 to 2.8 was applied to the elastically scaled seismic stresses for seismic events with probabilities of occurrence of 10E-6 from actual plant seismic-hazard curves. (That correction factor was a function of the crack size with 2.8 corresponding to unflawed pipe and 1 for elastic piping response with a very large flaw.) It is comforting that the margins seen in the analyses of these JNES tests of the tolerable accelerations relative to the SSE design PGA values for U.S. plants are much larger than the maximum nonlinear stress correction factors used in the Transition Break Size seismic consideration analyses. Although analyses as conducted in this report would have to be conducted for the crack sizes and typical pipe system used in the Transition Break Size seismic analysis to better quantify the margins that might exist. Similar margins would also affect LBB analyses, ASME code criteria, and on-going probabilistic pipe fracture analyses such as the NRC's xLPR efforts that are just starting up.

Table 1 Summary of margins for different cases

Case	Temperature	Margins on applied moments	Margins on applied accelerations
1/3-scale model Crack in GTAW	Room temperature	1.26	5
1/3-scale model Crack in GTAW	288°C (550°F)	1.19	3
Full-scale Crack in GTAW/SMAW using JSME Z-factor*	288°C (550°F)	1.06 = 1.19/Z(711/200)	~ 1.92 to 2.39 (Not actually conducted)

* JSME Z-factor for 200-mm diameter pipe = 1.31, and for 711-mm diameter pipe = 1.48. Z(711/200) = 1.48/1.31 = 1.127, which is the ratio of the failure stresses expected from a 200-mm versus 711-mm diameter pipe due to elastic-plastic fracture mechanics.

4 CONCLUSIONS AND RECOMMENDATIONS

The connector element in ABAQUS was used to simulate the global response of a cracked pipe, i.e., it performed like a "cracked-pipe element" that could be placed at any node point in the FE model. All validations were good, albeit some improvements can be made with the element formulation to get better agreement with some of the experimental results. This has been discussed with the ABAQUS staff. The beauty of the current "cracked-pipe element" approach is that it is capable of automatically capturing low-cycle fatigue with large-scale plasticity, hysteresis energy due to the plasticity at the crack during the seismic loading, and ductile tearing at the ultimate load capacity of the cracked-pipe section under complicated seismic loading without any tedious post processing. High-cycle fatigue crack growth from elastic loading or low-cycle fatigue with small-scale yielding is not automatically captured by this current approach, and currently requires a second fatigue crack growth analysis using the applied cyclic moment. Moreover, this type of element tremendously reduces computational time, i.e., ~1 hour of CPU time was used per FTP system run (using eight 64-bit processors in parallel). Only 25 elements were needed in the FTP-4 system model, whereas a full 3D analysis with the three cracks would probably require about 45,000 elements for similar full three dimensional nonlinear analyses of surface cracked pipe performed by the authors in past work or proper mesh refinement at each crack locations, and even then, this FE mesh would not allow for crack growth so multiple meshes and FE runs would be necessary.

The viscous damping value for the FTP-4 test system runs was specified as 2.0%, which was obtained based on test data [23], while the entire piping system was allowed to deform plastically, including plasticity development at cracks (i.e., connector elements). These modeling specifications led to good agreement between experimental displacements and strains and the corresponding analytical results, confirming the validity of the 2% viscous damping ratio and the plasticity modeling in the elbows and the cracks. The analysis also showed that there was only small-scale yielding loads at the crack locations, so that only classical fatigue failure should occur. The dynamic FE analyses showed that the piping system model could accurately predict displacement and damage responses for various input motions.

In the JNES combined-component experiment where leakage occurred (FTP-4), it was determined that the loading at the crack location was in the small-scale plasticity range of the "cracked-pipe elements." Hence the leakage was caused by low-cycle fatigue with very small-scale yielding, rather than by ductile tearing or low-cycle fatigue with larger plasticity that would occur if the loading were near the ultimate-load capacity of the cracked pipe. The procedure used to make predictions of low-cycle fatigue crack growth were based on the Dowling ΔJ procedure, which is an extension of linear-elastic-based fatigue-crack-growth methodology extended into the nonlinear plasticity regime. The predicted moments from the CPE approach were used using a cycle-by-cycle crack growth procedure outside of the dynamic FE analyses. Only moments large enough to produce significant crack growth per cycle need be included, and the U.S. Air Force fatigue crack growth code, AFGROW, was used to make these predictions. The predictions using this approach compare quite well with the experimental measurements where leakage occurred during the sixth load block.

It would be advantageous to develop an automated procedure to permit both cyclic ductile tearing (as with the "cracked-pipe element"), and low-cycle fatigue crack growth (as with Dowling ΔJ approach) within the full dynamic finite element analysis. It is possible that a crack may grow under low-cycle fatigue conditions to a size where ductile tearing may occur and the "cracked-pipe element" modeling will take over. As such, there is an interaction between the two approaches that should be accounted for. The FTP-4 analyses were performed in two separate ways, neglecting interaction. In reality, it is likely for the FTP-4 analysis, that low-cycle fatigue dominated the early portion of the test and then cyclic tearing may dominate after the crack grows to a certain depth. This combined analysis could be done in an ABAQUS finite element framework by writing a user routine (a UMAT) that can account for both types of damage.

Margins for failure in one loading block were calculated for the FTP-4 test for the applied moment to the maximum moment capacity of the cracks for the room temperature testing that was done, as well as for the calculated case of the tests being done at BWR service temperature of 288°C (550°F). Those margins on the applied moments were 1.26 and 1.19, respectively. The lower calculated margins on the moments at service temperatures were expected since the strength and toughness of stainless steel decreases with increasing temperature.

Perhaps a more important margin assessment involved how much more the accelerations needed to be increased to cause the pipe to break in one seismic loading event. (Six seismic loading blocks were applied in Experiment FTP-4.) The margins on moment and accelerations are not linearly related since the plasticity at the crack and the elbows absorbs energy like increased damping. These calculations were performed for the FTP-4 room temperature case, as well as considering the FTP-4 system with material properties at the BWR service temperature of 288°C (550°F). Compared to the applied accelerations in the FTP-4 test (2000 gal), the margins of the acceleration needed to cause failure in just one load cycle were determined to be 5 and 3 at room temperature and 288°C (550°F), respectively. These are lower bound margins, since the damping from the rest of the uncracked-pipe system would slightly increase above 2% at the higher-level excitations.

Finally, an estimate was made as to what the margins on the moments and accelerations would be if elastic-plastic fracture mechanics considerations were made for the full-scale pipe system. To do this, first the appropriate Z-factor relationship needed to be determined. That was done using the monotonic component test EM-3. Using the failure stress from that JNES component test, the calculated Z-factor was 1.38, which is extremely close to the JSME Z-factor value of 1.31 for GTAW/SMAW welds. To predict the margins that might exist for a full-scale pipe system, the JSME Z-factor equation was then used. This resulted in a conservative estimate that the full-scale pipe system might have a margin of 1.06 on the failure load. Although the dynamic "cracked-pipe element" analysis was not conducted for the full-scale pipe system, the margins on acceleration were scaled to the FTP moment and acceleration margins, and estimated to be between 1.92 and 2.39. New seismic design criteria are being developed in Japan as a results of the earthquake event at the Kashiwazaki nuclear plant site. Qualitatively, these results show that larger crack sizes could be tolerated with margins, although more precise analyses are needed.

In conclusion, these analyses showed that the JNES FTP-4 pipe test should have failure due to low-cycle fatigue with small-scale yielding, and there were large margins on acceleration needed to cause failure even for extrapolated results to full-scale behavior and design PGA values. These analyses showed large margins for the acceleration to cause failure relative to the typical design PGA values for U.S. plants. These margins are lower bounding since the viscous damping could slightly increase at large accelerations, and qualitatively instructive in understanding the safety factors that might actually exist under seismic loading. In the Transition Break Size work[(3)], it was known that such margins might exist between elastically calculated seismic stresses for fracture analysis involving beyond-design-basis earthquakes using nonlinear-fracture behavior. A correction factor of 1 to 2.8 was applied to the elastically scaled seismic stresses for events with probabilities of occurrence of 10E-6 from actual plant seismic-hazard curves. (The correction factor of 1 corresponds to the stresses being purely elastic for flawed pipe failure and the factor of 2.8 corresponds to stresses that would cause failure of unflawed pipe.) The correction factor of 1 to 2.8 changes as the flaw size changes. This result is consistent with results from the BINP program[(21)]. It is comforting that the margins seen in the analyses of these JNES tests of the tolerable accelerations relative the SSE design PGA values for U.S. plants are much larger than the maximum nonlinear stress correction factors used in the Transition Break Size work. However, analyses as conducted in this report would have to be conducted for the larger crack sizes and typical pipe system used in the Transition Break Size seismic analysis to better quantify the margins that might exist.

Similar margins would also affect LBB analyses, ASME code criteria, and on-going probabilistic pipe fracture analyses such as the NRC's xLPR efforts that are just starting up.

Other issues that deserve further study include the effect of cyclic loading on crack initiation, the constraint effects on ductile tearing, and constraint effects on low-cycle fatigue crack growth. When plasticity at the crack tip is important, voids that develop in front of the blunted crack (prior to initiation) may sharpen and cause initiation to occur at a lower value of J. It is known that constraint effects are important for surface cracks in pipe during elastic-plastic fracture. Improvement of the J-estimation schemes and developing a factor to apply compact tension J-R curves to make them more appropriate for use in surface-cracked pipe is needed. Finally, constraint effects on fatigue is a topic of interest in the elastic high-cycle fatigue field at present. It may be even more important for low-cycle fatigue since plasticity is more important.

5 REFERENCES

(1) K. Suzuki and H. Kawauchi, "Test Programs for Degraded Core Shroud and PLR System Piping (Seismic Test Results and Discussion on JSME Rules Application," 2008 ASME PVP conferences, July 27-31, Chicago, IL.

(2) Wilkowski, G. M., Olson, R. J., and Scott, P. M., "State-of-the-Art Report on Piping Fracture Mechanics," U.S. Nuclear Regulatory Commission report, NUREG/CR-6540, BMI-2196, February 1998.

(3) Chokshi, N.C., Shaukat, S.K., Hiser, A.L., DeGrassi, G., Wilkowski, G., Olson, R., and Johnson, J.J., "Seismic Considerations for the Transition Break Size," NUREG-1903, February 2008.

(4) Suzuki, K., Kawauchi, H., and Abe, H., "Test Programs For Degraded Core Shroud and BWR Piping (Simulated Crack Models And Input Seismic Waves For Shaking Test)," *Proceedings of PVP2006-ICPVT-11*, July 23-27, 2006, paper # PVP2006-ICPVT-11-93118.

(5) Wilkowski, G., and others, "International Piping Integrity Research Group (IPIRG) Program, Final Report," NUREG/CR-6233 Vol. 4, June 1997.

(6) Hopper, A. T., Wilkowski, G. M., Scott, P. M., Olson, R. O., Rudland, D., Kilinski, T., Mohan, R., Ghadiali, N., and Paul, D., "The Second International Piping Integrity Research Group (IPIRG 2) Program - Final Report," NUREG/CR-6452, February 1997.

(7) P. M. Scott, R. J. Olson, and G. M. Wilkowski, "Development of Technical Basis for Leak-Before-Break Evaluation Procedures," NUREG/CR-6765, May 2002.

(8) Wilkowski, G. M., and others, "Degraded Piping Program - Phase II, Summary of Technical Results and Their Significance to Leak-Before-Break and In-Service Flaw Acceptance Criteria," NUREG/CR-4082, Vol. 8, March 1989.

(9) Wilkowski, G. M. and others, "Short Cracks in Piping and Piping Welds," Seventh Semiannual Report, NUREG/CR-4599, Vol. 4, No. 1, April 1995.

(10) Ghadiali, N., and Wilkowski, G. M., "Fracture Mechanics Database for Nuclear Piping Materials (PIFRAC)," in Fatigue and Fracture - 1996 - Volume 2, PVP - Vol. 324, July 1996, pp. 77-84.

(11) Hays, R. A., and others, "Fracture Analysis of Welded Type 304 Stainless Steel Pipe," NUREG/CR-4538 Vol. 1, May 1986.

(12) Scott, P. and others, "Crack Stability in a Representative Piping System Under Combined Inertial and Seismic/Dynamic Displacement-Controlled Stresses - Subtask 1.3 Final Report," NUREG/CR-6233 Vol. 3, BMI-2177, June 1997.

(13) Olson, R., Wolterman, R., and Wilkowski, G. M., "Validation of Analysis Methods for Assessing Flawed Piping Subjected to Dynamic Loading," NUREG/CR-6234, ANL-94/22, BMI-2178, August 1994.

(14) Scott, P., Francini, R., Rahman, S., Rosenfield, A. and Wilkowski, G, "Fracture Evaluations of Fusion Line Cracks in Nuclear Pipe Bimetallic Welds," U.S. Nuclear Regulatory Commission report NUREG/CR-6297, BMI-2182, April 1995.].

(15) Tada, H., Paris, C. and Irwin, G., *The Stress Analysis of Cracks Handbook*, Paris Productions Inc, St. Louis, 1985.

(16) Rice, J. R., "A Path-Independent Integral and Approximate Analysis of Strain Concentration by Notches and Cracks," *Journal of Applied Mechanics*, 35, pp 376-386, 1968.

(17) Dowling, N. E., and Begley, J. A., "Fatigue Crack Growth during Gross Plasticity and the J-Integral," *Mechanics of Crack Growth*, ASTM STP 590, pp 82-103, 1976.

(18) Wilkowski, G., Rahman, S., and Mohan, R., "Low-Cycle Fatigue Crack Growth Considerations in Pipe Fracture Analyses," ASME PVP Vol. 280, June 1994, pp. 281-298.

(19) Rudland, D. L., Brust, F., and Wilkowski, G. M., "The Effect of Cyclic and Dynamic Loading on the Fracture Resistance of Nuclear Piping Steels," NUREG/CR-6440, December 1996.

(20) Ghadiali, N., and Wilkowski, G. M., "Fracture Mechanics Database for Nuclear Piping Materials (PIFRAC)," in *Fatigue and Fracture - 1996* - Volume 2, PVP - Vol. 324, July 1996, pp. 77-84.

(21) Scott, P. M. et al., "The Battelle Integrity of Nuclear Piping (BINP) Program Final Report," NUREG/CR-6837, Vol. 2, June 2005.

(22) AFGROW (Air Force Fatigue Crack Growth Software), Version 4, 10/2008.

(23) Nie, J., R.J. Morante, H.C. Hofmayer, and S.A. Ali, "Assessing Equivalent Viscous Damping Using Piping System Test Results," 2010 ASME PVP conferences, July 18-22, Bellevue, Washington.

NRC FORM 335
(9-2004)
NRCMD 3.7

U.S. NUCLEAR REGULATORY COMMISSION

BIBLIOGRAPHIC DATA SHEET

(See instructions on the reverse)

1. REPORT NUMBER
(Assigned by NRC, Add Vol., Supp., Rev., and Addendum Numbers, if any.)

NUREG/CR-7015
BNL-NUREG-91346-2010

2. TITLE AND SUBTITLE

Analysis of JNES Seismic Tests on Degraded Piping

3. DATE REPORT PUBLISHED

MONTH	YEAR
July	2010

4. FIN OR GRANT NUMBER

JCN: N-6076

5. AUTHOR(S)

T. Zhang, F.W. Brust, D.J. Shim, and G. Wilkowski (Engineering Mechanics Corp. Of Columbus)
J. Nie and C. Hofmayer (Brookhaven National Laboratory)

6. TYPE OF REPORT

Technical

7. PERIOD COVERED *(Inclusive Dates)*

8. PERFORMING ORGANIZATION - NAME AND ADDRESS *(If NRC, provide Division, Office or Region, U.S. Nuclear Regulatory Commission, and mailing address; if contractor, provide name and mailing address.)*

Energy Sciences & Technology Department
Brookhaven National Laboratory
P.O. Box 5000
Upton, NY 11973-5000

9. SPONSORING ORGANIZATION - NAME AND ADDRESS *(If NRC, type "Same as above"; if contractor, provide NRC Division, Office or Region, U.S. Nuclear Regulatory Commission, and mailing address.)*

Division of Engineering
Office of Nuclear Regulatory Research
U.S. Nuclear Regulatory Research
Washington, DC 20555-0001

10. SUPPLEMENTARY NOTES

Syed Ali, NRC Project Manager.

11. ABSTRACT *(200 words or less)*

This report describes efforts conducted by Engineering Mechanics Corporation of Columbus (Emc^2) under subcontract to Brookhaven National Laboratory (BNL) for the U.S. Nuclear Regulatory Commission to analyze and better understand a series of degraded pipe tests under seismic loading that were conducted in Japan. These efforts were undertaken as part of collaborative efforts between the United States Nuclear Regulatory Commission (NRC) and the Japan Nuclear Energy Safety Organization (JNES), who conducted a multi-year test program for the Ministry of Economy, Trade and Industry (METI) of Japan to investigate the behavior of typical Nuclear Power Plant piping systems under large seismic loads. JNES provided the test results for the evaluations given in this report. Emc^2 worked with BNL on the degraded piping system analyses. This report describes Emc^2's post-test analyses of the large-scale piping system tests and discusses insights gained from this program. The analyses in these efforts are of value to understanding margins that degraded piping has under seismic loading for: (a) Transition Break Size rule for CFR 50.46a applications, (b) Leak-Before-Break analyses in NRC's SRP 3.6.3, and (c) pipe flaw tolerance by ASME code evaluations.

12. KEY WORDS/DESCRIPTORS *(List words or phrases that will assist researchers in locating the report.)*

Seismic analysis, seismic testing, piping design, ASME code evaluation, fracture mechanics, low cycle fatigue failure, crack growth, plasticity, transition break size, leak-before-break analysis, cracked pipe element, seismic margin

13. AVAILABILITY STATEMENT

unlimite

14. SECURITY CLASSIFICATION

(This Page)
unclassified

(This Report)
unclassified

15. NUMBER OF PAGES

94

16. PRICE

PRINTED ON RECYCLED PAPER